iScience

CellPress
OPEN ACCESS

Article

A Phylogenetic Networks perspective on reticulate human evolution

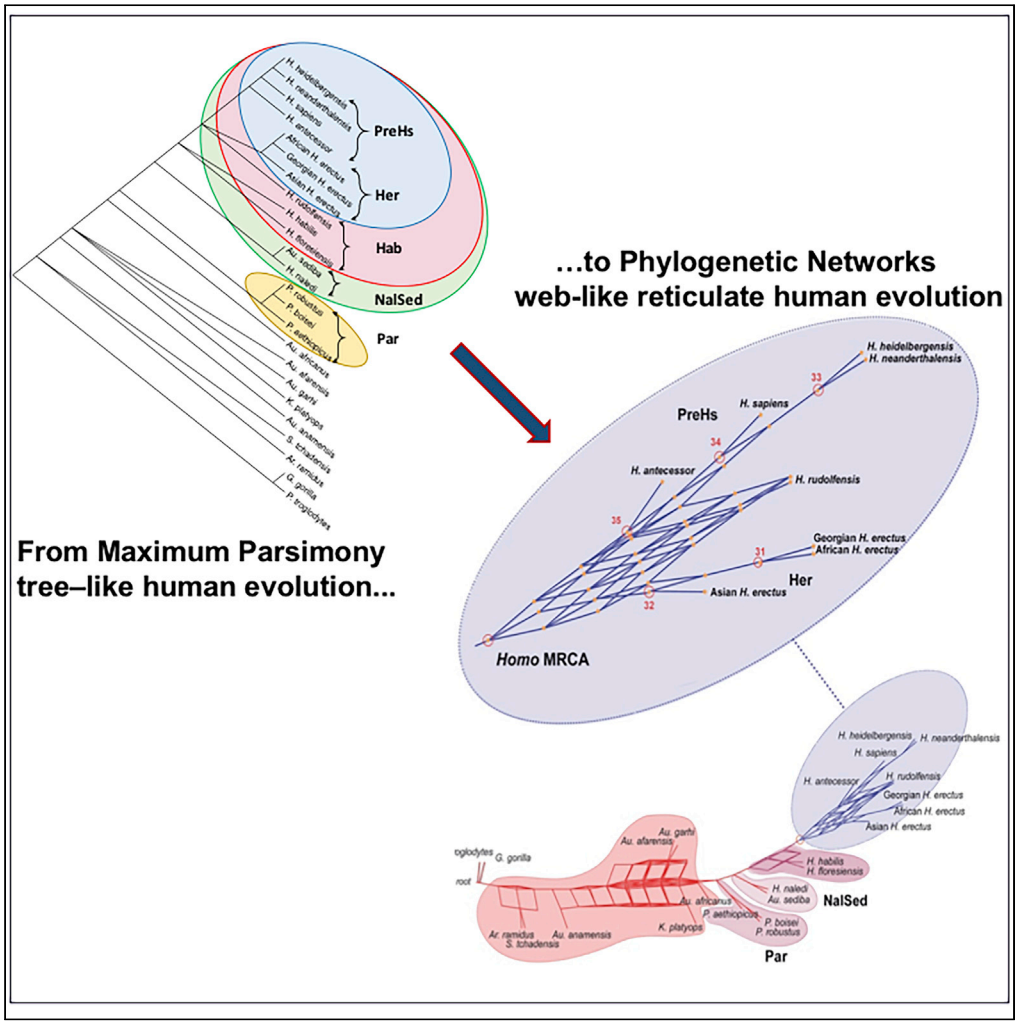

Miguel Caparros, Sandrine Prat

capmig@aol.com (M.C.)
sandrine.prat@mnhn.fr (S.P.)

Highlights

Integrate Maximum Parsimony and Phylogenetic Networks methods in study of human evolution

Most parsimonious tree-like scenario shows 3 alternative genus *Homo* definitions

We suggest that homoplastic reversals play an important role in human evolution

Phylogenetic Networks analysis shows probable reticulate mode of evolution in genus *Homo*

Caparros & Prat, iScience *24*, 102359
April 23, 2021
https://doi.org/10.1016/j.isci.2021.102359

iScience

CellPress
OPEN ACCESS

Article

A Phylogenetic Networks perspective on reticulate human evolution

Miguel Caparros[1,2,*] and Sandrine Prat[1,*]

SUMMARY

We present a methodological phylogenetic reconstruction approach combining Maximum Parsimony and Phylogenetic Networks methods for the study of human evolution applied to phenotypic craniodental characters of 22 hominin species. The approach consists in selecting and validating a tree-like most parsimonious scenario out of several parsimony runs based on various numerical constraints. An intermediate step from tree to network methods is implemented by running an analysis with a reduced apomorphous character dataset that generates multiple parsimonious trees. These most parsimonious trees are then used as input for a Phylogenetic Networks analysis that results in consensus and reticulate networks. We show here that the phylogenetic tree-like definition of the genus *Homo* is a relative concept linked to craniodental characters that come in support of hypothetical Last Common Ancestors of the most parsimonious scenario and infer that the *Homo* reticulate network concords with recent findings in paleogenomic research regarding its mode of evolution.

INTRODUCTION

The process that best describes the species diversity apparent in hominin evolution remains an open question. Traditionally, two modes of evolution have prevailed in the study of human origins (Cela-Conde and Ayala, 2007): a linear one, anagenesis synonymous of phyletic gradualism with transformation of species along an evolutionary lineage based on the concept of grades (Mayr and Ashlock, 1991), and a dichotomous one, cladogenesis representing the splitting of species by speciation into two or several species as portrayed by the cladistic method with findings expressed as a tree with branches in accord with the concepts of Phylogenetic Systematics (Hennig, 1966). To illustrate the application of these evolutionary concepts, we make reference to the two extreme models of *Homo sapiens* origins that have been the object of intense debates. The scenario of recent African origin of *H. sapiens* (Stringer and Andrews, 1988), with replacement of archaic populations without genetic contribution, is more attuned to the phylogenetic species concept based on the recognition of morphological features that define groups of monophyletic species further to speciation events (cladogenesis). In this scenario, the emergence of modern humans in Africa between 100 and 300 thousand years ago with the subsequent colonization of Eurasia represents the latest speciation of the genus *Homo*. On the opposite side of the spectrum, the advocates of the multiregional hypothesis (Wolpoff et al., 1984) maintain that hominin fossil species are anatomically polytypic and proclaim that *H. sapiens* emerged in various geographical locations of Africa and Eurasia by a phyletic process of gene flow exchanges among archaic populations. This scenario is more in line with the concept of anagenesis in the course of human evolution, although its proponents accept that there was speciation by cladogenesis when *Homo* emerged in Africa. Advances in the field of molecular anthropology, such as the sequencing of the Neanderthal genome (Green et al., 2008), the identification of the extinct Denisova lineage (Meyer et al., 2012), and findings of multiple evidence of introgressive hybridization between modern humans and archaic taxa (Rogers et al., 2020), raise some doubts on the coherence of the two extreme scenarios of *H. sapiens* origins, and whether anagenesis or cladogenesis represents reliable explanatory modes of evolution that would shed some light on the emergence and geographic expansion of the genus *Homo* (Ackermann et al., 2019). A third evolutionary process has been proposed on the basis of studies of natural genetic hybridization and phenotypic mosaic variability (Arnold, 2006, 2009), namely, reticulate evolution, which we believe from a paleoanthropological standpoint requires further investigation.

Moreover, there remain today unresolved and debated issues in paleoanthropology, namely, the morphological delimitation of species within the *Homo* genus, their relatedness, the number of species within the

[1]UMR 7194 "Histoire naturelle de l'Homme préhistorique" CNRS-MNHN-UPVD, Alliance Sorbonne Université, Musée de l'Homme, Palais de Chaillot, 17 place du Trocadéro, 75116 Paris, France

[2]Lead contact

*Correspondence: capmig@aol.com (M.C.), sandrine.prat@mnhn.fr (S.P.)

https://doi.org/10.1016/j.isci.2021.102359

Homo hypodigm, and the definition of the genus *Homo* (Antón et al., 2014; Haile-Selassie et al., 2016; Hublin, 2015; Leakey et al., 1964; Prat, 2005; Strait and Grine, 2004; Villmoare, 2018; Wood, 2014; Wood and Boyle, 2016; Wood and Collard, 1999; Wood and Lonergan, 2008). Two recent discoveries illustrate the contradictory taxonomic interpretations related to species diversity within the genus *Homo*. First, the publication of the *Homo naledi* remains (Berger et al., 2015) rekindled the questions of what constitutes this genus and from which ancestral morphotype it originates; some critics proclaiming that this new species is an example of artificial species inflation in paleoanthropology (Randolph-Quinney, 2015). Second, the discovery of early *Homo* (2.8 Ma) from Ledi-Geraru (Villmoare et al., 2015a) was the object of criticisms by competing researchers (Hawks et al., 2015; Villmoare et al., 2015b). It is clear that the use of the term "early *Homo,*" given the multiplicity of fossils it encompasses (non-*Homo erectus* specimens such as *Homo* sp. indet., *Homo habilis,* or *Homo rudolfensis*), blurs the taxonomic diversity of paleospecies belonging to this genus. In light of these two examples of diverging interpretations, some authors advocate discarding the historical constructs inherited from the Linnaean binomial classification and adopting a more rigorous approach to hominin systematics (Schwartz and Tattersall, 2015). The lack of a widely accepted comparative methodology to establish a coherent diagnosis of hominin species recognition and consensus-based definition of the genus *Homo* demonstrates that a comprehensive phylogenetic analysis to address these issues is long overdue (Strait et al., 2015).

The objective of the present study is to present a methodology combining a cladistic Maximum Parsimony (MP) protocol and a Phylogenetic Networks (PN) method applied to a comprehensive hominin dataset of craniodental characters. Our approach will aim to clarify the phylogenetic definition(s) of the genus *Homo* and test the hypothesis of phylogenetic reticulation in its mode of evolution. The methodology is described in the section experimental design of Transparent Methods, and the analytical framework is schematically summarized in Figure S1.

To carry out our study with the greatest number of hominin taxa and morphological traits, and to enable the comparison of its results with those of an alternative methodology, we selected the supermatrix assembled by Dembo et al. (2016) among large published datasets of pre-established species. This supermatrix of 391 craniodental characters was compiled by the authors from matrices used in 14 previous studies, with some alterations made to a mix of trait observations as described in their publication. They analyzed it using primarily Bayesian phylogenetic methods compared with a bootstrap MP analysis. All craniodental datasets in paleoanthropological studies are based on morphological characters observed on hominin fossils and coded subjectively by researchers. Some might consider that either the choice of characters is not adequate, or the coding might be missing, incorrect, or subject to observational biases. The dataset has a large percentage of missing data, due in part to the fragmentary nature of some specimens of the late Miocene-Pliocene paleospecies, which may have an impact on the results. However, for comparative purposes with the findings of Dembo et al. (2016) we have not made any changes to the list of characters and the coding and thus have taken the data at face value. The sample of taxa consists of two extant outgroup hominoids (*Gorilla gorilla* and *Pan troglodytes*) and the following 22 hominins covering the geological period from late Miocene to Holocene (Figure S2): *Sahelanthropus tchadensis*, *Ardipithecus ramidus, Australopithecus anamensis*, *Australopithecus afarensis*, *Australopithecus garhi*, *Kenyanthropus platyops*, *Australopithecus africanus*, *Australopithecus sediba*, *Paranthropus boisei, Paranthropus robustus*, *Paranthropus aethiopicus*, *Homo naledi*, *Homo rudolfensis, Homo habilis*, African *Homo erectus*, Georgian *Homo erectus*, Asian *Homo erectus*, *Homo floresiensis*, *Homo antecessor*, *Homo heidelbergensis, Homo neanderthalensis,* and *H. sapiens*.

With our combined MP and PN analyses, we endeavor to demonstrate the following points:

- Methodologically, MP (a non-statistical numerical method based on graph theory) has a superior phylogenetic explanatory power in the study of hominin evolution than statistical Bayesian methods.
- Resemblance not inherited from a close common ancestor, defined as homoplasy, manifests itself either by irreversible convergence-parallelism or reversal of characters. We advance the hypothesis that reversal, which is generally dismissed in evolutionary studies, plays a significant adaptive role in human evolution.
- The taxonomic definition of the genus *Homo* is a relative concept linked to the appearance and sharing of morphological novelties (apomorphies) among groups of species, and thus, rather than

one inclusive definition, researchers should take into consideration the possibility of using several definitions encompassing different hierarchical sister groups.

- The PN method shows that reticulation represents a more informative conceptual framework than anagenesis or cladogenesis to explain the phylogenetic links between the genus *Homo* species, as well as the evolutionary process that led to their diversity. Such a diversity is deemed to have arisen through speciations by introgressive hybridization during the Pleistocene.

RESULTS

Tree-based Maximum Parsimony (MP) phylogenetic analysis

MP, epistemologically associated with Phylogenetic Systematics also known as cladistics (section Foundations of the phylogenetic concept of Maximum Parsimony in Transparent Methods), is a non-statistical method of mathematical programming with optimization of an objective function subject to linear constraints (Darlu and Tassy, 2019). The objective function is to find out of millions of tree combinations, the one (unoriented graph) that maximizes the number of one-time character-state changes (apomorphies), subject to some constraints. In our analysis we take into consideration three kinds of constraints: the type of characters (Fitch, Wagner, Camin-Sokal or Dollo) determined by four models of parsimony (Transparent Methods 1); the presence of polymorphic characters in multistate taxa (Transparent Methods 2), i.e., species showing all the states for some specific characters with two possible numerical settings ("polymorphic" or "uncertain" in PAUP software); and whether characters should have the same weight or be reweighed after an initial run (Transparent Methods 3). It is essential to discard preconceived subjective biases with regard to the constraints and conduct the MP analysis with all possible numerical options available in order to objectively select the evolutionary scenario that is truly the most parsimonious, without postulating *a priori* how morphological character changes evolve, what type of multistate taxa setting to use, and whether characters should be reweighed or not.

Selection of MPMAX optimal scenario

Our MP protocol is implemented with the PAUP software (Swofford, 2020). Based on the dataset of 391 morphological characters of 22 hominin paleospecies and 2 outgroup taxa, we execute 16 MP runs by heuristic search with the four main character types, uncertainty or polymorphic setting for multistate taxa and either equally weighed or reweighed characters, and generate 16 phylogenetic MP trees (Figures S3–S6) with the main results summarized in Table 1. These MP trees represent 16 hypothetical scenarios of what hominin evolution might have been in a dichotomous phylogenetics perspective based on the dataset. To assess the branch support of each the 16 MP trees, we also show in Figures S3–S6 the bootstrap 50% majority rule consensus trees executed with the same parsimony settings.

The best available estimator of maximization of apomorphies to select the most reliable MP evolutionary scenario is the tree retention index (RI) (Transparent Methods 4). Tree run 15 executed with the Dollo parsimony model that favors reversals (with characters reweighed by the rescaled consistency (RC) index and uncertainty setting for multistate taxa) shows the highest RI = 0.8805 and is thus the most coherent and informative MP scenario (Figure S6E). We will name this scenario MPMAX (Figure 1).

In evaluating the 16 possible scenarios to select the most parsimonious one, some may object to the use of the tree RI. As an alternative, we conduct a Popperian elimination of evolutionary scenarios based on three inconsistencies (Table 2; Transparent Methods 4). Our results show that there exists a strong inverse correlation (- 0.721) between the RI of the 16 scenarios and the sum of inconsistencies, and between the RI and inconsistency 3 (- 0.715), whereas there is practically no correlation between the consistency index (CI) and the sum of inconsistencies (- 0.041) and a low negative correlation of the CI with inconsistency 3 (- 0.342). The negative correlation of the RI (the lower the sum of inconsistencies, the higher the RI, the more coherent the scenario) demonstrates that it is an informative and decisive indicator when it comes to selecting evolutionary scenarios, contrary to the CI, which shows a low discriminating value. Weighing characters with the RC index in a second set of runs results in higher RI values and is effective in identifying more coherent MP cladograms with better resolution. The Popperian elimination of attempted solutions with the least number of inconsistencies confirms the selection of the MPMAX scenario (Figures 1 and S6E) based on the use of the Dollo optimality criterion (Transparent Methods 1), with only one inconsistency related to the inverted positions in the tree of *S. tchadensis* and *Ar. ramidus*. However, this inconsistency might not be relevant in light of the suggestion by some authors (Haile-Selassie et al., 2004) that the Late

Table 1. Summary of main MP parameters of 16 evolutionary scenarios related to Figures S3–S6

Character type		Equal weight - Uncertainty					Equal weight - Polymorphism					RC weighed - Uncertainty					RC weighed - Polymorphism				
		Trees	*Steps*	*RI*	*CI*		*Trees*	*Steps*	*RI*	*CI*		*Trees*	*Steps*	*RI*	*CI*		*Trees*	*Steps*	*RI*	*CI*	
Fitch parsimony (unordered)	**R1**	8	796	0.6035	0.5741	**R2**	8	1425	0.6016	0.7628	**R3**	1	308.86	0.8316	0.8061	**R4**	1	230.78	0.8409	0.8406	
Wagner parsimony (ordered)	**R5**	3	859	0.6062	0.5425	**R6**	3	1506	0.6046	0.7397	**R7**	1	298.4	0.8347	0.7826	**R8**	1	224.02	0.8364	0.8049	
Camin-Sokal parsimony (convergence)	**R9**	6	1093	0.689	0.4263	**R10**	1	1941	0.6309	0.5892	**R11**	1	309.12	0.8463	0.6397	**R12**	1	232.97	0.7936	0.6158	
Dollo parsimony (reversal)	**R13**	2	1021	0.7158	0.4564	**R14**	1	1930	0.6431	0.5843	**R15**	1	334.61	0.8805	0.7085	**R16**	1	267.17	0.8406	0.6871	

Run numbers corresponding to the character types with equal weight-reweigh and multistate taxa settings are highlighted in bold. The parameters are: the number of most parsimonious trees resulting from each run, the corresponding number of steps (character changes on the tree), and their tree retention index RI and consistency index CI.

Miocene hominin fossils do not represent three separate genera (*Ardipithecus*, *Orrorin*, and *Sahelanthropus*), but only one genus with specific or sub-specific variation within the group, although some authors suggest that *Ar. ramidus* is more derived relative to *Sahelanthropus* (Mongle et al., 2019).

In summary, we show here (Figure 1) that (1) sister group D = (H, (G, F)) = (Hab, (Her, PreHs)) corresponds to genus *Homo sensu lato* (sl); (2) sister group E = (G, F) = (Her, PreHs) concords with the recommendation to exclude *H. rudolfensis* and *H. habilis* from the genus *Homo* (Wood and Collard, 1999), and is thus recognized as genus *Homo sensu stricto* (ss); and (3) the extended monophyletic group C = (I, (H, (G, F))) = (NalSed, (Hab, (Her, PreHs))) that includes *H. naledi* and *Au. sediba* (Berger et al., 2010) could tentatively be called genus *Homo sensu amplo* (sa).

Comparative validation of MPMAX optimal scenario

In order to validate the MPMAX scenario, we compare it with the results of a Bayesian inference-based Markov chain Monte Carlo (BMCMC) analysis with the same dataset (Dembo et al., 2016). We call the tree from Figure 2 of this study, the BMCMC Dembo tree, and compare the proportions of bootstrap replicates P_{boot} of the MPMAX bootstrap tree (Figure S6F) to the posterior probability values P_{post} of the BMCMC Dembo tree on the basis of their equivalence (Transparent Methods 5). We use an elliptic graphical representation for the comparative analysis (Hennig, 1966, Figure 18, p.71). For illustrative purposes, we highlight in Figure S7 the similarities between the elliptic representation and the MP cladogram of Figure 1.

With the exception of the inverted topological position of *S. tchadensis* and *Ar. ramidus*, and considering the previously mentioned non-diagnostic morphological and chronological caveat (Haile-Selassie et al., 2004), the phylogenetic sections comprising the outgroup *G. gorilla* and *P. troglodytes*, and the taxa *Au. anamensis*, *Au. afarensis*, *Au. garhi*, and *K. platyops*, are identical in the MPMAX and BMCMC Dembo trees; consequently, the comparison (Figure 2) is applied to the remaining 16 Pleistocene terminal taxa, and both tree phylogenies are reproduced partially in a modified graphical elliptic manner. The elliptic boundaries of MPMAX scenario (Figure 2A) corresponding to the nodes of the MP tree (Figure 1) are deemed to represent phylogenetically the Last Common Ancestors (LCAs).

Elliptic boundary A in the MPMAX scenario (Figure 2A) with bootstrap support 46 is the LCA of the *Au. africanus*, *Paranthropus*, and *Homo* lineages, whereas boundary B with support 52 is the stem lineage that gave rise to the *Paranthropus* and *Homo* sister groups. This supports the hypothesis that the *Paranthropus* genus (Par) belongs to a separate and distinct evolutionary lineage from the upstream *Australopithecus* genus, sharing a common ancestor with the genus *Homo* and possibly concomitant chronologically with

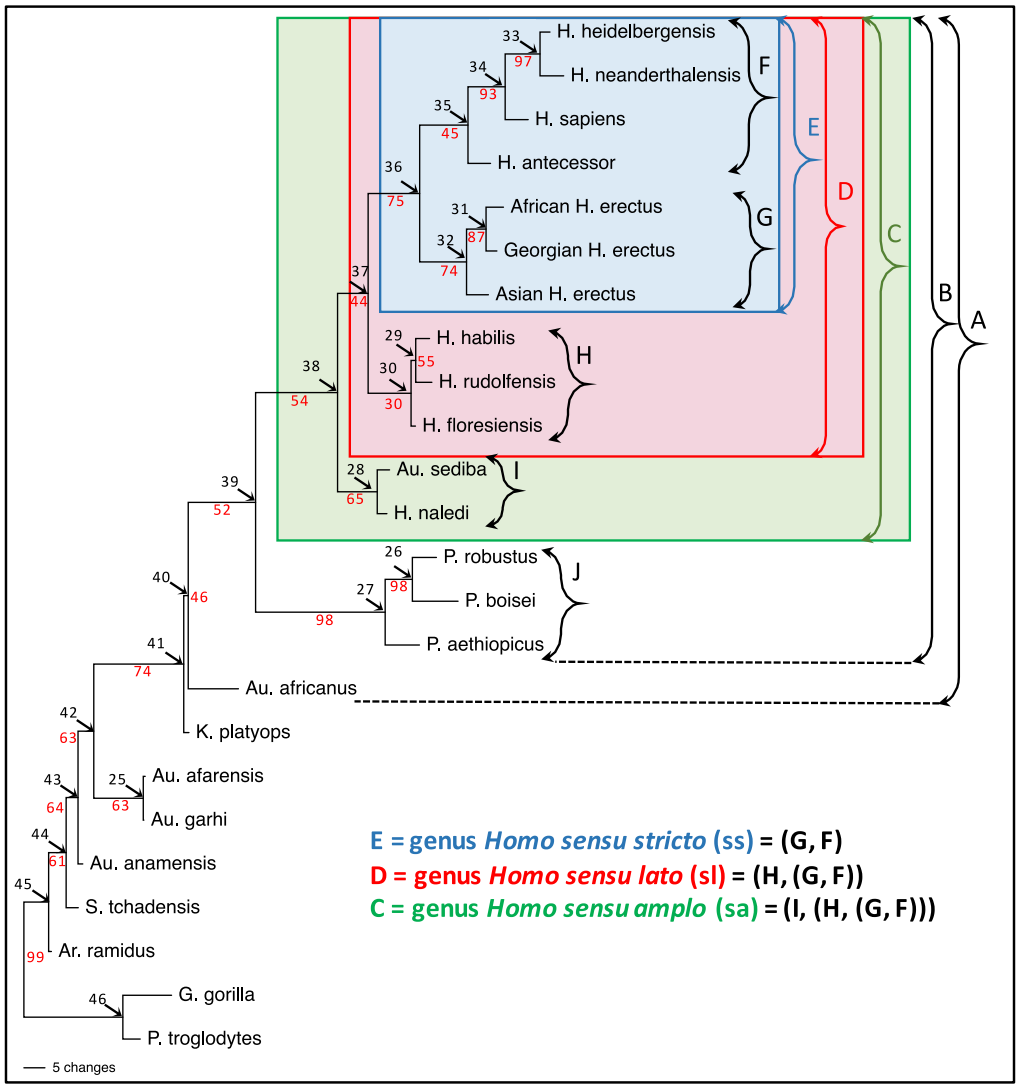

Figure 1. MPMAX scenario

MP tree of run 15 executed with the PAUP software (Figures S6E) with Dollo parsimony characters reweighed by the RC and uncertainty setting for multistate taxa. The 50% majority-rule bootstrap replicate values of the structurally identical bootstrap tree with same settings (Figure S6F) are indicated in red. Node numbers representing hypothetical ancestors are indicated by arrows. Pleistocene sister groups are indicated in capital letters and are attributed coded labels for ease of discussion in the text. All terminal taxa are also given a coded label. We identify five highly resolved Pleistocene monophyletic sister groups:

F = (((*Homo heidelbergensis*, *Homo neanderthalensis*), *H. sapiens*), *Homo* antecessor) = (((*Hhei*, *Hnea*), *Hsap*), *Hant*) = PreHs

G = ((African *Homo erectus*, Georgian *Homo erectus*), Asian *Homo erectus*) = ((*AfHer*, *GeoHer*), *AsHer*) = Her

H = ((*Homo rudolfensis*, *Homo habilis*), *Homo floresiensis*) = ((*Hrud*, *Hhab*), *Hflo*) = Hab

I = (*Homo naledi*, *Australopithecus sediba*) = (*Hnal*, *Ased*) = NalSed

J = ((*Paranthropus boisei*, *Paranthropus robustus*), *Paranthropus aethiopicus*) = ((*Pboi*, *Prob*), *Paet*) = Par

and recognize five higher monophyletic sister groups:

E = (G, F) = (Her, PreHs), D = (H,E) = (H, (G, F)) = (Hab, (Her, PreHs)), C = (I,D) = (I, (H, (G, F))) = (NalSed, (Hab, (Her, PreHs))), B = (J,C) = (J, (I, (H, (G, F)))) = (Par, (NalSed, (Hab, (Her, PreHs)))), A = (*Australopithecus africanus*, B) = (Auaf, (J, (I, (H, (G, F))))) = (Auaf, (Par, (NalSed, (Hab, (Her, PreHs)))))

Six other late Miocene - Pliocene paleospecies are also recognized: *Ardipithecus ramidus* (*Arram*), *Salehantropus tchadensis* (*Stchad*), *Australopithecus anamensis* (*Auana*), *Australopithecus afarensis* (*Auafar*), *Australopithecus garhi* (*Augar*), and *Kenyanthropus* platyops (*Kplat*).

Table 2. Inconsistencies for the Popperian elimination of evolutionary scenarios

Parsimony scenario	Inconsistency 1 Chronological order satisfied in bootstrap tree			Inconsistency 2 Presence of clade ((*H. heid, H. neand*), *H. sap*)	Inconsistency 3 Bootstrap support # Clades <20%	Sum of inconsistencies	CI	RI
	S. tchadensis	*K. platyops*	*Au. africanus*					
Run 1 Fitch equal weight - Uncertainty	1	1	1	0	3	6	0.57	0.60
Run 2 Fitch equal weight - Polymorphism	1	1	1	0	2	5	0.76	0.60
Run 3 Fitch RC weighed - Uncertainty	1	1	1	1	0	4	0.81	0.83
Run 4 Fitch RC weighed - Polymorphism	1	1	1	1	0	4	0.84	0.84
Run 5 Wagner equal weight - Uncertainty	1	1	1	1	2	6	0.54	0.61
Run 6 Wagner equal weight - Polymorphism	1	1	1	1	4	8	0.74	0.60
Run 7 Wagner RC weighed - Uncertainty	1	1	1	1	0	4	0.78	0.83
Run 8 Wagner RC weighed - Polymorphism	1	1	1	1	0	4	0.80	0.84
Run 9 Camin-Sokal equal weight - Uncertainty	0	1	0	0	2	3	0.43	0.69
Run 10 Camin-Sokal equal weight - Polymorphism	0	1	1	0	8	10	0.59	0.63
Run 11 Camin-Sokal RC weighed - Uncertainty	0	1	1	0	0	2	0.64	0.85
Run 12 Camin-Sokal RC weighed - Polymorphism	0	1	1	0	0	2	0.62	0.79
Run 13 Dollo equal weight - Uncertainty	1	1	0	0	1	3	0.46	0.72
Run 14 Dollo equal weight - Polymorphism	1	1	1	0	3	6	0.58	0.64
Run 15 Dollo RC weighed - Uncertainty MPMAX	1	0	0	0	0	1	0.71	0.88
Run 16 Dollo RC weighed - Polymorphism	1	1	0	0	2	4	0.69	0.84

The list of inconsistencies based on 16 MP bootstrap trees (Figures S3–S6) is determined according to the following criteria: (1) chronological placement of *S. tchadensis*, *K. platyops*, and *Au. africanus* (1 = out of order chronologically, 0 = consistent chronologically); (2) presence of clade ((*H. heidelbergensis, H. neanderthalensis*), *H. sapiens*) (1 = no presence of clade, 0 = presence of clade); and (3) number of branches with bootstrap support values of less than 20%.

Correlations: RI versus Sum of Inconsistencies = −0.721, RI versus Inconsistency 3 = −0.715, CI versus Sum of Inconsistencies = −0.041, CI versus Inconsistency 3 = -0.342.

the speciation events that gave rise to both lineages (Strait et al., 1997). Although the *Paranthropus* clade J = Par has an equivalent support in both representations (98 & 99), the BMCMC Dembo scenario (Figure 2B) shows a different relationship with *Au. africanus*, closely related only to the *Paranthropus* group with a lower support of 38.

We observe in the MPMAX scenario a clear phylogenetic association between *H. naledi* and *Au. sediba* supported by an appreciable bootstrap value of 65, and the clade of both terminals NalSed has an intermediate position between the upstream *Australopithecus* and *Paranthropus* sister groups, and the downstream *Homo* sister groups, which begs the question whether these two paleospecies belong to the genus

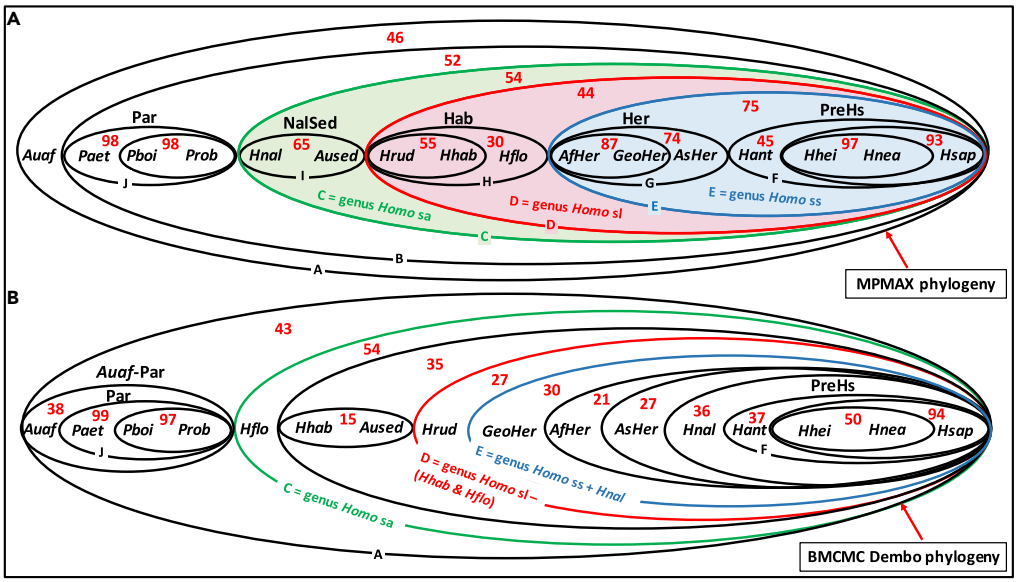

Figure 2. Phylogenetic support comparison illustrated with elliptic graphic representation of MPMAX scenario and the best BMCMC Dembo scenario based on 16 Pleistocene terminal taxa

(A) MPMAX bootstrap elliptic representation with replicate P_{boot} values from Figure S6F.

(B) BMCMC Dembo elliptic representation with posterior probability values P_{post}.

P_{boot} and P_{post} are shown in red and expressed in %. Refer to the legend of Figure 1 for sister group definitions.

Homo. We also observe in the 16 executed MP and bootstrap runs that *H. naledi* and *Au. sediba* systematically share a close common ancestor (Figures S3–S6; Table S4). Dembo et al., (2016) ran a MP bootstrap analysis with a dataset split of 288 unordered characters and 103 ordered characters (Figure S7 of their Supplementary Online Material [SOM]). For comparative purposes, we applied our MP protocol to their data split; the results of the 4 MP runs (equal weight and RC reweighing with uncertainty or polymorphism setting for multistate taxa) and the corresponding bootstrap runs executed with this mix are shown in Figure S11. The bootstrap run with equal character weights and uncertainty setting for multistate taxa (Figure S11B) produces a consensus tree that is topographically identical to the tree of Dembo et al., (2016) (Figure S7 of their SOM) with the slight difference of *Au. sediba* and *H. naledi* shown as a sister group instead of successive terminals. We also applied the Popperian elimination of evolutionary scenarios protocol using the bootstrap consensus trees of Figures S11B, S11C, S11E, and S11G, with the results shown in Table S5. Compared with the MPMAX scenario that shows the highest tree RI of 0.8805 (Table 1) and only one inconsistency (Table 2), all the Dembo scenarios with the split character dataset are phylogenetically suboptimal and clearly not as coherent and informative as evidenced by their MP tree RIs (Figure S11) and their number of Popperian elimination inconsistencies (Table S5). As a matter of fact, in Dembo et al. (2016) the results of two Bayes factor tests used to evaluate the strength of support concerning the hypothesis of which clade *H. naledi* is nested in show that the best model evidence is: *H. naledi* forms a sister taxon to *Au. sediba* and no other members of the genus *Homo*, and is nested in the clade of *Homo* + *Au. sediba*. These tests come in contradiction to the positions reflected in BMCMC Dembo scenario where *Au. sediba* forms a sister taxon with *H. habilis* with very low support (15), whereas *H. naledi* is nested away with the clade F = PreHs also with low support of 36. However, these tests are in accord with the MPMAX scenario where *H. naledi* forms a clade I = NalSed with *Au. sediba*, and together represents a sister group of the higher order monophyletic group D, taxonomically defined as *Homo* genus *sensu lato* (sl).

In MPMAX, the H = Hab group has a low support 30 reflecting the tenuous association of *H. floresiensis* within this group, which might favor the exclusion of this clade from the genus *Homo* (Collard and Wood, 2015), despite the slightly higher support 55 of the (*H. rudolfensis, H. habilis*) clade. These three species are dispersed in three successive clades in BMCMC Dembo with the higher clade including *H. habilis* showing a low support of 35 and the one including *H. rudolfensis* showing a lower support of 27.

The sister group E (genus *Homo sensu stricto*) in MPMAX is highly supported and cohesive with a bootstrap value of 75, and within it the *H. erectus* sister group G shows significant support of 74, with high support of 87 for the clade (African *H. erectus*, Georgian *H. erectus*). In BMCMC Dembo the three geographical *H. erectus* species belong successively to 3 separate sister groups with, respectively, very low support of 30, 21, and 27. F = PreHs, the other sister group within E in MPMAX shows a low support value of 45 due probably to the presence of *H. antecessor*. In BMCMC Dembo scenario, *H. antecessor*, although in the same position in the PreHS group, has a lower support of 37. In MPMAX the clade (*H. heidelbergensis, H. neanderthalensis*) has a robust 97 support when compared with a substantially lower support of 50 in BMCMC Dembo.

The comparison of both phylogenies shows that the MPMAX scenario (Figure 2A) has a systematically higher support than the Bayesian BMCMC Dembo scenario (Figure 2B) in practically all the sister groups, and a clearer and higher resolution concordant, we believe, with generally accepted paleoanthropological paradigms. Thus the bootstrap tree (Figure S6F), topographically identical to the MP tree (Figure S6E) with the same settings (Dollo parsimony characters, uncertainty for multistate taxa, and RC reweighed characters), validates the most phylogenetically informative and coherent MPMAX evolutionary scenario (Figure 1).

Contrary to probability based methods of phylogeny reconstruction, MP identifies clearly the character-state changes that support the various clades. For illustrative purposes, we show in supplemental information the 74 apomorphies in support of the LCAs. These apomorphies are identified from the MPMAX run output with character RI = 1 (Transparent Methods 6; Figure S8; Table S1) and are listed in Table S2. In Figure S9 we show the apomorphies in support of the LCA elliptic boundaries of Figure 2A; most of them are unambiguous, which explains in part the higher resolution and coherence of this part of the phylogeny. In Figure S10 we highlight the apomorphies in support of the late Miocene-Pliocene species groups up to *K. platyops* of MPMAX (nodes/elliptic boundaries 46 to 41); these are ambiguous in their majority (Transparent Methods 7), i.e., of uncertain sister group attribution.

Intermediate step from MP protocol to PN method

Could the sequential hierarchical order of the various *Homo* sister groups C, D, and E in the MPMAX scenario (Figure 1) be indicative of a process of reticulate evolution in the genus *Homo*? Before answering this question, we need to verify the phylogenetic signal related to the taxonomic threshold between the genus *Homo* and other hominin sister groups.

The fundamental principle of Phylogenetic Systematics is that the hierarchical evolutionary history of taxa is reconstituted from characters by the sharing of apomorphies, whereas homoplasies, resemblance not due to inheritance from a recent common ancestor, represent features of an adaptive nature that are less phylogenetically informative. In keeping with this principle, we re-run the analysis with the 74 apomorphous characters from the MPMAX scenario (Table S2), with the Dollo type algorithm and uncertainty setting for multistate taxa. There is no need to reweigh because all characters have an RI = 1 and CI = 1 and the RC = RI × CI = 1 is identical to the original equal weights. The run generates a set of 3,211 MP trees, which we call MMPT (multiple most parsimonious trees), with perfect tree congruence indices RI = 1 and CI = 1. The 50% majority consensus tree of MMPT is shown in Figure 3A. For comparative purposes we also run the MP analysis based on 74 apomorphous characters with the other character types (Fitch, Wagner, and Camin-Sokal) and same settings. The equal weight Fitch, Wagner, and Dollo runs result in a similar 50% majority consensus tree (Figure 3A) with RI = 1 and CI = 1. The Camin-Sokal algorithm shows a closely similar topology (Figure 3B) but with slightly lower consistency scores after RC reweighing; the main difference with Figure 3A is *H. rudolfensis* associated with the *H. erectus* group instead of being in a polytomy. The fact that for three algorithms the tree RI = CI = 1 is proof that the selection of apomorphies by the character RI = 1 is effective and robust.

In the analysis runs with the full dataset, homoplasies generate a background noise that varies depending on the algorithmic constraints used (character type, multistate taxa, and weighing/reweighing) and is related to the tree topographies. We define this background noise as the difference between the best RI from the run with 74 apomorphies having a value = 1 (Figure 3A) and the tree RI with value <1 from an analysis run with 391 characters (Table 1); in short, the background noise of a run with the full dataset is (1 - RI). Conceptually, it represents the contribution of the 317 homoplastic characters to the diminution

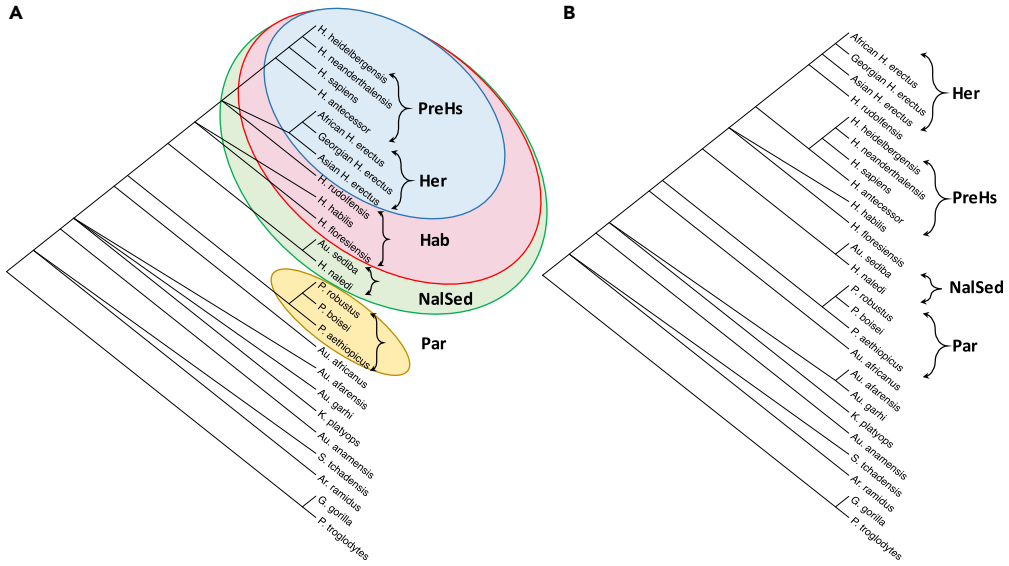

Figure 3. 50% Majority consensus MP trees from PAUP analysis run with dataset of 74 apomorphies selected from MPMAX scenario

Runs were executed with the four character types and uncertainty setting for multistate taxa.

(A) Identical consensus tree of 3,211 MP Fitch trees (95 steps), 3,057 MP Wagner trees (96 steps), and 3,213 Dollo MP trees (96 steps) with RI = 1 and CI = 1 for all the trees.

(B) Consensus tree of 609 MP Camin-Sokal trees based on RC reweighed characters (91.42 steps) with RI = 0.9862 and CI = 0.9401.

of the RI between the two types of analyses. A perfect tree RI = 1 means that phylogenetically there is no noise in the run with the reduced apomorphy dataset, whereas there is noise with the runs executed with the full dataset, and the MPMAX R15 scenario is the one with the least noise. As in the present study, it has been observed that more polytomies become apparent when the number of homoplastic characters describing the taxa decreases and the number of most parsimonious trees increases substantially (Caparros, 1997). Polytomies are thought to be generally uninformative, but they will result in being of utmost importance in the PN analysis, i.e., neutralizing the background noise will allow to conduct the PN analysis.

Polytomies are prevalent among late Miocene-Pliocene hominin species upstream from *Au. africanus* in both consensus trees because most of the apomorphous character-state changes in that part of the tree are ambiguous with uncertain assignments (Figure S10), and to the many missing characters that contribute to the multiplication of trees of minimal length. This group could be split possibly into two sub-groups (*S. tchadensis/Ar. ramidus*) and (*K. platyops/Au. garhi/Au. afarensis*), with *Au. anamensis* and *Au. africanus* in intermediate positions. The characters of the dataset are not sufficiently informative to discriminate more precisely among these taxa. On the other hand, as in MPMAX (Figure 1) we observe the appearance of recurrent and very stable sister groups across the four MP character type runs (Fitch, Wagner, Camin-Sokal, or Dollo) with the dataset of 74 apomorphies, such as PreHs = (((*H. heidelbergensis, H. neanderthalensis*), *H. sapiens*), *H. antecessor*), Her = ((African *H. erectus*, Georgian *H. erectus*), Asian *H. erectus*)), NalSed = (*H. naledi*, *Au. sediba*), and Par = ((*P. boisei, P. robustus*), *P. aethiopicus*). The Hab group is now split in two, with on one hand the polytomy (*H. naledi/H. floresiensis*) and on the other *H. rudolfensis* in a polytomy itself with (PreHs, Her) in Figure 3A or as a sister taxon of the Her group in Figure 3B. Given that the consensus tree of Figure 3A has the highest tree score R = 1, we may infer that *H. rudolfensis* is more closely linked to (PreHs, Her) than *H. habilis* as proposed by Leakey et al. (2012). The MP analysis with 74 apomorphies would indicate that the evolutionary topography of Figure 1 downstream of *Au. africanus* provides a highly informative and coherent phylogenetic signal. This signal confirms the hierarchical order of 3 sister groups (PreHS = F, Her = G and NalSed = I) within the genus *Homo sensu amplo* definition of the MPMAX scenario (Figure 1) regardless of the constraints used, with, however, some uncertainty in the sister group Hab = H given its polytomous nature. This represents, we believe, a significant paleoanthropological

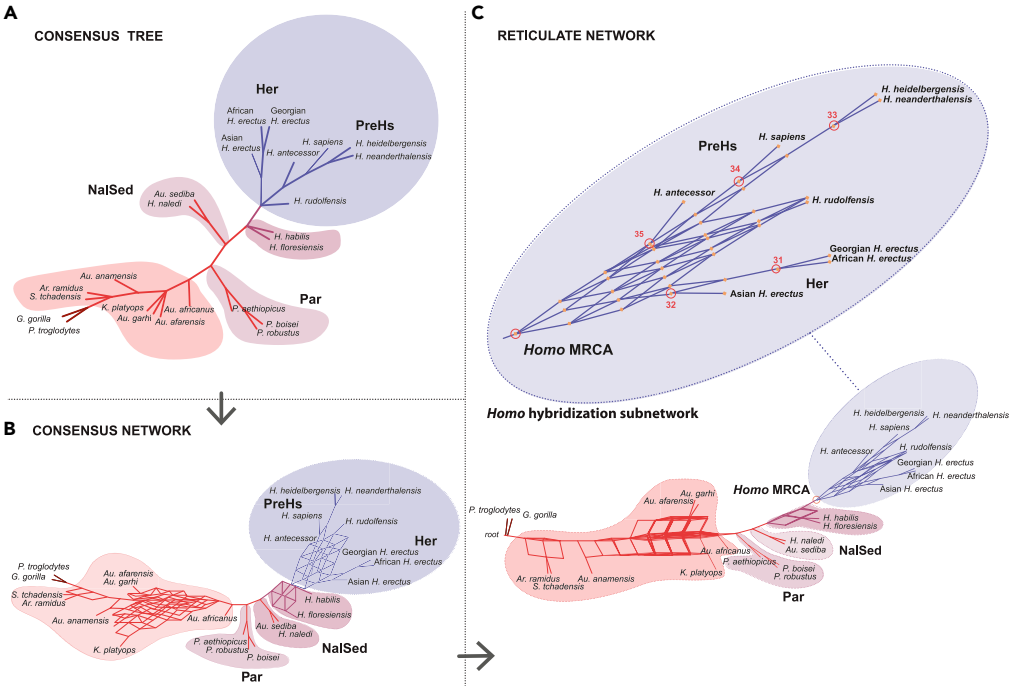

Figure 4. Phylogenetic Networks graphical results

Figure360▷ For a Figure360 author presentation of this figure, see https://doi.org/10.1016/j.isci.2021.102359.

Tree and network computations were executed with the program SplitsTree (Huson and Bryant, 2006) with input of 3,213 trees (MMPT) from Dollo parsimony run with 74 apomorphous characters. These apomorphies were selected based on their character RI = 1 from the output (Table S1) of the MPMAX run with the full dataset.

(A) Unrooted majority consensus tree with mean edge weights (pipeline Taxa = 24 [Trees > ConsensusTree > EqualAngle]).

(B) Consensus network computed with threshold = 0.10, mean edge weights, and splits convex hull transformation (pipeline Taxa = 24 [Trees > ConsensusNetwork > ConvexHull]).

(C) Rooted reticulate network with first taxon as outgroup and 180 equal angle (pipeline Taxa = 24 [Trees > ConsensusNetwork > ReticulateNetwork]).

finding, particularly as it relates to the much debated phylogenetic positions of *H. naledi* and *Au. sediba*. The question remains whether this tree-based analysis is indicative of a process of reticulation?

To shed some further light on the taxonomic threshold between the genus *Homo* and other hominin sister groups, we test the hypothesis of phenotypic hominin evolutionary reticulation by using a PN conceptual approach extensively employed in molecular biology (section Phylogenetic Networks in Transparent Methods; Huson et al., 2010; Morrison, 2011). To establish a link between the PN analysis and the MP analysis with 74 apomorphous characters, we make two empirical assumptions: (1) apomorphous character-state changes represent analogous proxies of gene sequence changes evolving from common ancestors and (2) the 3,213 MP trees (MMPT) resulting from the Dollo parsimony PAUP run with 74 apomorphies are methodologically analogous to gene trees from a set of species, and are thus used as input in the PN analysis.

Phylogenetic Networks (PN) analysis

We use the SplitsTree software (Huson and Bryant, 2006) to compute the majority consensus tree, consensus network, and reticulate network based on the MMPT dataset. Common combinations of sister groups sharing homologous characters are displayed in the unrooted majority consensus tree (Figure 4A), which is topographically equivalent to the one of Figure 3A, i.e., well-supported dichotomous branches PreHs (F), Her (G), NalSed (I), and Par (J) are identified, whereas the least-supported groups are identically expressed as polytomies. The conflicting data patterns of polytomies are highlighted in the consensus network (Figure 4B) by means of parallelograms, with high intensity in the group up to *Au. africanus*

correlating with a high number of incompatibilities essentially due to a substantial proportion of ambiguous characters difficult to position at the nodes, and missing data.

In the reticulate network (Figure 4C) we observe three evolutionary patterns. First, there is no evidence of tree-like or web-like ancestral relationships among the two groups (*S. tchadensis-Ar. ramidus*, *Au. anamensis*) and (*Au. garhi, Au. afarensis, K. platyops*), but a chronological punctuated succession of taxa that eventually would give rise to the emergence of *Au. africanus* shown here as an isolated single edge (White et al., 2015). The conflicting character incompatibilities, low discriminating power of the state changes, and uncertain direction of character transformations of these variable morphoclines may be interpreted as the expression of evolutionary adaptive events that would favor the classification of anagenetic grade instead of clade for these hominin taxa. Second, the side-edges Par = (*P. aethiopicus,* (*P. boisei, P. robustus*)), NalSed = (*H. naledi, Au. sediba*) and (*H. habilis, H. floresiensis*) represent probable phylogenetic divergences that might be construed as evolutionary dead-ends, eventually becoming extinct without contributing meaningfully to the lineages of the upstream *Homo* web-like subnetwork, as suggested for *Au. sediba* (Du and Alemseged, 2019). The recent discovery of *Homo luzonensis* (Détroit et al., 2019), showing mosaic dental and postcranial morphological features shared with *Homo* species and *Australopithecus*, would suggest also a probable dead-end trajectory without evolutionary continuity as is the case with *H. floresiensis*. Third, the end-part of the network with the most recent common ancestor (*Homo* MRCA) shows a clear reticulate radiative structure encompassing sister group E, genus *Homo sensu stricto* (Figures 1 and 2A), plus *H. rudolfensis*; we call it the *Homo* hybridization subnetwork. After three successive events (edges), the network splits into two clades Her and PreHs with their own LCA nodes of origin 32 and 35, in parallel with the leaf *H. rudolfensis*. The association of *H. rudolfensis* with the *Homo sensu stricto* group would seem to confirm its phylogenetic position as an early taxon closely related to the genus *Homo*, and separate from *H. habilis* shown here as an edge outside the *Homo* hybridization subnetwork (Leakey et al., 2012). The *H. erectus* sister group (Her) is coherent (Antón et al., 2014; Lordkipanidze et al., 2013), whereas *H. antecessor* is correctly linked within the sister group (((*H. heidelbergensis, H. neanderthalensis*), *H. sapiens*), *Homo antecessor*) rather than the *H. erectus* group (Bermúdez de Castro et al., 2017), and the splits ((*H. heidelbergensis*, *H. neanderthalensis*), *H. sapiens*) indicates accurately an early genetic divergence of *H. sapiens* and *H. neanderthalensis* (Mendez et al., 2016), also corroborated by dental evolutionary rates (Gómez-Robles, 2019). We must stress that in SplitsTree runs conducted with input MP trees obtained from the Wagner and Fitch PAUP analysis with 74 apomorphous characters, the subnetwork distribution of the taxa remains the same and so does the position of *H. rudolfensis*. The *Homo* MRCA rooted subnetwork may be considered as the expression of reticulate evolutionary processes with apomorphous novelties evolving along the network edges, and experiencing one-time changes along the path. Based on the commonly used PN definitions (internal nodes are ancestors, edges represent evolutionary events, nodes of in-degree 1 and out-degree of at least 2 represent genetic divergences, and nodes of in-degree > 1 show pooling of genetic material), we infer that the phylogenetic events that generated the terminal taxa of the MRCA rooted group may represent probable biological mechanisms of reticulate hybridization in the genus *Homo*, possibly resulting at times in speciation by introgression (Arnold, 2006).

A short video (Figure360) illustrating the significance of Figure 4 is provided in supplemental information.

DISCUSSION

Comparative suitability of Maximum Parsimony (MP) versus Bayesian inference-based Markov chain Monte Carlo methods (BMCMC)

MP is the most commonly used method of phylogenetic reconstruction in paleoanthropology (Strait et al., 2015). It is associated with Phylogenetic Systematics (section Foundations of the phylogenetic concept of MP in Transparent Methods), otherwise called cladistics, the school of thoughts in taxonomy that conceptually allows the identification and numerical classification of extant or fossil biological organisms, and to draw inferences about their evolutionary history (Hennig, 1966). Methods of phylogeny reconstruction can be divided into statistical methods requiring an explicit model of evolution, such as Bayesian phylogenetic Markov chain Monte Carlo methods (BMCMC) used by Dembo et al. (2016), and non-statistical methods such as MP used in the present study that do not require a model of evolution (Goloboff and Pol, 2005).

Dembo et al. (2016) highlight three major differences between MP and BMCMC to make phylogenetic inferences:

1. BMCMC requires one explicit model of character-state change for all characters, whereas with MP each character evolves with distinct evolutionary processes and rates of change.
2. Geological chronology can be used in the Bayesian framework to infer the expected amount of change leading to dated taxa, whereas with MP, geological dates can only be used *a posteriori* by comparing the tree to the stratigraphic record.
3. In the Bayesian approach, trees are assessed and compared based on their posterior probability of being true given the data and the assumptions of the evolutionary model, with preference of trees of higher probability, whereas MP relies on a single number, the minimization of the number of character-state changes appearing on the tree as reflected by the tree RI.

To support the assertion that BMCMC allows the testing of phylogenetic hypotheses with statistical rigor, and is more suitable than MP, Dembo et al. (2016) refer to a simulation study (Wright and Hillis, 2014), which supposedly shows that the Bayesian phylogenetic approach outperforms MP when applied to discrete characters evolving at a high rate; however, Figure 3 of Wright and Hillis study shows that although the BMCMC model performs better (less error) than MP at high evolutionary rates, the two methods do not differ at middle rates or low rates. As the real evolutionary rates of characters that have an incidence on the level of homoplasy are unknown, the supposedly superior statistical attraction of the BMCMC method remains uncertain. BMCMC assumes that each character follows an identical statistical distribution while MP posits that each character follows its own rate of change along every branch of the tree in a heterogeneous manner; MP is more in agreement with evolutionary theory (Wright, 1982) than BMCMC with regard to the assumption of different character evolutionary rates. The suggestion that Bayesian analysis is more reliable than MP analysis is not corroborated by another simulation study showing that when rates at which genetic sequences differ over time (heterogeneity), BMCMC can become strongly biased and inconsistent, whereas MP performs substantially better, even under moderate heterogeneity (Kolaczkowski and Thornton, 2004). Doubts have been expressed as to whether phylogeny reconstruction ought to be considered as a statistical question, with the suggestion that phylogenetic inference is best viewed in non-statistical terms: "the statistical approach to phylogenetic inference was wrong from the start, for it rests on the idea that to study phylogeny at all, one must first know in great detail how evolution has proceeded. That cannot very well be the way in which scientific knowledge is obtained … Phylogenetic analysis is necessarily based on parsimony, both because it is precisely that criterion that leads to grouping according to putative synapomorphy and because empirical investigation is impossible without avoiding ad hoc hypotheses" (Farris, 1983).

In light of the contrary views concerning the adequacy of MP or BMCMC to make phylogenetic inferences, caution must be exercised with regard to the question of statistical consistency, the complexity and empirical basis of the evolutionary models used, and what epistemological considerations support the use of specific models of evolution. In studies of phylogenetic reconstruction both the non-statistical method such as MP and the statistical ones, such as BMCMC and bootstrap analysis, ought to be used and compared for a better interpretation of the data. Here we show that the MP executed MPMAX scenario, confirmed by a bootstrap resampling run (Figure 2A), has systematically a higher phylogenetic support than the Bayesian BMCMC Dembo scenario (Figure 2B), with an informative topographic species distribution in accord with a significant number of accepted paleoanthropological paradigms as indicated below.

Considerations on evolutionary reversal

The MPMAX tree (Figure 1) was obtained from the numerical search with the Dollo character state optimality criterion where homoplasies are explained by reversal to the ancestral plesiomorphic state as opposed to the Camin-Sokal model of irreversible convergent evolution (Transparent Methods 1). Hall (2003) defines reversal as "a feature that is phenotypically similar to a feature in earlier members within a lineage, not present continuously in the lineage but present in all members of a later species" and specify that "the term reversal thus applies to a phenotype arising in a descendant from a developmental program retained from an ancestor but not expressed in intervening taxa." The expression "Dollo parsimony" should not be confused with "Dollo's law" (Dollo, 1893), which stipulates that reversal to the ancestral state is impossible. In fact, the parsimony model that follows "Dollo's law" is the Camin-Sokal parsimony model. Referring to Dollo's Law, Simpson (1953), a major contributor to the neo-Darwinian modern synthesis, expressed what would become the prevailing view among evolutionary biologists: "The statistical probability of a complete

reversal or of essential reversal to a very remote condition is extremely small …. ….Evolution is irreversible because it results from its own past and its past is irrevocable." Later on Simpson (1961) did not refer at all to reversal as a mode of homoplasy, whereas Hennig (1966), founder of the phylogenetic systematics school of thought, kept an open mind stating "the possibility that characters that have disappeared may reappear again is probably often underestimated." The uncompromising position of the neo-Darwinians seems to be at odds with the observations of Darwin who bred domestic pigeons. Referring to the coloring of pigeons and in light of the reappearances of various colors in some breeds, Darwin (1859, p. 25) concluded that: "We can understand these facts, on the well-known principle of reversion to ancestral characters, if all the domestic breeds have descended from the rock-pigeon." The prevailing view of Dollo's law of irreversibility in evolution has been challenged and occurrences of trait loss and reversal across many levels of biological entities have been identified (Hall, 2003, 2007), while incidentally it has been shown that methodologically removing convergence-prone characters improves phylogenetic accuracy (Zou and Zhang, 2016). A review of various phylogenetic studies demonstrates that complex features, such as digits in lizards and wings in insects, have been reacquired due to the retention of the underlying developmental pathways and genetic architecture within time periods of several million years, and that there is a distinction between the loss (re-evolution) of characters and the reversal of character states (Collin and Miglietta, 2008). The re-evolution of lost mandibular teeth in frogs and the mechanism that may facilitate trait re-evolution is unequivocably documented (Wiens, 2011). Various studies examining the genotypes and phenotypes in reverse suggest that one of the most important factors of reversibility is the environment's effect on interaction of traits and their underlying genetic background (Porter and Crandall, 2003). More relevant to the present MP analysis are studies of muscle reversion in primate phylogeny, with myology-based cladistic analyses highlighting the importance of evolutionary reversions in the morphological evolution of primate clades and providing examples of reversions that violate Dollo's law due to the retention of ancestral developmental pathways (Diogo and Wood, 2012, 2013). An example of possible reversal in paleoanthropology is linked to the derived maxillary developmental pattern of the immature ATD6-69 *H. antecessor* fossil showing some affinity with *H. sapiens*. This would imply that deriving the Sima de los Huesos and Neanderthal facial morphologies from that of the *H. antecessor* child would demand evolutionary reversals in their ontogeny (Stringer, 2016). The most coherent results emanating from the application of the Dollo parsimony optimality criterion demonstrates that empirically the choice of an MP model should not be based *a priori* on a postulate of how evolution proceeds, but rather on the algorithm that fits the data in the most consistent explanatory manner. Convergence or parallelism are the most common explanations used to substantiate the appearance of similar morphological features in distantly related species, whereas reversal as an adaptive evolutionary explanation seems to be generally dismissed (Morris, 2010). In light of the results of the present study and the fact that the prevailing view of irreversibility in evolution has been challenged, we encourage researchers in human evolution to pay more attention to occurrences of trait loss and reversal in the hominin fossil record.

Taxonomic definition of the genus *Homo*

We addressed first the issues of number of species within the *Homo* hypodigm, their relatedness. and the definition of the genus *Homo* with an MP protocol. Based on the complete dataset of pre-established species with 391 features, the MP analysis allowed us to identify three hypothetical genus *Homo* phylogenetic definitions from the MPMAX scenario (Figure 1), well supported by bootstrap replicate values (Figure 2A), as follows: genus *Homo sensu lato* = D that includes among others *H. rudolfensis* and *H. habilis*, genus *Homo sensu stricto* = E that excludes them, and a broader definition including *H. naledi* and *Au. sediba* we call genus *Homo sensu amplo* = C. Furthermore, regardless of the constraints used in the prior analysis (character types, multistate taxa settings, and reweighing of characters or not), the MP runs with 74 apomorphous characters produced consensus trees (Figure 3) that confirm the existence of four coherent monophyletic sister groups: Par = J= ((*P. boisei, P. robustus*), *P. aethiopicus*), NalSed = I = (*H. naledi, Au. sediba*), Her = G = ((African *H. erectus*, Georgian *H. erectus*), Asian *H. erectus*), and PreHs = F = (((*H. heidelbergensis, H. neanderthalensis*), *H. sapiens*), *H. antecessor*).

The results of our combined MP and PN analyses shed some light on issues related to much debated paradigms in paleoanthropology, which we highlight as follows:

- The *Paranthropus* genus Par is the most supported sister group thanks to singular autapomorphies (Figure S9) related to masticatory forces affecting mandibular, maxillar, and postorbital morphology, along with a robust cranial architecture. Its position demonstrates that species of this group

represent a distinct evolutionary lineage from the upstream *Australopithecus* genus, and might have shared a common ancestor with the genus *Homo* (Kimbel et al., 2004; Strait et al., 1997).

- *H. naledi* is the most recent major complete fossil hominin discovery that gave rise to the naming of a new *Homo* species (Berger et al., 2015). Despite its young age of 236–335 ka (Dirks et al., 2017) and on the basis that its anatomical configuration may have existed since the origin of *Homo*, Berger et al. (2017) suggest that *H. naledi* may be placed among the sister group that led to *H. habilis*, *Au. sediba*, and *H. rudolfensis*. Our MP analyses are close to the scenario suggested by the discoverers with regard to the position of *H. naledi* together with *Au. sediba*, and would favor their inclusion in a broad definition of the genus *Homo*, we conceptually call genus *Homo sensu amplo* (Figures 1 and 2). We observe that they systematically share a close common ancestor in the 16 executed MP and bootstrap runs (Table S4; Figures S3–S6), while they make up a sister group that precedes but is not included in the *Homo* hybridization subnetwork of the PN analysis (Figure 4C).
- The H = Hab group in the MPMAX scenario (Figures 1 and 2) incorporates *H. floresiensis,* which confirms its possible phylogenetic link with *H. habilis*, as observed in the analysis with 104 cranial and 29 postcranial characters of 11 hominin species of Argue et al. (2017). However, in the Fitch, Wagner, and Dollo consensus trees (Figure 3A) and in the *Homo* hybridization subnetwork (Figure 4C), *H. rudolfensis* stands out of the Hab group and is in a polytomy with the Her and PreHs groups, which given the chronology and geographic proximity points toward a greater morphological affinity of this taxon with African *H. erectus* of the genus *Homo sensu stricto* than with *H. habilis* (Leakey et al., 2012).
- The *H. erectus* sister group HER ((African *H. erectus*, Georgian *H. erectus*), Asian *H. erectus*) is phylogenetically coherent (Lordkipanidze et al., 2013) and confirms a probable early radiation of *H. erectus* in Asia (Antón et al., 2014).
- *H. antecessor* presents derived features shared with both Neanderthals and modern humans, to the exclusion of other taxa, which validates the position of this terminal in the PreHs group rather than among the *H. erectus* group Her (Bermúdez de Castro et al., 2017).
- Within the group PreHs, the sister group ((*H. heidelbergensis, H. neanderthalensis*), *H. sapiens*) is in accord with the results of recent paleogenomics studies (Mendez et al., 2016).

Which definition of the genus *Homo* is phylogenetically the most relevant according to the MP analysis depends on the taxonomic value that one attributes to the craniodental apomorphies (Table S2; Figure S9) in support of the stem species (tree nodes/boundaries/LCAs) of the three monophyletic groups C, D, and E (Figure 1). Given the nested nature of the stem boundaries of the genus *Homo* as illustrated graphically in Figure 2A, we show here that its phylogenetic tree-like definition (Figure 1) is a relative concept rather than an absolute taxonomic classification norm. However, the PN analysis demonstrates that the *Homo* hybridization subnetwork of Figure 4C associating the *Homo sensu stricto* sister groups of the MP analysis (Her = ((African *H. erectus*, Georgian *H. erectus*), Asian *H. erectus*) and PreHs = (((*H. heidelbergensis, H. neanderthalensis*), *H. sapiens*), *H. antecessor*)) with *H. rudolfensis* might be a more coherent phylogenetic definition of the genus *Homo* with regard to its mode of evolution and offers a highly informative explanation as to how it emerged, diffused, and extended its geographical reach in a reticulate manner.

Mode of evolution of the genus *Homo*: a shifting paradigm toward reticulation

The African origin of *H. sapiens* is traditionally represented by two extreme models of evolution. The recent out of Africa scenario with replacement of archaic populations (Stringer and Andrews, 1988) proposes the appearance of a new species by a tree-like process of cladogenetic speciation, whereas the multiregional hypothesis (Wolpoff et al., 1984) proclaims that *H. sapiens* emerged by a process of gene flow exchanges between archaic populations isolated by distance and meeting at the edge, a model akin to anagenesis or linear phyletic gradualism. In between, but closer to the multiregional one, the assimilation model (Smith et al., 1989), which agrees that the anatomically modern morphology appears in Africa, posits that the genetic advantages of the modern anatomy are not transmitted by migrations but by a process of assimilation resulting from absorption of selective genic fluxes. This model proclaims, for example, that there might have been genetic continuity between Neanderthals and modern humans in Eastern Europe. The assimilation model would appear to be the closest to recent findings in hominin introgressive hybridization, with genetic/genomic and phenotypic studies as supporting evidence (Smith et al., 2017).

Numerous paleogenomics studies have shown that hybridization by means of gene exchanges between divergent taxonomic groups might be the rule rather than the exception in human evolution, particularly as it relates to the origin of *H. sapiens* (Ackermann et al., 2016). Furthermore, interbreeding with parental backcrossing between individuals of genetically differentiated but not too distant taxa, a process known as introgressive hybridization, may be the principal cause of the appearance of phenotypic novelties and the evolutionary emergence of new species (Arnold, 1992, 1997). The logical consequence of hybridization by gene exchanges leading to multiple human groups joining back and forth and resulting in new lineages would be that evolution becomes reticulate and as such would resemble a network rather than a tree. This web-like process of sorting out hominin species with presumed speciations by introgressive hybridization would therefore negate the suitability of cladogenesis or anagenesis as modes of evolution.

Most inferences about reticulation and natural hybridization in paleoanthropology are drawn to a great extent from studies of nonhuman primates such as baboons (Jolly, 2001); paleogenomics studies of Neanderthals, Denisovans, fossil and extant *H. sapiens* (Nielsen et al., 2017; Steinrücken et al., 2018; Villanea and Schraiber, 2019); and to a lesser extent from human fossil phenotypic analyses (Duarte et al., 1999; Trinkaus et al., 2003; Gunz et al., 2018; Bailey et al., 2019). The assertions of introgression or genetic admixture in phenotypic studies are based on observed mosaic anatomical features of supposed transitional fossils, oftentimes described as mixed intermediate morphologies (Ackermann, 2010). However, detecting hybridization in the fossil record is rather challenging and in most hominin species cannot be assessed. Furthermore, defining the morphological effects of hybridization with fossil specimens has been in many cases the subject of disputes (Ackermann et al., 2019). This is due in part to the lack of convincing evidence as to what are the developmental heritable and environmental adaptive factors that can support inferences drawn from mixed intermediate morphologies.

Uncertainties in recognizing admixture in the fossil record and drawing inferences of introgression from phenotypic studies require a phylogenetic conceptual framework to formally explain reticulation. Phylogenetic trees may not be the best tool to represent phylogenetic history in light of the complex biological processes such as hybridization that generate reticulation. Networks are therefore the solution, if one conceives that a network is a tree with reticulations. The question methodologically is how do we make the transition from a tree to a network to explain evolution. In a hybrid species, its genome comes partly from one parent and partly from the other, so the resulting hybrid genome will have different evolutionary histories; therefore, the analysis will endeavor to reconstruct and blend the different phylogenetic trees of the genome. In the construction of a hybridization network the conflicting gene trees will be processed, and not the original character data (Morrison, 2011). Using this analogy, we present here a methodological framework to investigate hominin evolution by combining a phylogenetic network approach with a prior MP tree analysis based on a comprehensive dataset of craniodental morphological features. Our results come to a certain extent in support of recent findings of introgression and hybridization emerging in paleogenomic research of the genus *Homo* and confirm that reticulation is the most probable mode of evolution of the genus *Homo*.

CONCLUSION

The field of molecular anthropology has made significant advances in the past decade with the sequencing of the Neanderthal genome, the identification of the extinct lineage Denisova, and multiple evidence of introgression between *H. sapiens* and these two extinct human groups. Despite exceptional fossil discoveries in the last few years such as Denisova, Dmanisi, *Au. sediba*, *H. naledi*, *Homo floresiensis*, and recently *Homo luzonensis*, progress in paleoanthropology has not kept pace conceptually in redrawing and clarifying the human tree (Scerri et al., 2019). The last significant phylogenetic study on hominin evolution by Dembo and co-authors (2016) relied on a Bayesian inference-based Markov chain Monte Carlo (BMCMC) method using the most complete up-to-date craniodental features dataset available. In the present study using the same dataset, we show that our MP protocol, backed by a bootstrap analysis, produces a more coherent hominin phylogenetic reconstruction (Figure 1), in accord with broadly accepted paleoanthropological paradigms, than the Bayesian BMCMC method, and illustrates three definitions of the genus *Homo*. However, the explanatory utility of commonly used dichotomous tree-like models of phylogenetic reconstruction is limited, as they do not explain the nature of underlying evolutionary processes and mode of evolution of the genus *Homo*.

The molecular proof today of introgression in the genus *Homo* is well established, with documented cases of genetic admixture in recent and extinct *Homo* groups (Nielsen et al., 2017; Steinrücken et al., 2018;

Villanea and Schraiber, 2019). This evidence comes in support of the hypothesis of introgressive hybridization that probably resulted in multiple speciations in the genus *Homo* (Arnold, 2006, 2009). It is clear that to gain a better understanding of the phenotypic diversity observed in the course of human evolution, reticulation has displaced the use of the other two modes of evolution that prevailed historically, namely, anagenesis and cladogenesis (Ackermann et al., 2019). To overcome the limitations of tree-based phylogenetic reconstructions, we conducted a PN analysis based on multiple most parsimonious trees obtained from a prior parsimony analysis with 74 apomorphies, and generated a consensus tree, a consensus network, and a reticulate network. The reading of the reticulate network (Figure 4C) does not provide evidence of diffuse ancestral radiations, but rather directional adaptive changes with uncertain cladogeneses for the late Miocene-Pliocene taxa up to *Au. africanus*, which may be considered by some as a linear punctuated phyletic evolutionary process (White et al., 2006). However, based on the dataset we show that the evolutionary events that gave rise to the species of the genus *Homo* are best represented by a Most Recent Common Ancestor rooted phylogenetic reticulate network. This reticulation might be interpreted as probable hybridization processes that led to the emergence of the extant species *H. sapiens*, further to the extinction of other paleospecies of the genus *Homo*.

The results from our PN analysis come to a certain extent in support of recent findings of introgression and hybridization emerging in paleogenomic research of the genus *Homo* and confirm a paradigm shift in the study of human evolution in favor of reticulation (Winder and Winder, 2014). We hope that our methodological approach combining MP and PN analytical methods is helpful in visualizing the reticulate mode of evolution of the genus *Homo* and provides incentives to rethink and conduct further research in the complex field of hominin phylogeny by means of PN.

Limitations of the study and future avenues of research

Based on a methodological analogy from molecular biology, the present research relying on phenotypic features represents an attempt to combine a tree-based phylogenetic reconstruction method in the study of human evolution with a PN approach. The interpretation of the topography of the resulting most parsimonious tree and network may be subject to debate if one is to argue with the quality of the dataset; however, the phylogenetic information sheds some light on the much debated issue of the emergence of the genus *Homo*, and its reticulate mode of evolution. Further work will be focused on the causal influence of the morphological apomorphous novelties on the nodes of the *Homo* hybridization subnetwork, and what phylogenetic information can be extracted from the tangles reflecting polytomous incompatibilities in the section of the network covering the late Miocene-Pliocene taxa up to *Au. africanus*, in order to elucidate whether there were directional linear adaptive changes of an anagenetic nature. A future avenue for research will also be to supplement the dataset with postcranial characters. Postcranial data would be helpful to confirm the intermediate phylogenetic position of *Au. sediba* and *H. naledi* between australopiths and *Homo* genus *sensu lato*, shed some light on the placement of *H. habilis* and *H. floresiensis* as inferred by Argue et al. (2017), and refine our understanding of the appearance and modes of bipedal locomotion. The diagnosis of hominin species in the present dataset is based on cranial remains, as is generally the case in paleoanthropology. However, we must stress that it is often difficult to assign postcranial remains to a specific species when several contemporaneous species have been identified in a site, but are not associated with cranial remains.

Resource availability

Lead contact

Further information and requests for resources should be directed to Miguel Caparros (capmig@aol.com).

Materials availability

No materials were newly generated for this paper.

Data and code availability

The data and code supporting the findings of this study are available as follows:

- Fossil hypodigms, character matrix, and nexus file of the data (Dembo et al., 2016) are freely available at Dryad Digital Repository https://doi.org/10.5061/dryad.d7r4g.2.
- Characters, character definitions, and character states are available from Supplemental information (Dembo et al., 2016) at https://doi.org/10.1016/j.jhevol.2016.04.008.

- The MP trees (MMPT) generated as output from the Dollo optimality PAUP run with 74 apomorphous characters and used as input data for the Phylogenetic Networks analyses may be provided upon request.
- Code availability. All software packages used for the analyses are publicly available as follows:

PAUP http://phylosolutions.com/paup-test/,

SplitsTree https://software-ab.informatik.uni-tuebingen.de/download/splitstree4/welcome.html.

MacClade http://www.macclade.org/download.html.

METHODS

All methods can be found in the accompanying Transparent Methods supplemental file.

SUPPLEMENTAL INFORMATION

Supplemental information can be found online at https://doi.org/10.1016/j.isci.2021.102359.

ACKNOWLEDGMENTS

We thank Mana Dembo and Arne Mooers for providing the workable Nexus file of the dataset. We thank David Swofford for his explanations regarding the numerical treatment of multistate characters in PAUP, and we assume all errors of interpretation. We thank the three anonymous reviewers for their comments and suggestions that were very helpful in improving the presentation of our work, and Josephine Herbelin/atelier Nous Travaillons Ensemble for her help in the graphic design of Figure 4. We would also like to express our appreciation to the editor Dr. Alessio Bolognesi for his guidance during the review process. S.P. is partly supported by Agence Nationale de la Recherche (France) ANR-17-CE27-0005. One of us (M.C.) would like to pay homage and express thanks to the late professors Pierre Rosenstiehl and Gérard Worms who taught him the intricacies of operations research and graph theory during his years as undergraduate at HEC.

AUTHOR CONTRIBUTIONS

M.C. and S.P. conceived the study, interpreted the results, and wrote the manuscript. M.C. designed the methodology and conducted all analyses.

DECLARATION OF INTERESTS

The authors declare no competing interests.

Received: November 28, 2019
Revised: May 4, 2020
Accepted: March 23, 2021
Published: April 23, 2021

REFERENCES

Ackermann, R.R. (2010). Phenotypic traits of primate hybrids: recognizing admixture in the fossil record. Evol. Anthropol. *19*, 258–270.

Ackermann, R.R., Mackay, A., and Arnold, M.L. (2016). The hybrid origin of "modern humans". Evol. Biol. *43*, 1–11.

Ackermann, R.R., Arnold, M.L., Baiz, M.D., Cortés-Ortiz, L., Evans, B.J., Grant, B.R., Hallgrimsson, B., Humphreys, R.A., Cahill, J.A., et al. (2019). Hybridization in human evolution- Insights from other organisms. Evol. Anthropol. *28*, 189–209.

Antón, S.C., Potts, R., and Aiello, L.C. (2014). Evolution of early *Homo*: an integrated biological perspective. Science *345*, 1236828.

Argue, D., Groves, C.P., Lee, M.S.Y., and Jungers, W.M. (2017). The affinities of *Homo floresiensis* based on phylogenetic analyses of cranial, dental, and postcranial characters. J. Hum. Evol. *107*, 107–133.

Arnold, M.L. (1992). Natural hybridization as an evolutionary process. Annu. Rev. Ecol. Syst. *23*, 237–261.

Arnold, M.L. (1997). Natural Hybridization and Evolution (Oxford University Press).

Arnold, M.L. (2006). Evolution through Genetic Exchange (Oxford University Press).

Arnold, M.L. (2009). Reticulate Evolution and Humans: Origins and Ecology (Oxford University Press).

Bailey, S.E., Hublin, J.J., and Antón, S.C. (2019). Rare dental trait provides morphological evidence of archaic introgression in Asian fossil record. Proc. Natl. Acad. Sci. U S A *116*, 14806–14807.

Berger, L.R., de Ruiter, D.J., Churchill, S.E., Schmid, P., Carlson, K., Dirks, P., and Kibii, J. (2010). *Australopithecus sediba*: a new species of *Homo*-like australopith from South Africa. Science *328*, 195–204.

Berger, L.R., Hawks, J., de Ruiter, D.J., Churchill, S.E., Schmid, P., Delezene, L.K., Kivell, T.L.,

Garvin, H.M., Williams, S.A., DeSilva, J.M., et al. (2015). *Homo naledi*, a new species of the genus *Homo* from the Dinaledi Chamber, South Africa. eLife *4*, e09560.

Berger, L.R., Hawks, J., Dirks, P.H., Elliot, M., and Roberts, E.M. (2017). *Homo naledi* and Pleistocene hominin evolution in subequatorial Africa. eLife *6*, e24234.

Bermúdez de Castro, J.M., Martinon-Torres, M., Arsuaga, J.L., and Carbonell, E. (2017). Twentieth anniversary of *Homo antecessor* (1997-2017): a review. Evol. Anthropol. *26*, 157–171.

Caparros, M. (1997). *Homo sapiens* archaïques: un ou plusieurs taxons (espèces)? Analyse cladistique et morphométrique. PhD dissertation (Muséum national d'Histoire naturelle).

Cela-Conde, C.J., and Ayala, F.J. (2007). Human Evolution. Trails from the Past (Oxford University Press).

Collard, M., and Wood, B.A. (2015). Defining the genus *Homo*. In Handbook of Paleoanthropology, W. Henke and I. Tattersall, eds. (Springer-Verlag), pp. 2107–2144.

Collin, R., and Miglietta, M.P. (2008). Reversing opinions on Dollo's law. Trends Ecol. Evol. *23*, 602–609.

Darlu, P., and Tassy, P. (2019). La reconstruction phylogénétique: Concepts et méthodes (Editions Matériologiques).

Dembo, M., Radovčić, D., Garvin, H., Laird, M., Schroeder, L., Scott, J., Brophy, J., Ackermann, R., Musiba, C., de Ruiter, D.J., et al. (2016). The evolutionary relationships and age of *Homo naledi*: an assessment using dated Bayesian phylogenetic methods. J. Hum. Evol. *97*, 17–26.

Détroit, F., Mijares, A.S., Corny, J., Daver, G., Zanolli, C., Dizon, E., Robles, E., Grün, R., and Piper, P. (2019). A new species of *Homo* from the late Pleistocene of the Philippines. Nature *568*, 181–186.

Diogo, R., and Wood, B.A. (2012). Violation of Dollo's Law: evidence of muscle reversions in primate phylogeny and their implications for the understanding of the ontogeny, evolution and anatomical variations of modern humans. Evolution *66*, 3267–3276.

Diogo, R., and Wood, B.A. (2013). The broader evolutionary lessons to be learned from a comparative and phylogenetic analysis of primate muscle morphology. Biol. Rev. *88*, 988–1001.

Dirks, P., Hilbert-Wolf, H., Kramers, J., Hawks, J., Dosseto, A., Duval, M., Elliott, M., Evans, M., Grün, R., Hellstrom, J., et al. (2017). The age of *Homo naledi* and associated sediments in the Rising Star Cave, South Africa. eLife *6*, e24231.

Dollo, L. (1893). Les lois de l'évolution. Bull. Soc. Belge Geol. Pal. Hydr. VII, 164–166.

Du, A., and Alemseged, Z. (2019). Temporal evidence shows *Australopithecus sediba* is unlikely to be the ancestor of *Homo*. Sci. Adv. *5*, eaav9038.

Duarte, C., Mauricio, J., Pettitt, P., Souto, P., Trinkaus, E., Van der Plicht, H., and Zilhão, J. (1999). The early Upper Paleolithic human skeleton from the Abrigo do Lagar Velho (Portugal) and modern human emergence in Iberia. Proc. Natl. Acad. Sci. U S A *96*, 7604–7609.

Farris, J.S. (1983). The logical basis of phylogenetic analysis. In Advances in Cladistics 2: Proceedings of the Second Meeting of the Willi Hennig Society, N.I. Platnick and V.A. Funk, eds. (Columbia U. Press), pp. 7–36.

Goloboff, P.A., and Pol, D. (2005). Parsimony and bayesian phylogenetics. In Parsimony, Phylogeny, and Genomics, V.A. Albert, ed. (Oxford University Press), pp. 148–159.

Gómez-Robles, A. (2019). Dental evolutionary rates and its implications for the Neanderthal–modern human divergence. Sci. Adv. *5*, eaaw 1268.

Green, R.E., Malaspinas, A.S., Krause, J., Briggs, A.W., Johnson, P.L.F., Uhler, C., Meyer, M., Good, J.M., Maricic, T., Stenzel, U., et al. (2008). A complete Neandertal mitochondrial genome sequence determined by high-throughput sequencing. Cell *134*, 416–426.

Gunz, P., Tilot, A.K., Witfield, K., Teumer, A., Shapland, C.Y., van Erp, T.G.M., Danneman, M., Vernot, B., Neubauer, S., Guadalupe, T., et al. (2018). Neandertal introgression sheds light on modern human endocranial globularity. Cur. Biol. *29*, 120–127.

Haile-Selassie, Y., Melillo, S.M., and Su, D.F. (2016). The Pliocene hominin diversity conundrum: do more fossils mean less clarity? Proc. Natl. Acad. Sci. U S A *113*, 6364–6371.

Haile-Selassie, Y., Suwa, G., and White, T.D. (2004). Late miocene teeth from middle awash, Ethiopia, and early hominid dental evolution. Science *303*, 1503–1505.

Hall, B.K. (2003). Descent with modification: the unity underlying homology and homoplasy as seen through an analysis of development and evolution. Biol. Rev. *78*, 409–433.

Hall, B.K. (2007). Homoplasy and homology: Dichotomy or continuum? J. Hum. Evol. *52*, 473–479.

Hawks, J., de Ruiter, D.J., and Berger, L.R. (2015). Comment on early *Homo* at 2.8 Ma from Ledi-Geraru, Afar, Ethiopia. Science *348*, 1326-b.

Hennig, W. (1966). Phylogenetic Systematics, Translated by D. Davis and R. Zangerl (University of Illinois Press).

Hublin, J.-J. (2015). Paleoanthropology: how old is the oldest Human? Curr. Biol. *25*, R 453–455.

Huson, D.H., and Bryant, D. (2006). Application of phylogenetic networks in evolutionary studies. Mol. Biol. Evol. *23*, 254–267.

Huson, D.H., Rupp, R., and Scornavacca, C. (2010). Phylogenetic Networks: Concepts, Algorithms and Applications (Cambridge University Press).

Jolly, C.J. (2001). A proper study for mankind: Analogies from papionin monkeys and their implications for human evolution. Yearb. Phys. Anthropol. *44*, 177–204.

Kimbel, W.H., Rak, Y., and Johanson, D.C. (2004). The Skull of *Australopithecus afarensis* (Oxford University Press).

Kolaczkowski, B., and Thornton, J.W. (2004). Performance of maximum parsimony and likelihood phylogenetics when evolution is heterogeneous. Nature *431*, 980–984.

Leakey, L.S.B., Tobias, P.V., and Napier, J. (1964). A new species of the genus *Homo* from Olduvai Gorge. Nature *202*, 7–9.

Leakey, M.G., Spoor, F., Dean, C.M., Feibel, C., Antón, S.C., Kiarie, C., and Leakey, L. (2012). New fossils from Koobi Forain northern Kenya confirm taxonomic diversity in early *Homo*. Nature *488*, 201–204.

Lordkipanidze, D., Ponce de León, M., Margvelashvili, A., Rak, Y., Rightmire, G.P., Vekua, A., and Zollikofer, C. (2013). A complete skull from Dmanisi, Georgia, and the evolutionary biology of early *homo*. Science *342*, 326–331.

Mayr, E., and Ashlock, P.D. (1991). Principle of Systematic Zoology (McGraw-Hil).

Meyer, M., Kircher, M., Gansauge, M.T., Li, H., Racimo, F., Mallick, S., Schraiber, J.G., Jay, F., Prüfer, K., de Filippo, C., et al. (2012). A high-coverage genome sequence from an archaic Denisovan individual. Science *338*, 222–226.

Mendez, F.L., Poznik, G.D., Castellano, S., and Bustamante, C.D. (2016). The divergence of neandertal and modern human Y chromosomes. Am. J. Hum. Genet. *98*, 728–734.

Mongle, C.S., Strait, D.S., and Grine, F.E. (2019). Expanded character sampling underscores phylogenetic stability of *Ardipithecus ramidus* as a basal hominin. J. Hum. Evol. *131*, 28–39.

Morris, S.D. (2010). Evolution: like any other science it is predictable. Philos. Trans. R. Soc. B *365*, 133–145.

Morrison, D.A. (2011). An Introduction to Phylogenetic Networks (RJR Productions).

Nielsen, R., Akey, J.M., Jakobsson, M., Pritchard, J.K., Tishkoff, S., and Willersley, E. (2017). Tracing the peopling of the world through genomics. Nature *541*, 302–310.

Porter, M.L., and Crandall, K.A. (2003). Lost along the way: the significance of evolution in reverse. Trends Ecol. Evol. *18*, 541–547.

Prat, S. (2005). Characterising early *Homo*. In From Tools to Symbols, from Hominids to Modern Humans, L. Backwell and F. D'errico, eds. (Witwatersrand University Press), pp. 198–228.

Randolph-Quinney, P.S. (2015). The mournful ape: Conflating expression and meaning in the mortuary behaviour of *Homo naledi*. S. Afr. J. Sc. *111*, 1–5.

Rogers, A.R., Harris, N.S., and Achenbach, A.A. (2020). Neanderthal-Denisovan ancestors interbred with a distantly related hominin. Sc. Adv. *6*, eaay5483.

Scerri, M.L., Chikhi, Lounès, and Thomas, M.G. (2019). Beyond multiregional and simple out-of-Africa models of human evolution. Nat. Ecol. Evol. *3*, 1370–1372.

Schwartz, J.H., and Tattersall, I. (2015). Defining the genus *Homo*. Science *349*, 931–932.

Simpson, G.G. (1953). The Major Features of Evolution (Columbia University Press).

Simpson, G.G. (1961). Principles of Animal Taxonomy (Columbia University Press).

Smith, F.H., Falsetti, A.B., and Donnelly, S. (1989). Modern human origins. Yearb. Phys. Anthropol. *32*, 35–68.

Smith, F.H., Ahern, J.C.M., Janković, I., and Karavanić, I. (2017). The assimilation model of modern human origins in light of current genetic and genomic knowledge. Quater. Inter. *450*, 126–136.

Steinrücken, M., Spence, J.P., Kamm, J., Wieczorek, E., and Song, Y.S. (2018). Model-based detection and analysis of introgressed Neanderthal ancestry in modern humans. Mol. Ecol. *27*, 3873–3888.

Strait, D.S., Grine, F.E., and Moniz, M.A. (1997). A reappraisal of early hominid phylogeny. J. Hum. Evol. *32*, 17–82.

Strait, D.S., and Grine, F.E. (2004). Inferring hominoid and early hominid phylogeny using craniodental characters: the role of fossil taxa. J. Hum. Evol. *47*, 399–452.

Strait, D.S., Grine, F.E., and Fleagle, J.G. (2015). Analyzing hominin phylogeny: cladistic approach. In Handbook of Paleoanthropology, W. Henke and I. Tattersall, eds. (Springer-Verlag), pp. 1989–2014.

Stringer, C.B. (2016). The origin and evolution of Homo sapiens. Philos. Trans. R. Soc. B *371*, 20150237.

Stringer, C.B., and Andrews, P. (1988). Genetic and fossil evidence for the origin of modern humans. Science *239*, 1263–1268.

Swofford, D.L. (2020). Phylogenetic Analysis Using Parsimony (PAUP) (Version 4.0a169). http://phylosolutions.com/paup-test/.

Trinkaus, E., Moldovan, O., Milota, S., Bîlgār, A., Sarcina, L., Athreya, S., Bailey, S., Rodrigo, R., Mirces, G., Higham, T., et al. (2003). An early modern human from the Pestera cu Oase, Romania. Proc. Natl. Acad. Sci. U S A *100*, 11231–11236.

Villanea, F.A., and Schraiber, J.G. (2019). Multiple episodes of interbreeding between Neanderthal and modern humans. Nat. Ecol. Evol. *3*, 39–44.

Villmoare, B., Kimbel, W., Seyoum, C., Campisano, C.J., DiMaggio, E., Rowan, J., Braun, D.R., Arrowsmith, J.R., and Reed, K.E. (2015a). Early *Homo* at 2.8 Ma from Ledi-Geraru, Afar, Ethiopia. Science *347*, 1352–1355.

Villmoare, B., Kimbel, W., Seyoum, C., Campisano, C.J., DiMaggio, E., Rowan, J., Braun, D.R., Arrowsmith, J.R., and Reed, K.E. (2015b). Response to comment on early *Homo* at 2.8 Ma from Ledi-Geraru, Afar, Ethiopia. Science *348*, 1326–c.

Villmoare, B. (2018). Early *Homo* and the role of the genus in paleoanthropology. Am. J. Phys. Anthrop. *165*, 72–89.

White, T.D., Woldegabriel, G., Asfaw, B., Ambrose, S., Beyene, Y., Bernor, R., Boisserie, J.-R., Currie, B., Gilbert, W., Haile-Selassie, Y., et al. (2006). Asa Issie, Aramis and the origin of *Australopithecus*. Nature *440*, 883–889.

White, R.D., Lovejoy, C.O., Asfaw, B., Carlson, J.P., and Suwa, G. (2015). Neither chimpanzee nor human, *Ardipithecus* reveals the surprising ancestry of both. Proc. Natl. Acad. Sci. U S A *112*, 4877–4884.

Wiens, J.J. (2011). Re-evolution of lost mandibular teeth in frogs after more than 200 Million years, and re-evaluation Dollo's Law. Evolution *65*, 1283–1296.

Winder, I.C., and Winder, N.P. (2014). Reticulate evolution and the human past: an anthropological perspective. Ann. Hum. Biol. *41*, 300–311.

Wolpoff, M.H., Zhi, W.X., and Thorne, A.G. (1984). Modern Homo sapiens origins: a general theory of hominid evolution involving the fossil evidence from East Asia. In The Origins of Modern Humans: A World Survey of the Fossil Evidence, F.H. Smith and F. Spencer, eds. (Alan Liss), pp. 411–483.

Wood, B.A., and Collard, M. (1999). The human genus. Science *284*, 65–71.

Wood, B.A., and Lonergan, N. (2008). The hominin fossil record: taxa, grades and clades. J. Anat. *212*, 354–376.

Wood, B.A. (2014). Fifty years after *Homo habilis*. Nature *508*, 31–33.

Wood, B.A., and Boyle, E.K. (2016). Hominin taxic diversity: fact or fantasy? Yearb. Phys. Anthrop. *159*, S37–S78.

Wright, A.M., and Hillis, D.M. (2014). Bayesian analysis using a simple likelihood model outperforms parsimony for estimation of phylogeny from discrete morphological data. PLoS One *9*, e109210.

Wright, S. (1982). Character change, speciation, and the higher taxa. Evolution *36*, 427–443.

Zou, Z., and Zhang, J. (2016). Morphological and molecular convergences in mammalian phylogenetics. Nat. Commun. *7*, 12758.

iScience, Volume *24*

Supplemental information

A Phylogenetic Networks perspective on reticulate human evolution

Miguel Caparros and Sandrine Prat

Supplemental Information

A Phylogenetic Networks perspective on reticulate human evolution

Miguel Caparros and Sandrine Prat

Transparent Methods

Detailed methods include the following:

Foundations of the phylogenetic concept of Maximum Parsimony

In the Origin of Species, Darwin stated that extant species are linked by successive dichotomies with nodes up to common ancestral species, and linked time and lineage in a tree figure for the first time (Darwin, 1859, p.117). He proposed a model of descent with modification stipulating "that the characters which naturalists consider as showing true affinity between any two or more species, are those which have been inherited from a common parent" (Darwin, 1859, Chapter 13). For Darwin character affinities between species, construed as homologous similarities, are the proof of their common descent while differences would indicate modifications that are driven by natural selection. However, further to his pronouncement two uncertainties remained: should one try to find only resemblance revealing common descent, or should one also try to take dissimilarities into account. The choice between these two approaches had a bearing on the results of descent-ancestral analysis among darwinian naturalists, namely the shape and structure of the phylogenetic tree (Tassy, 1998).

By integrating in a "modern synthesis" the mendelian genetic principles of inheritance to the theory of darwinian selection, the neo-darwinian naturalist school (Mayr, 1942) conceived evolution as a gradual phenomenom driven by the accumulation of small genetic mutations and chromosomic rearrrangements, genetic variation being determined by natural selection. The question of ancestor-descendant relationships became secondary given that evolution was considered as a linear anagenetic gradual process with the appearance of similar characters in distant species explained by adaptive convergence or parallelism. In essence the phylogenetic dichotomic tree became a trunk with branches of variable widths representing ancestral groups of species and classes (Tassy, 1998). For this school of thought the search of primitive characters became the basis of comparative anatomy with a revised concept of homology as the cornerstone of evolutionary systematics and proof of evolution.

In Principles of Animal Taxonomy, Simpson (1961, p.78) defines Homology as “resemblance due to inheritance from a common ancestor” and “Homoplasy is resemblance not due to inheritance from a common ancestor”. For Simpson, only resemblance linked to homologous traits allowed a phylogenetic reconstruction of species, but he did not specify if this homologous inheritance came from a close or remote ancestor. As illustrated below and based on a given inferred phylogeny, on the right tree Simpson’s homology definition of global similarity applies to character state a

of taxa X and V, and to character state a' of taxa Y, Z and W. One may argue that the primary aim of neo-darwinian evolutionists was to untangle ancestor-descendant relationships by bringing to light convergence (homoplasies) explained by adaptive mechanisms, while to a lesser extent searching primitive characters that reveal deeply rooted similarities (homologies) and common descent.

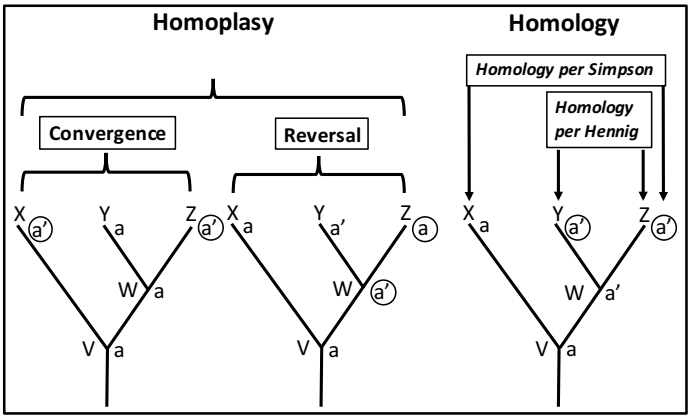

Illustration of Homology and Homoplasy taxonomic concepts: X, Y and Z are species under study, V and W are ancestor species, a is the primitive character state and a' the derived character state.

Although Hennig (1966), founder of the modern Phylogenetic Systematics school of thought, did not explicitly use the term homoplasy, he referred to its component concepts and covered them extensively as non-homology, namely convergence, parallelism and reversibility. His major contribution to phylogenetic systematics however may be summarized simply: he refined the concept of homology articulated by Simpson by further splitting the notion of homology into two, as shown on the right of the above illustration. He distinguished similarity from a primitive state (a), he called plesiomorphy, from similarity from a derived state (a') considered as the appearance of an evolutionary novelty, and proposed the principle that only the sharing of novelties by two species, he called apomorphies (a' in species Y and Z on the right tree), is a sign of close relatedness: " It is evident that the presence of corresponding characters in two or more species is a basis for assuming that these species form a monophyletic group only if the characters are apomorphous, if their correspondence rests on synapomorphy" (Hennig, 1966, p. 90). Homology became synapomorphy. In essence the association of primitive traits and derived traits as homology, i.e. global similarity, was invalidated and substituted by a new way of reconstructing phylogeny based on the sharing of character apomorphies. This new paradigm was in line with the darwinian theory of evolution of descent with modification, now applied to characters. Without consideration of evolutionary concepts such as adaptive zone, divergence rate or genetic cohesion to explain convergence, the hierarchical history of taxa was reconstituted from characters by the sharing of apomorphies and not from taxa. In the Hennigian model the cladogram made up of nested monophyletic sister groups allowed one to identify the hypothetical Last Common Ancestors (LCAs) at the tree nodes that bear the synapomorphies, denying any relevance to primitive traits (plesiomorphies).

Hennig did not originate the concept of parsimony, but given the common occurrence of convergence and parallelism implicitly alluded to it by postulating that " The common occurrence of parallelisms and homoiologies, if not of pronounced convergences, indicates the necessity for phylogenetic systematics to take into account as many characters as possible in deciding kinship relations. The more certainly characters interpretable as apomorphous (not characters in general) are present in a number of different species, the better founded is the assumption that these species form a monophyletic group" (Hennig, 1996, p.121). He suggested that the appearance of a derived character in two closely related species should not be construed *a priori* originating from convergence, and proposed the principle of bringing into congruence several series of characters to ascertain kinship relations by "checking, correcting and rechecking". Congruence of characters would enable the identification of non-apomorphies (homoplasies), with the most informative character-state changes being the ones that appear once which he named apomorphies. In essence the only criterion that satisfies Hennig's congruence concept of homologous characters to build a phylogenetic tree is the criterion of parsimony which consists in choosing a cladogram that maximizes the number of shared derived characters (apomorphies) and minimizes homoplasies. Hennig's method of congruence gave rise subsequently to algorithmic parsimony which was based on concepts developed by Wagner (1961, 1963) and formalized by Kluge and Farris

(1969) and Farris (1970). The PAUP software (Swofford, 2020), built according to the principle of Hennigian phylogenetic systematics just described, is used in our parsimony analyses with the most common character state optimality criteria.

Experimental design

The objective of our study is to present a conceptual phylogenetic reconstruction framework, summarized schematically in Figure S1, that combines tree-based Maximum Parsimony (MP) cladistics with a web-like Phylogenetic Networks (PN) method. We will test its application by using the phenotypic craniodental dataset of Dembo et al. (2016), with the aim of clarifying the taxonomic definition(s) of the genus *Homo* and ascertaining whether its mode of evolution leading up to the emergence of *Homo sapiens* was of a web-like reticulate nature or not.

Our methodological approach follows three logical steps as follows:

1. Implementation of a tree-based MP protocol with the complete dataset to select the most parsimonious tree scenario out of 16 numerical runs based on various algorithmic constraints. This scenario will highlight hypothetical ancestor-descendant relationships among the 22 hominin species that will serve to suggest phylogenetic definitions of the genus *Homo*. We use the PAUP software (Swofford, 2020) for this step.
2. Intermediate step to establish a methodological link between the MP and PN analyses. We execute an MP run based on apomorphies identified from the most parsimonious tree obtained in step 1 and generate multiple most parsimonious trees (MMPT) as input for the PN analysis. This run will serve to verify the phylogenetic signal of the most coherent scenario from step 1. We use the PAUP software (Swofford, 2020) for this step.
3. PN analysis based on input of MMPT from step 2 that produces a consensus tree, a consensus network and a reticulate network. From the reticulate network we will infer whether or not the phylogenetic relationships among the hominin species of the dataset are of a reticulate nature. We use the SplitsTree software (Huson and Bryant, 2006) for this step.

Step 1. Tree-based MP protocol

Execution of 16 MP tree runs with original dataset

There are four main character types available to conduct an MP analysis (Transparent Methods 1). In most MP published studies in palaeoanthropology, authors commonly use the unordered character type (Fitch parsimony) or ordered type (Wagner parsimony), or a combination of both (Collard and Wood, 2000; Strait and Grine, 2004), whereas the ones favoring convergent homoplasies (Camin-Sokal parsimony) or reversals (Dollo parsimony) are never selected. This common approach would indicate that authors make *a priori* assumptions about the process of evolution with regard to character-state changes. Many authors tend to discard polymorphic characters in multistate taxa. Ignoring polymorphism results in a loss of information (Wiens, 1999); fortunately, this is not the case in the present dataset that includes several taxa showing all the states for some specific characters. However, given that the choice of setting ("polymorphic" or "uncertain") is non-trivial and lead to different tree topologies (Swofford, 2020), a word of caution is necessary with regard to which setting is used for multistate taxa (Transparent Methods 2). Should the characters with originally equal weight be reweighed after the first run? Some authors argue that characters should have the same weight, stating that reweighing the characters in a second run to minimize the importance of homoplastic characters may negatively affect the tree topography, and therefore falsify the phylogenetic results. It is empirically demonstrated that reweighing characters in a second run with the character Rescaled Consistency (RC) indices obtained from the first run is efficient, and in accord with the principle of maximum parsimony (Transparent Methods 3). In light of these observations, it is necessary to conduct the MP analysis with all possible numerical options available in order to objectively select the scenario that is truly the most parsimonious. With the PAUP software (Swofford, 2020), we execute 16 MP runs corresponding to 16 different evolutionary tree scenarios (Figures S3-S6) based on 4 character types (Fitch, Wagner, Camin-Sokal or Dollo, the last two with "Up" polarity) with equal weight and RC reweighing, and uncertainty or polymorphism multistate taxa setting. Thus, for each character type there will be 4 runs: 2 first search runs with equal weights and uncertainty or polymorphism setting, and 2 second search runs with RC reweighed characters and uncertainty or polymorphism setting. All the runs are conducted by heuristic search (simple stepwise addition and TBR branch swapping), and all the character RCs used for the reweighing in the second search are obtained from the ouput of the first search (Mounier and Caparros, 2015). If the runs result in more than one tree, such as in R1, R2, R5, R6, R9 and R13, we post the 50% majority rule maximum parsimony consensus tree

of the resulting minimal trees (Transparent Methods 7). The main parameters resulting from the 16 MP runs are summarized in Table 1. Concurrently to assess the branch support of each the 16 MP tree scenarios, we execute bootstrap runs with the same parsimony settings used in each MP run, and show in the same Figures S3-S6 the respective 50% majority rule bootstrap consensus trees along with the corresponding bootstrap branch support values (Transparent Methods 5).

Selection of MPMAX tree scenario

The Hennigian principle of congruence (Hennig, 1966) postulates that the most parsimonious tree is the one that reveals the maximum number of apomorphies or equivalently minimizes the number of homoplasies inherent to the tree, and supposedly minimizes the number of character-state changes (steps) on the cladogram. The total number of steps of the 16 MP analysis runs is not a reliable parameter to select the most parsimonious scenario due to the fact that the constraints (models of character types, equal weight or reweighing, and multistate taxa settings) affect the scale of the number of steps, as evidenced in Table 1. The best parameter to select the most informative run is the one that measures accurately the overall degree of synapomorhy of the MP tree. The Retention Index (RI) of the resulting 16 tree runs happens to be the most reliable congruence index for the selection of the most parsimonious scenario (Transparent Methods 4), i.e, the scenario with the highest tree RI is the most coherent and phylogenetically informative. If the tree RI is objectionable to select the most parsimonious scenario, we present as an alternative a selection procedure that follows the scientific method advocated by Popper (1963) of empirical falsification based on scrutiny of all the available evidence (Transparent Methods 4).

Validation of MPMAX scenario by comparing MP and BMCMC results

Given that we use the same dataset as Dembo et al. (2016), contrasting the results of the BMCMC analysis from Dembo et al. (2016, Figure 2) with the MP results of the most parsimonious scenario MPMAX of the present study (Figure 1) ought to be an empirical objective to interpret the data. However, the two methods are not directly comparable since MP is a numerical method based on mathematical graph theory (Darlu and Tassy, 2019), while BMCMC is a statistical method (Goloboff and Pol, 2005). The measure of coherence of MP such as the tree RI is not comparable to the posterior probabilities produced by BMCMC. An indirect way of comparing the two methods is to execute a bootstrap run with the same settings as the MPMAX run, and compare the proportions of bootstrap replicates values P_{boot} of the bootstrap tree (Figure S6E) to the posterior probability values P_{post} of the BMCMC tree. The branch support equivalence of P_{boot} to P_{post} is well documented (Transparent Methods 5). We validate the MPMAX scenario by comparing the replicate values (P_{boot}) of the bootstrap tree obtained with the same settings, with the posterior probabilities (P_{post}) of the best tree resulting from a Dembo et al. (2016) Bayesian analysis.

Step 2. Intermediate step to establish methodological link between MP and PN analyses

Execution of MP run with 74 apomorphous characters

The character retention index ri is a measure of the phylogenetic information content of a character (Farris, 1989b, Transparent Methods 6, Figure S8), i.e., it determines whether it is an apomorphy or a homoplasy. From the output of the MPMAX run (Table S1), the dataset may be split in two: 74 apomorphies (Table S2) with character ri = 1 (18.93%), and 317 homoplasies with character $0 < ri < 1$ (81.07%). The fundamental principle of Phylogenetic Systematics is that the evolutionary history of taxa is reconstituted from characters by the sharing of apomorphies while homoplasies, resemblance not due to inheritance from a common ancestor, represent features of an adaptive nature and are therefore phylogenetically less informative: "The more characters certainly interpretable as apomorphous (not characters in general) are present in a number of different species, the better founded is the assumption that these species form a monophyletic group (Hennig, 1966)". In essence, only apomorphies are relevant in finding monophyletic groups " not characters in general". Thus, in keeping with this principle, we re-run the parsimony analysis with the 74 apomorphous characters.

Verification of MPMAX phylogenetic signals

The analysis run with 74 apomorphous characters will generate a certain number of multiple most parsimonious trees (MMPT) with perfect RI and CI scores equal to 1. We compute a 50% majority consensus tree (Transparent Methods 7) that will confirm the existence of highly resolved monophyletic sister groups identified in step 1 with the full set of characters. The MMPT will be used as input for the PN analysis.

Step 3. PN analysis

In a final stage, in order to elucidate the mode of hominin evolution, and in particular the evolution of the genus *Homo*, we use a web-like innovative Phylogenetic Networks conceptual approach (Transparent Methods-Phylogenetic Networks method) that takes over where the tree-based MP protocol ends, i.e. with the MMPT of step 2. We conduct a PN analysis (Huson et al., 2010) based on the MMPT as input with the application software SplitsTree (Huson and Bryant, 2006), and generate an un-rooted consensus tree (structurally identical to the 50% majority consensus tree of step 2), a consensus network and a reticulate network.

Tree-based Maximum Parsimony (MP)

Maximum Parsimony is an integral part of the Phylogenetic Systematics school of thoughts, commonly known in taxonomy as cladistics (Hennig, 1996). In essence, it is the analysis of individual characters (anatomical or genetic) free to evolve independently with the application of the principle of maximization of the number of novelties on the cladogram (tree), and the consequent discovery of the hierarchical order of the various groups of species of the dataset. By its computational nature it allows one to identify clearly the character-state changes that support the various clades (branches), and thus enhances the evolutionary analysis of observed anatomical modifications, be they of an adaptive nature or the result of epigenetic processes.

Transparent Methods 1. Maximum Parsimony (MP) optimality criteria

MP optimality criteria are options of character types available in the PAUP software (Swofford, 2020) before executing the runs. They model evolutionary character-state changes based on imposed algorithm constraints. The four main choices are Fitch, Wagner, Camin-Sokal or Dollo parsimony.

1. In Fitch parsimony (Fitch 1971) characters are unordered and therefore have no constraint, i.e., any state can transform into any other state, and a state change is counted as one step. All resulting homoplasies (multiple state changes at some nodes for certain characters) by convergence or reversal are allowed.

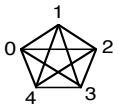

2. In Wagner parsimony (Farris, 1970; Swofford and Maddison, 1987) characters are ordered, and the ordering results in the number of steps from one state to another counting as the absolute difference between their state numbers, e.g., for a character with 4 states (0, 1, 2, 3), a change from 0 to 3 (or from 3 to 0) will count as 3 steps while under Fitch parsimony it counts as 1. Convergence and reversal are allowed. Since there is only one possible path between the two states of a binary character (0, 1), the ordered type applies only to characters that have more than two states.

$$0 \leftrightarrow 1 \leftrightarrow 2 \leftrightarrow 3 \leftrightarrow 4$$

3. Camin-Sokal parsimony (Camin and Sokal, 1965) postulates that character evolution is irreversible, i.e., only parallelism or convergence state changes are allowed while reversals are excluded. The number of state changes is the difference between their state numbers, and decreases in state numbers is not allowed, e.g., for a character with 4 states (0, 1, 2, 3), a state change from 2 to 4 is counted as 2 steps, but change from 4 to 2 is impossible.

$$0 \rightarrow 1 \rightarrow 2 \rightarrow 3 \rightarrow 4$$

4. In Dollo parsimony (Farris, 1977) all homoplasies are accounted for by reversal to the ancestral plesiomorphic state, and state changes by convergence or parallelism are not allowed. A character can change from the plesiomorphic state to the derived state only once, and multiple reversals are allowed, i.e., the number of steps is the difference of the numbers attributed to the states and an increase in state number happens once.

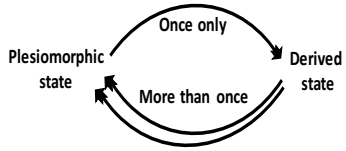

The four parsimony optimality criteria represent four models of evolutionary paths applied to character changes, subject to constraints as to the polarity or reversibility of the characters. If one does not want any constraint with regard to the type of characters, one then uses unordered setting (Fitch) which permits any state of a character to transform directly to any other state. If one wants to impose a constraint as to the direction (polarity) of the state changes, one uses ordered setting (Wagner) which is bidirectional, i.e. in a three states 0,1,2 character there is no requirement that 0 be the ancestral state, only the resulting tree will determine which state is ancestral after orienting the tree (graph) with an outgroup. Wagner parsimony makes convergence and reversion possible, as in Fitch parsimony. If one considers that evolution is irreversible as suggested by Simpson (1953), then one chooses the Camin-Sokal criterion which is equivalent to ordered characters with the additional constraint of irreversibilty, or unidirectionality from a plesiomorphic state or less derived state to a more derived state. Finally, if one assumes that a derived character can change only once from the plesiomorphic state to the derived state, and can revert more than once to the plesiomorphic state, then the Dollo criterion, which only allows homoplasy under the form of reversal, is required.

Transparent Methods 2. Treatment of multistate taxa

The treatment of multistate taxa remains contentious (Kornet and Turner, 1999). Two setting options (uncertainty and polymorphism) are available for the treatment of multistate taxa in PAUP (Swofford, 2020), and their choice affects the results and interpretation of the parsimony analysis. To clarify, let us assume that a taxon has been coded with two states 0 and 1. For the uncertainty setting PAUP chooses the state 0 or 1 that minimizes the tree length and assumes that the ancestral taxon at the node could have either one of the two states. For the polymorphism setting, the program chooses both states 0 and 1 to find the most parsimonious tree which might result in a longer tree; conceptually the polymorphic taxon is split into 2 subtaxa, one with the state 0 and the other with 1, the terminals are "polymorphic", and the ancestors are still assumed to have one state or the other. Both uncertainty and polymorphism setting options are considered as "ambiguity". For uncertainty, we assume that each taxon (terminal or at the node) has a single state; we just do not know which one. For polymorphism, we assume that the terminal may have both. The only difference between these interpretations is in the tree length: if a terminal is polymorphic with "0" and "1", then an extra step is added because there must be at least one change between the two states within the terminal clade. Caution is required in interpreting the results: after running the parsimony algorithm, PAUP assigns one of the states of a multistate character to the terminal taxon, i.e. the algorithm treats the multistate character as an ambiguity, and by optimization assigns one of the features to the terminal in the output. Conceptually one may construe the selected chosen state in the output terminal as if the polymorphism had resulted in the monomorphic dominant fixation of the trait in the concerned species.

Transparent Methods 3. Reweighing characters

Weighing of characters in cladistics is a controversial issue, one argument being that reweighing characters after an initial run leads to unparsimonious hypotheses (Kluge, 1997). However, Farris (1983) considered that characters with more homoplasy are less reliable and noted that parsimony is not equivalent to equal weights; he argued on the basis that some characters represent stronger evidence than others, that consequently they should be weighed. Successive weighing is successful when cladistically reliable characters such as apomorphies are outnumbered by homoplasies as in the present study (Farris, 1969), and the use of the rescaled consistency index RC (= Retention Index (RI) x Consistency Index (CI)) from a first run is recommended as a weighing criterion (Farris, 1989b). Reweighing of morphological data sets produces substantial increases in jackknife frequencies, and results compared to equal weighing become more stable with lower error rates (Goloboff et al, 2008). This supports the affirmation that “it is not that parsimony does not preclude weighing, but rather that it requires weighing" (Goloboff, 1993). In the present study, we execute 16 runs with the PAUP software (Swofford, 2020) based on 4 character types (Fitch, Wagner, Camin-Sokal or Dollo, the last two with "Up" polarity), two settings for weights and two settings for multistate taxa (uncertainty or polymorphism). With regard to character weights, in a first search we will use equal weights while in a second search we will reweigh the characters with the character RCs obtained from the first search (Caparros, 1997; Mounier and Caparros, 2015). Thus, for each character type there will be 4 runs: 2 first search equal weight runs with uncertainty or polymorphism setting, and 2 second search runs with RC reweighed characters and uncertainty or polymorphism setting. All the runs are conducted by heuristic search (simple stepwise addition and TBR branch swapping), and the character RCs used for the reweighing in the second search are obtained from the ouput of the first

search. The parameters of the 16 MP runs are summarized in Table 1. In this Table, we note that in first runs with equal weights showing multiple parsimonious trees summarized by a consensus tree (R1, R2, R5, R6, R9 and R13 of Figures S3-S6), reweighing in a second run with the same constraints (character type and multistate taxa) produces one single parsimonious tree (R3, R4, R7, R8, R11 and R15 of Figures S3-S6). Such a reduction is also evidenced in Mounier and Caparros (2015).

Transparent Methods 4. Criteria to select the most parsimonious tree

Tree Retention Index (RI)

To select the most parsimonious tree among the 16 scenarios, there exist several computational character congruence indices, considered as cumbersome, such as for example the homoplasy excess ratio HER (Archie, 1989), the data decisiveness index DD (Goloboff, 1991) and the homoplasy slope ratio HSR (Meier et al., 1991). The Consistency Index (CI) and Retention Index (RI) are two measures of homoplasy that are commonly and extensively used (Farris, 1989a; Farris, 1989b). However, the CI, unlike the RI, is negatively correlated with the number of taxa, and thus is not an absolute measure of the degree of homoplasy, and its measure of convergence or reversal might also take into account background noise due to the presence of a large number of highly variable and poorly informative characters within and between taxa (Caparros, 1997). The overall tree retention index RI is the sum over all the individual-character retention indices r (Transparent Methods 6 and Figure S8) calculated with the formula $(\sum g - \sum s) / (\sum g - \sum m)$. The RI is a better indicator of the level of synapomorphy than the CI, and represents a robust proxy for confidence and accuracy estimate in the selection of the most informative and coherent MP scenarios (Caparros, 1997; Farris, 1989a; Farris, 1989b; Mounier and Caparros, 2015; Mounier et al., 2016). A high value of the RI index is indicative of a high degree of overall synapomorphy inherent to the tree, and thus of its phylogenetic information content.

Popperian approach.

Popperian hypothesis testing must follow a three stage model (Popper, 1999): 1) problem: delineate the evolutionary threshold between *Homo* and other hominin species; 2) attempted solutions: 16 identified scenarios; and 3) elimination of these solutions by subjecting them to criticism to select the most parsimonious. Two options are available to refute the attempted solutions of Popper's stage 3 in order to select the most parsimonious scenario: a narrative one by a process of argumentation based on existing paleoanthroplogical paradigms, which would lead to unending discussions and disagreements, or an empirical one focused on identifying inconsistencies by blending low boostrap support of tree scenarios with some paleoanthropological commonly accepted paradigms (one paradigm based on chronology and one based on a well-established pre-formed clade). We use the empirical option to eliminate scenarios that appear inconsistent, and rely on three inconsistency criteria (Table 2) obtained from 16 bootstrap runs (Figures S3-S6) executed with the same settings of the MP runs: 1) the chronological order of the emergence of pre-*Homo* taxa is deemed in general terms to be as follows (Figure S2): *S. tchadensis* --> *Ar. ramidus* --> *Au. anamensis* --> *Au. afarensis* --> *K. platyops* --> *Au. africanus* --> *Au. garhi* --> *Paranthropus* cohesive sister group; any deviation of *S. tchadensis, K. platyops* and *Au. africanus* from this chronological order showing significant variation in their positions in the bootstrap trees will be deemed to be inconsistent; 2) The clade ((*H. heidelbergensis, H. neanderthalensis*), *H. sapiens*) is consistent with bootstrap results (Mounier and Caparros, 2015); any deviation from this clade sequence such as for example ((*H. heidelbergensis, H. sapiens*), *H. neanderthalensis*) will be deemed to be inconsistent; 3) branch support values of less than 20 % in the bootstrap trees will be deemed to be inconsistent.

Transparent Methods 5. Comparative equivalence of MP bootstrap P_{boot} v.s. BMCMC P_{post}

Bootstrapping is a random resampling method developed by Efron (1979) to evaluate the accuracy of statistical estimates. Felsenstein (1985) proposed to use bootstraping to assess the confidence intervals in phylogenetic analyses, and PAUP has implemented this method. In a PAUP bootstrap analysis, the number of taxa of the dataset is held constant while the characters are randomly sampled with replacement to build a series of new data sets the same size as the original dataset which are called bootstrap replicate datasets (BSD). As indicated by Felsenstein (1985), each BSD consists of a new data table with the same set of species, but with some of the original characters duplicated and others dropped by the process of sampling n characters from the original dataset with replacement. These BSDs are then executed by a maximum parsimony search and generate bootstrap replicate trees (BRT). Finally, a majority-rule bootstrapping consensus tree (MRBCT) is constructed from all of the BRTs, with the same computational criteria as

for a Maximum Parsimony majority-rule consensus tree. It is assumed that if a sister group appears in x percent of a MRBCT branch, the confidence level associated with that group is taken as x percent. We call the x percentage value P_{boot}. The proportion of bootstrap replicate value P_{boot} in which a clade is identified is subject to various interpretations in phylogenetic analysis (Soltis and Soltis, 2003). Some view P_{boot} as a measure of repeatability, others as a measure of accuracy, i.e. closeness to the true tree, or a measure of statistical confidence. Most systematists view bootstrap values as a relative assessment of clade support rather than a strict statistical confidence statement of the nodes, or joint confidence for the entire tree. The BMCMC method estimates stochastically the posterior probability P_{post} to assess the strength of support of the individual clades of the resulting tree topology (Dembo et al., 2016). The question is: are the values of P_{boot} and P_{post} comparable? Simulations of maximum likelihood bootstrap and BMCMC analyses performed on the same sequence dataset show that over various model spaces values P_{boot} and P_{post} are not significantly different (Cummings et al., 2003). These findings are corroborated in a set of simulations showing that P_{post} estimated by Mr Bayes software and P_{boot} calculated by PAUP software were almost exactly the same (Goloboff and Pol, 2005). Thus, in the two elliptic representations of Figure 2, values of P_{boot} of MPMAX tree and P_{post} of BMCMC Dembo tree will be deemed to be equivalent in the comparison of support of the various clades of both phylogenies. P_{post} values of the BMCMC Dembo tree are low but comparable to other Bayesian phylogenetic studies (Dembo et al., 2016), and the same qualification may be applied to P_{boot} values of the MPMAX tree; however, bootstrap values in general are negatively affected by the number of characters, the number of non-informative characters, the number of missing characters in some taxa, and by the sample size and the nature of the search algorithms (Soltis and Soltis, 2003). One should not exclude the possibility that a tree topography with very low support values of an extensive and complex dataset might still be phylogenetically closer to the "true" tree than a tree topology with higher support values from a limited and related dataset. It is thus paradoxical that the more extensive a dataset is, the lower the support values may be. The comparison of P_{boot} and P_{post} values of Figure 2 reflects the difference in clade support related to the search methods; thus, the method with the highest support values will indicate relatively a higher confidence level in the relationships expressed phylogenetically by the clades.

Transparent Methods 6. Character information content

A distinction should be made between the overall tree retention index RI and the single character retention index r. The character retention index r is "the fraction of apparent synapomorphy in the character that is retained as synapomorphy on the tree" (Farris, 1989b), i.e. it is a measure of the proportion of homoplasy observed in the character on a tree relative to the maximum possible homoplasy on any tree, and is a more informative estimator of a character homoplasy than the character consistency index. We illustrate graphically in Figure S8 the character retention index r behavior related to the coherence of the MP tree; it expresses the degree of *a posteriori* homology apparent in the character, i.e. its information content. If $r = 1$ the character change represents an apomorphy while values of $0 \leq r < 1$ represent homoplasies. The lower this index the more homoplastic the character is; thus, the quantity 1- r represents the degree of homoplasy inherent to this character in the MP tree.

Transparent Methods 7. MP consensus trees and treatment of ambiguities

Consensus trees are used when the maximum parsimony MP run generates more than one most parsimonious tree such as in the analysis with 74 apomorphous characters (Figure 3), or in runs with the entire dataset such as R1 & R2 (Figure S3A), R5 & R6 (Figure S4A), R9 (Figure S5A) and R13 (Figure S6A). Consensus trees are hierarchical summaries of the information common to a set of "rival" trees and represent a summary of agreement among trees. When the rival trees possess a certain number of similar branches (monophyletic sister groups), these are retained as such, while distinct branches not in agreement are expressed as polytomies. We use the Majority-rule model for the runs just mentioned and rely on 50% as percentage that allows one to retain all groups found in over half of the rival trees. The 50% Majority-rule consensus tree is the most robust commonly used method. Consensus trees summarize the concordance of trees of minimal length, and theoretically should not be interpreted as a phylogenetic tree. Their explanatory power comes from the fact that they identify informative coherent subgroups of taxa and provide a good indication of the information content of the dataset (Anderberg and Tehler, 1990). The multiplicity of MP trees of equal length obtained with 74 apomorphous characters (summarized by a consensus tree in Figure 3), as compared to the unique MPMAX tree with 391 characters (Figure 1A), is explained empirically by the fact that removing homoplastic characters in the analysis increases substantially the number of minimal trees (Caparros, 1997).

Further to a numerical run, some apomorphies and homoplasies may be subject to ambiguities regarding the possible assignment of character-state changes at nodes of the MP tree. Ambiguities may be resolved by a process of selective arguments, or by one commonly used optimization algorithm, such as ACCTRAN or DELTRAN (Agnarsson and Miller, 2008). In MPMAX, the most consistent scenario based on Dollo parsimony where homoplasies are accounted for by reversals, we use for illustration purposes the ACCTRAN optimization algorithm that assigns changes along the branches of the phylogenetic tree as close to the root as possible and minimize hypotheses of parallelism and favour reversals (Figures S9 and S10). A word of caution is required given that ACCTRAN (and also DELTRAN) may result in numerous equivocal resolutions when there is substantial amount of missing data as in the present dataset. For example, in Figure S10, character 55 (Projection nasal bones above frontomaxillary suture) is missing in *S. tchadensis*, *Ar. ramidus* and *Au. anamensis* but the change tapered to expanded is assigned by ACCTRAN at boundary 45, but could well be assigned at boundary 44 or 43, or even at the external boundary representing the first common ancestor which explains the symbol <--> given that eventuality.

Phylogenetic Networks method

The study of human evolution assumes a tree-like model represented by an optimal rooted phylogenetic tree with internal nodes (or elliptic boundaries in our analysis) symbolizing hypothetical last common ancestors (LCAs) emerging from speciation events. This dichotomous approach does not fully capture the complexity of evolutionary processes, particularly if the optimal solution is not unique such as the multiple MP trees (MMPT) obtained from running the analysis with 74 apomorphies summarized by a majority consensus tree (Figure 3). The amalgamation of conflicting hypotheses from incompatible multiple trees into a consensus tree represents a loss of phylogenetic information. The only way to decipher this loss of information from the collection of incompatible trees is by using the method of Phylogenetic Networks (PN) (Huson et al., 2010). PN is extensively employed in molecular biology, particularly to represent evolutionary relationships when the history of a set of taxa includes inheritance from multiple ancestors expressed as reticulate processes such as hybrid speciation or hybridization, horizontal gene-transfer and recombination (Morrison, 2011).

Standard concepts of graph theory are used to define phylogenetic networks; thus, the basic tool used to model them is a graph where taxa under study are represented by terminal nodes and evolutionary relationships between nodes are represented by edges (Huson and Scornavacca, 2010; Gross et al., 2019). For phylogenetic trees, edges are referred to as branches. As with phylogenetic trees, there are unrooted and rooted phylogenetic networks. Huson and Bryant (2006) distinguish three main types of phylogenetic networks: phylogenetic trees, splits networks and reticulate networks. Phylogenetic trees are used to summarize taxonomic relationships between biological entities, splits networks are used to represent incompatibilities in data sets reflected for example by polytomies of consensus trees, and reticulate networks are used to explain evolutionary histories with edges representing lineages of descent or reticulate events, and internal nodes representing hypothetical ancestors.

We run the PN analysis by using the SplitsTree software (Huson and Bryant, 2006) with the set of most parsimonious trees MMPT as input generated from the MP analysis run with 74 apormorphous characters, and produce graphically a consensus tree, a consensus network and a reticulate network (Figure 4). It is important to distinguish between data-display networks such as consensus trees and consensus networks, from evolutionary networks such as reticulation and hybridization. A consensus tree (Figure 4A, structurally identical to rooted consensus tree of Figure 3A) summarizes the parts of evolutionary scenarios that are in agreement; parts that are incompatible are suppressed and expressed as polytomies of unresolved nodes. On the contrary, a consensus network (Figure 4B) focuses on the alternative parts of the scenario that are incompatible and highlight the conflicting patterns that may cause reticulation by means of split parallelograms. Evolutionary networks (Figure 4C) display evolutionary events that have a causal relationship, the cause being subject to varying interpretation. Here, reticulation in coexisting taxa may be thought of as resulting from biological processes expressed by phenotypic apomorphies.

We must emphasize that, as illustrated in Figure 1 of Huson and Bryant (2006) summarizing the different types of Phylogenetic Networks concepts and the inputs required, our PN approach is not based on characters per se but on the multiple most parsimonious trees (MMPT) resulting from the MP analysis with apomorphous characters, in the same way that gene trees from a set of species are used to generate consensus networks and hybridization networks in

molecular biology. It is generally thought that polytomies have no value-added phylogenetic information in tree-based reconstruction. However, the reverse is true in the Phylogenetic Networks method. Polytomies represent conflicting patterns at certain nodes of incompatible multiple trees, and the information embedded in them allows the construction of consensus and reticulate networks in conjunction with the stable sister groups identified in the consensus tree.

There are conventions in defining a rooted PN (Morrison, 2011): "All of the internal nodes should be (inferred) ancestors and all of the edges (arcs) should represent inferred evolutionary events (with a direction of transformation). Nodes of in-degree 1 and out-degree at least 2 (one branch coming in and two or more going out) represent genetic divergence, and may be called “tree nodes”. Nodes of in-degree >1 (i.e. two or more lineages converge at what may be called a “reticulation node”) will indicate pooling of genetic material. The root node has in-degree 0 and out-degree at least 2 (no branches coming in and two or more going out). All of the branches are directed away from the root unless specified otherwise, and such specification will often be necessary for edges entering a reticulation node (or even to make clear which nodes are reticulation nodes). Such edges are called reticulation edges, while those associated with tree nodes are tree edges. The top node or origin of a reticulation cycle (or a complex tangle of reticulations) can be called the “split node” ". Many network methods are based on splits graphs where the edges denote bipartitions of the taxa with sets of parallel edges reflecting conflicting patterns in the form of parallelograms. A more elaborate set of definitions is available in Huson et al. (2010), and a summary interpretation of splits graphs in Morrison (2011).

Supplemental references

Agnarsson, I., and Miller, J. A. (2008). Is ACCTRAN better tha DELTRAN. Cladistics 24, 1–7.

Anderberg, A., and Tehler, A. (1990). Consensus trees, a necessity in taxonomic practice. Cladistics 6, 399–402.

Archie, J.W. (1989). Homoplasy Excess Ratios: New Indices for Measuring Levels of Homoplasy in Phylogenetic Systematics and a Critique of the Consistency Index. Systematic Zoology 38, 235– 269.

Camin, J. H., and Sokal, R. R. (1965). A method for deducing branching sequences in phylogeny. Evolution 19, 311–326.

Caparros, M. (1997). *Homo sapiens* archaïques : un ou plusieurs taxons (espèces) ? Analyse cladistique et morphométrique. PhD dissertation, Muséum National d'Histoire Naturelle, Paris.

Collard, M., and Wood, B.A. (2000). How reliable are human phylogenetic hypotheses? PNAS, 97, 5003–5006.

Cummings, M. P., Handley, S., Myers, S. D., Reed, D., Rokas, A., and Winka, K. (2003). Comparing Bootstrap and Posterior Probability Values in the Four-Taxon Case. Syst. Biol. 52, 477–487.

Darlu, P., and Tassy, P. (2019). La reconstruction phylogénétique: Concepts et méthodes (Editions Matériologiques).

Darwin, C. (1859). On the origin of species (Ed. John Murray).

Dembo, M., Radovčić, D., Garvin, H., Laird, M., Schroeder, L., Scott, J., Brophy, J., Ackermann, R., Musiba, C., de Ruiter, D. J., et al. (2016). The evolutionary relationships and age of *Homo naledi*: An assessment using dated Bayesian phylogenetic methods. J. Hum. Evol. 97, 17–26.

Efron, B. (1979). Bootstrapping methods: Another look at the jackknife. Ann. Stat. 7, 1–26.

Farris, J. S. (1969). A Successive Approximations Approach to Character Weighting. Syst. Zool. 18, 374–385.

Farris, J. S. (1970). Methods for computing Wagner Trees. Syst. Zool. 19, 83–92.

Farris, J. S. (1977). Phylogenetic analysis under Dollo's Law. Syst. Zool. 26, 77–88.

Farris, J. S. (1983). The logical basis of phylogenetic analysis. In: Platnick, N.I., Funk, V.A. (Eds.), Advances in Cladistics 2: Proceedings of the Second Meeting of the Willi Hennig Society, 7–36 (Columbia U. Press, NY).

Farris, J. S. (1989a). The retention index and homoplasy excess. Syst. Zool. 38, 406–407.

Farris, J.S. (1989b). The Retention Index and the Rescaled Consistency Index. Cladistics 5, 417–419.

Felsenstein, J. (1985). Confidence Limits on Phylogenies: An Approach Using the Bootstrap. Evolution 39 (4), 783–791.

Fitch, W. M. (1971). Toward defining the course of evolution: Minimal change for a specific tree topology. Syst. Zool. 20, 406–416.

Goloboff, P. A. (1991). Homoplasy and the choice among cladograms. Cladistics 7, 215–232.

Goloboff, P. A. (1993). Estimating character weights during tree search. Cladistics 9, 83–91.

Goloboff, P. A., and Pol, D. (2005). Parsimony and Bayesian Phylogenetics. In Parsimony, Phylogeny, and Genomics, V.A. Albert, ed. (Oxford University Press), pp. 148–159.

Goloboff, P. A, Carpenter, J. M., Arias, J. S., and Esquivel, D. R. M. (2008). Weighing against homoplasy improves phylogenetic analysis of morphological data sets. Cladistics 24, 758–773.

Gross, E., Long, C., and Rusinko, J. (2019). Phylogenetic Networks. arXiv:1906.01586v1 [q-bio.PE].

Hennig, W. (1966). Phylogenetic Systematics. Translated by D. Davis and R. Zangerl (University of Illinois Press).

Huson, D. H., and Bryant, D. (2006). Application of Phylogenetic Networks in Evolutionary Studies. Mol. Biol. Evol. 23, 254–267.

Huson, D. H., Rupp, R., and Scornavacca, C. (2010). Phylogenetic Networks: Concepts, Algorithms and Applications (Cambridge University Press).

Huson, D. H., and Scornavacca, C. (2011). A Survey of Combinatorial Methods for Phylogenetic Networks. Genom. Biol. and Evol. 3, 23–35.

Kornet, D. J., and Turner, H. (1999). Coding Polymorphism for Phylogeny Reconstruction. Syst. Zool. 48, 365–379.

Kluge, A. (1997). Sophisticated falsification and research cycles: consequences for differential character weighting in phylogenetic systematics. Zool. Scr. 26, 349–360.

Kluge, A. G. and Farris, J. S. (1969). Quantitative phyletics and the evolution of anurans. Syst. Zool. 18, 1-32.

Maddison, D.R., and W.P. Maddison (2005). MacClade software v. 4.08a, Sinauer Associates, Sunderland Massachusetts.

Mayr, E. (1942). Systematics and the origin of species from the viewpoint of a zoologist (Columbia Univ. Press).

Meier, R., Kores, P., and Darwin, S. (1991). Homoplasy slope ratio HSR: A better measurement of observed homoplasy in cladistic analyses. Syst. Zool. 40, 74–88.

Morrison, D. A. (2011). An Introduction to Phylogenetic Networks (RJR Productions).

Mounier, A., and Caparros, M. (2015). The phylogenetic status of *Homo heidelbergensis* - a cladistic study of Middle Pleistocene hominins. BMSAP 27**,** 110–134.

Mounier, A., Balzeau, A., Caparros, M., Grimaud-Hervé, D. (2016) Brain, calvarium, cladistics: A new approach to an old question, who are modern humans and Neandertals? J. Hum. Evol. 92, 22–36.

Popper, K. (1963). Conjectures and Refutations: The Growth of Scientific Knowledge (Routledge, London).

Popper, K. (1999). All life is problem solving (Routledge, London).

Simpson, G.G. (1953). The major features of evolution (Columbia University Press).

Simpson, G.G. (1961). Principles of Animal Taxonomy (Columbia University Press).

Soltis, P. S., and Soltis, D. E. (2003). Applying the Bootstrap in Phylogeny Reconstruction. Stat. Sci. 18 (2), 256–267.

Strait, D.S, and Grine, F.E. (2004). Inferring hominoid and early hominid phylogeny using craniodental characters: the role of fossil taxa. J. Hum. Evol. 47, 399–452.

Swofford, D. L. (2020). Phylogenetic Analysis Using Parsimony (PAUP), Version 4.0a.

Swofford, D. L., and Maddison, W. P. (1987). Reconstructing ancestral character states under Wagner parsimony. Math. Biosci. 87, 199–229.

Tassy, P. (1998). L'arbre à remonter le temps (Diderot Ed.).

Wagner, W. H. Jr. (1961). In *Recent Advances in Botany*. From lectures and symposia presented to the IX International Botanical Congress, Montreal, 1959, 841-844 (University of Toronto Press, 1961).

Wagner, W. H. Jr. (1963). Biosystematics and taxonomic categories in lower vascular plants. Regnum Veg. 27, 63–71.

White, T. D., Asfaw, B., Haile-Selassie, Y., Lovejoy, O., Suwa, G., and Woldegabriel, G. (2009). *Ardipithecus ramidus* and the Paleobiology of Early Hominids. Science 326, 75–86.

Wiens, J. J. (1999). Polymorphism in systematics and comparative biology. Ann. Rev. Ecol. Syst. 30, 327–362.

Supplementary Figures and Tables

- Figure S1. Methodological graphical framework. Related to Figures 1, 3 and 4
- Figure S2. Chronostratigraphic framework. Related to Figures 1, 2, 3 and 4
- Figure S3. MP and bootstrap trees from PAUP (Swofford, 2020) heuristic searches with Fitch parsimony unordered characters (Transparent Methods 1). Related to Tables 1 and 2
- Figure S4. MP and bootstrap trees from PAUP (Swofford, 2020) heuristic searches with Wagner parsimony ordered characters (Transparent Methods 1). Related to Tables 1 and 2
- Figure S5. MP and bootstrap trees from PAUP (Swofford, 2020) heuristic searches with Camin-Sokal parsimony irreversible characters (Transparent Methods 1). Related to Tables 1 and 2
- Figure S6. MP and bootstrap trees from PAUP (Swofford, 2020) heuristic searches with Dollo parsimony reversible characters (Transparent Methods 1). Related to Tables 1 and 2
- Figure S7. Elliptic representation of MPMAX cladogram. Related to Figure 1
- Figure S8. Character retention index ri formula and examples. Related to Figure 3, Transparent Methods 6 and Tables S1-S2
- Figure S9. Character-state changes (apomorphies) in support of stem species elliptic boundaries 40 to 26 (tree - nodes LCAs) of MPMAX scenario. Related to Figures 1 and 2A, and Table S3
- Figure S10. Character-state changes (apomorphies) in support of late Miocene - Pliocene stem species elliptic boundaries 46 to 41 (tree nodes - LCAs) of MPMAX scenario. Related to Figure 1
- Figure S11. MP and bootstrap trees from PAUP (Swofford, 2020) heuristic searches with dataset split of 288 unordered characters and 103 ordered characters as per Dembo et al. 2016 MP analysis in their Supplementary Online Material. Related to results concerning *H. naledi* and *Au. sediba* in main text *2. Comparative validation of MPMAX optimal scenario*, and Table S5

- Table S1. Character diagnostics from output of MPMAX run 15. Related to Figures 1 and S6E
- Table S2. List of 74 apomorphies in ascending identifying numbers in support of tree nodes / elliptic boundaries (LCAs) of MPMAX scenario. Related to Figures 3, S9 and S10
- Table S3. Apomorphies in support of stem elliptic boundaries/tree nodes 40 to 26. Related to Figures 1, 2A and S9
- Table S4. Summary of *H. naledi* and *Au. sediba* MP phylogenetic positions. Related to results concerning *H. naledi* and *Au. sediba* in main text *2. Comparative validation of MPMAX optimal scenario*, and Figures S3-S6
- Table S5. Inconsistencies for the Popperian elimination of evolutionary scenarios applied to dataset split of 288 unordered characters and 103 ordered characters as per Dembo et al. 2016. Related to results concerning *H. naledi* and *Au. sediba* in main text *2. Comparative validation of MPMAX optimal scenario*, and Figure S11

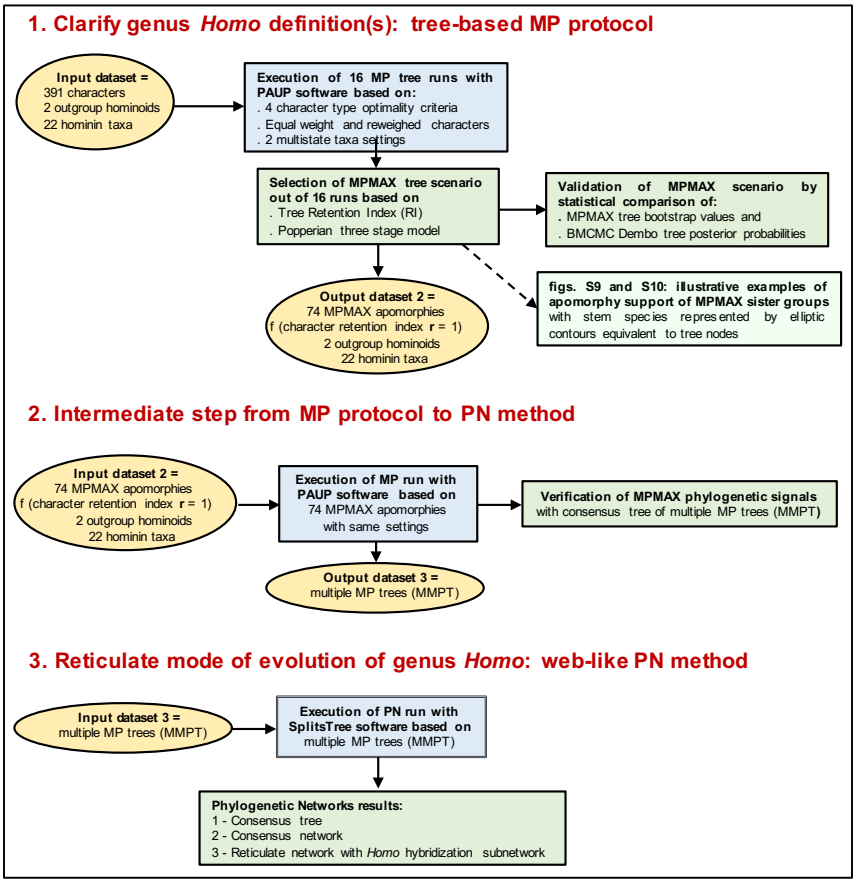

Figure S1. Methodological graphical framework. Related to Figures 1, 3 and 4
Phylogenetic reconstruction approach combining tree-based Maximum Parsimony (MP) protocol and web-like Phylogenetic Networks (PN) method.

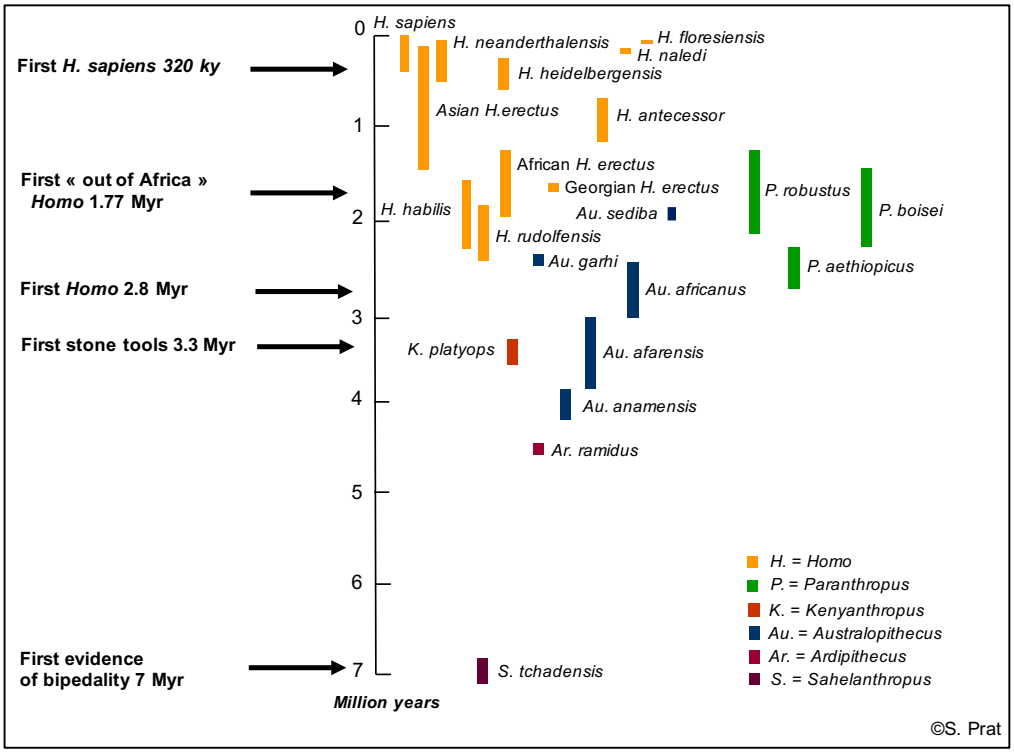

Figure S2. Chronostratigraphic framework. Related to Figures 1, 2, 3 and 4
Geological temporal ranges estimated from published research of fossil hominin species under study covering the period from late Miocene to Holocene.

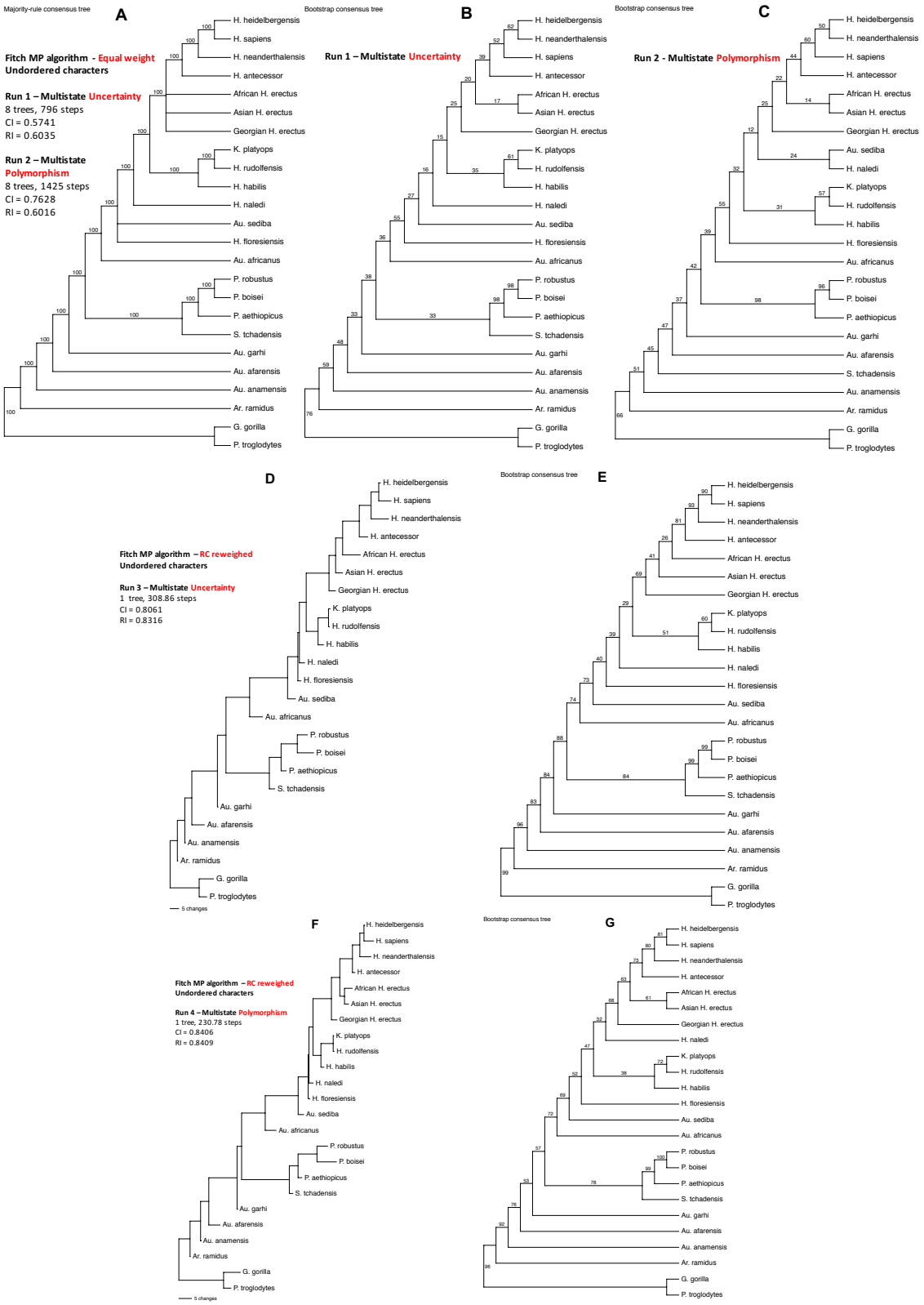

Figure S3. MP and bootstrap trees from PAUP (Swofford, 2020) heuristic searches with Fitch parsimony unordered characters (Transparent Methods 1). Related to Tables 1 and 2

Consensus MP and bootstrap trees include groups compatible with 50% majority-rule. Replicates P_{boot} indicated for all the clades in bootstrap trees.
(A) MP majority consensus tree of runs 1 and 2 with equally weighed characters and multistate taxa uncertainty or polymorphism settings.
(B) Bootstrap tree of run 1 (uncertainty).
(C) Bootstrap tree of run 2 (polymorphism).
(D) MP tree of run 3 with RC reweighed characters (Transparent Methods 3) and multistate taxa uncertainty setting.
(E) Bootstrap tree of run 3.
(F) MP tree of run 4 with RC reweighed characters and multistate taxa polymorphism setting.
(G) Bootstrap tree of run 4.

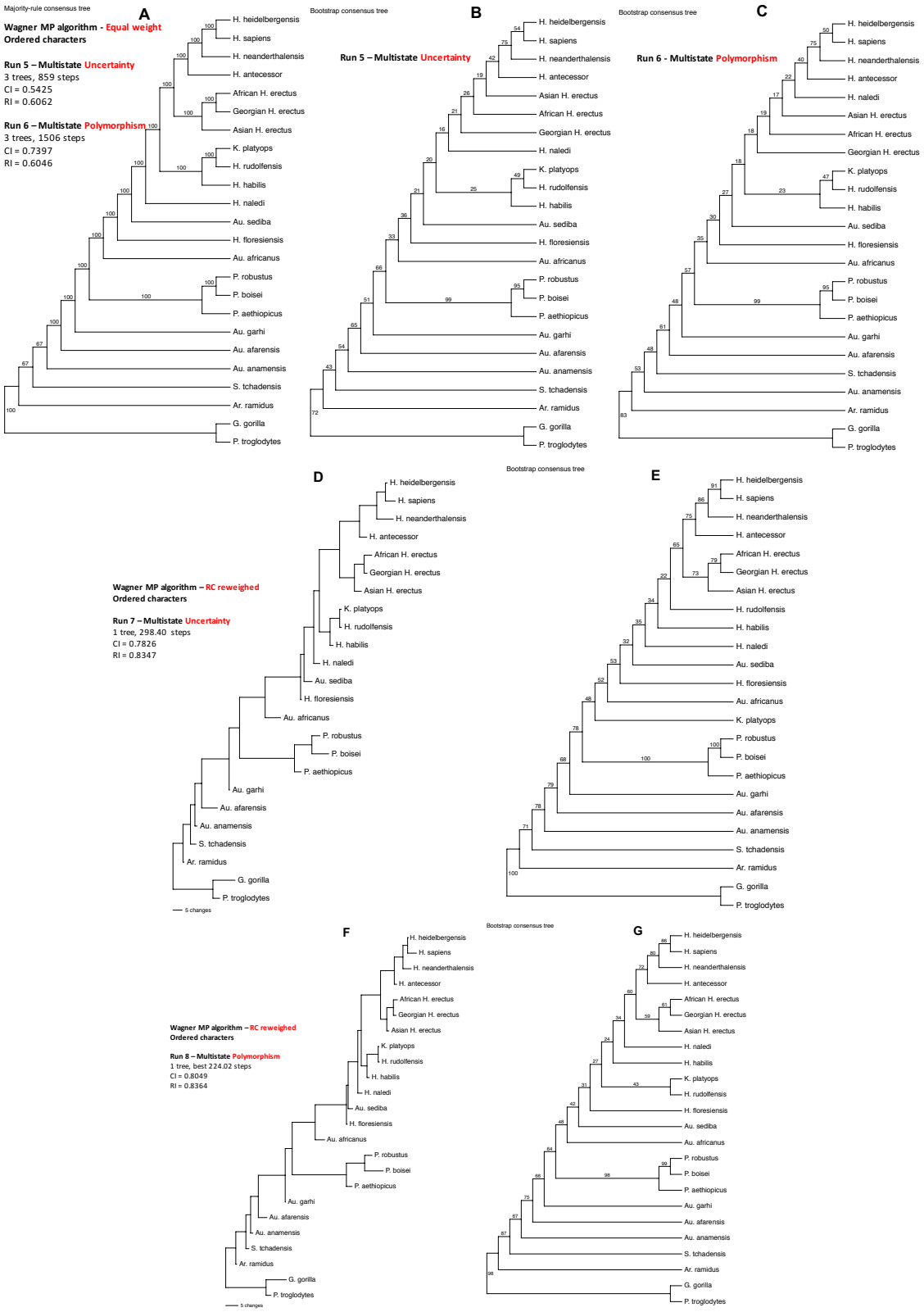

Figure S4. MP and bootstrap trees from PAUP (Swofford, 2020) heuristic searches with Wagner parsimony ordered characters (Transparent Methods 1). Related to Tables 1 and 2

Consensus MP and bootstrap trees include groups compatible with 50% majority-rule. Replicates P_{boot} indicated for all the clades in bootstrap trees.

(A) MP majority consensus tree of runs 5 and 6 with equally weighed characters and multistate taxa uncertainty or polymorphism settings.

(B) Bootstrap tree of run 5 (uncertainty).

(C) Bootstrap tree of run 6 (polymorphism).

(D) MP tree of run 7 with RC reweighed characters (Transparent Methods 3) and multistate taxa uncertainty setting.

(E) Bootstrap tree of run 7.

(F) MP tree of run 8 with RC reweighed characters and multistate taxa polymorphism setting.

(G) Bootstrap tree of run 8.

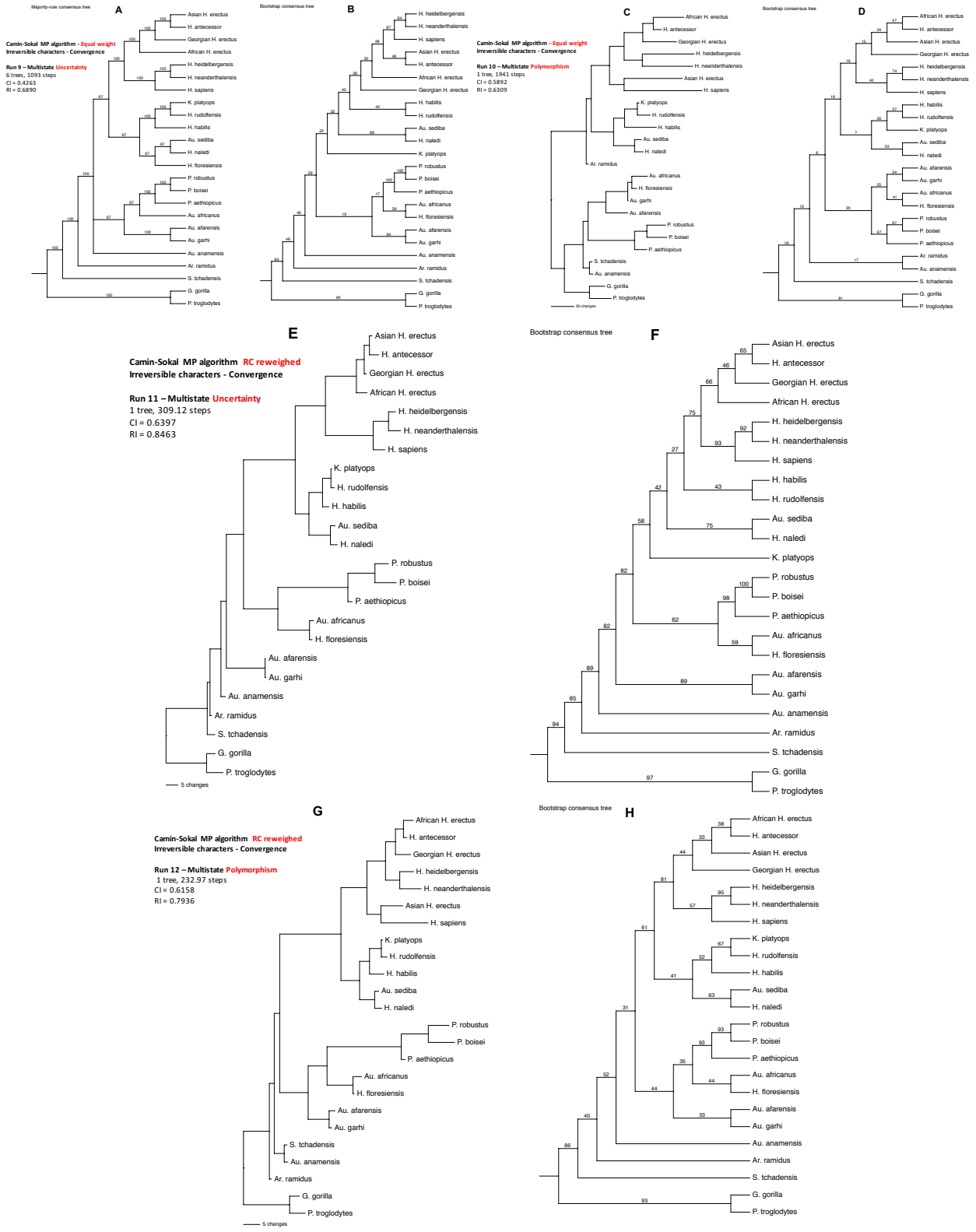

Figure S5. MP and bootstrap trees from PAUP (Swofford, 2020) heuristic searches with Camin-Sokal parsimony irreversible characters (Transparent Methods 1). Related to Tables 1 and 2

Consensus MP and bootstrap trees include groups compatible with 50% majority-rule. Replicates P_{boot} indicated for all the clades in bootstrap trees.
(A) MP majority consensus tree of run 9 with equally weighed characters and multistate taxa uncertainty setting.
(B) Bootstrap tree of run 9.
(C) MP tree of run 10 with equally weighed characters and multistate taxa polymorphism setting.
(D) Bootstrap tree of run 10.
(E) MP tree of run11 with RC reweighed characters (Transparent Methods 3) and multistate taxa uncertainty setting.
(F) Bootstrap tree of run 11. (G) MP tree of run 12 with RC reweighed characters and multistate taxa polymorphism setting.
(G) Bootstrap tree of run 12.

Figure S6. MP and bootstrap trees from PAUP (Swofford, 2020) heuristic searches with Dollo parsimony reversible characters (Transparent Methods 1). Related to Tables 1 and 2

Consensus MP and bootstrap trees include groups compatible with 50% majority-rule. Replicates P_{boot} indicated for all the clades in bootstrap trees.

(A) MP majority consensus tree of run 13 with equally weighed characters and multistate taxa uncertainty setting.

(B) Bootstrap tree of run 13.

(C) MP tree of run 14 with equally weighed characters and multistate taxa polymorphism setting.

(D) Bootstrap tree of run 14.

(E) MP tree of run15 (labelled MPMAX as most consistent informative phylogenetic scenario - Figure 1) with RC reweighed characters (Transparent Methods 3) and multistate taxa uncertainty setting.

(F) Bootstrap tree of run 15.

(G) MP tree of run 16 with RC reweighed characters and multistate taxa polymorphism setting. (G) Bootstrap tree of run 16.

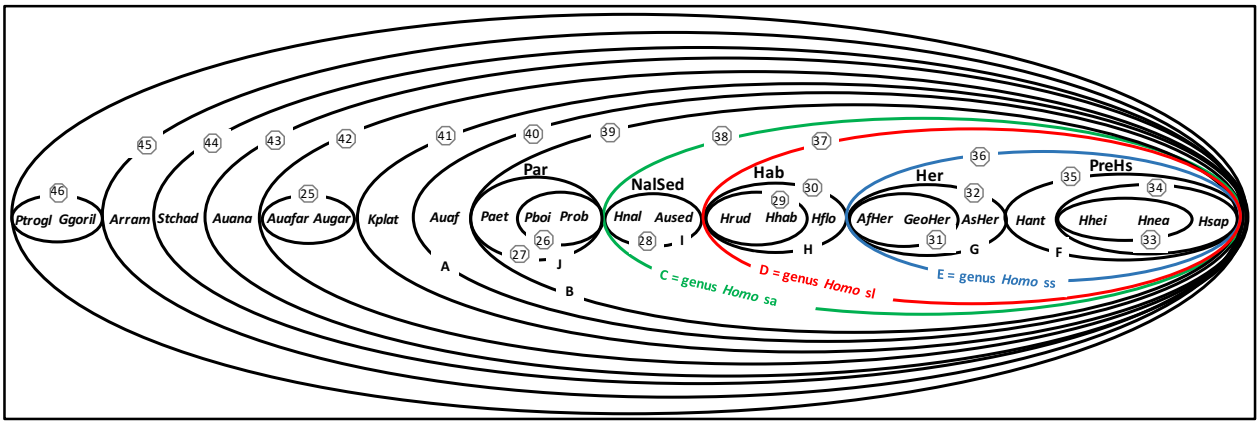

Figure S7. Elliptic representation of MPMAX cladogram. Related to Figure 1

The identifying node numbers of the hypothetical last common ancestors of the cladogram (Figure 1) are expressed as numbered stem species elliptic boundaries. The difference between the cladogram and the elliptic representation is the way the phylogenetic relationship is expressed between the stem species and its successor sister groups. In the cladogram, it is represented by the nodes (hypothetical ancestors) linking the dichotomous branches to its successors (two other nodes, or a node and a terminal, or two terminals). In the elliptic representation, the boundary lines of the stem species are drawn around their successor species, e.g. the elliptic boundary G is the *H. erectus* stem species (tree node 32 of Figure 1) from which three species have emerged ((African *H. erectus*, Georgian *H. erectus*), Asian *H. erectus*), and the stem species itself belongs to the sister group *H. erectus* = Her. The elliptic boundaries illustrate more accurately than the tree-based representation the formation of higher taxa monophyletic groups in conformity with the hierarchic system of phylogenetic systematics, and facilitate the interpretation of the ancestor-descendant relationships among the various hominin species under study. Refer to the legend of Figure 1 for sister group definitions.

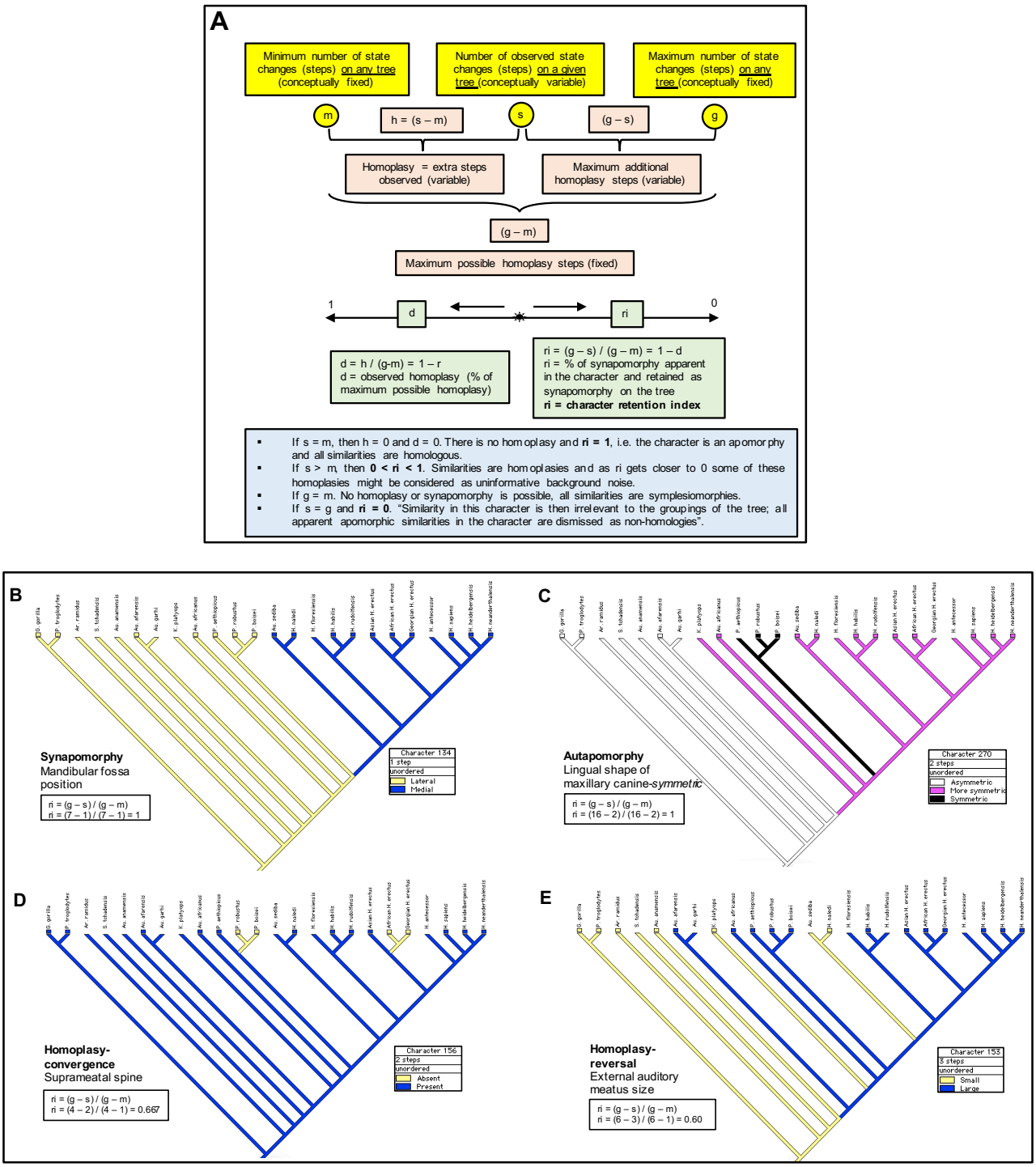

Figure S8. Character retention index ri formula and examples. Related to Figure 3, Transparent Methods 6 and Tables S1-S2

The examples are based on character diagnostics parameters from output of MPMAX run 15 (Table S1). Projection of characters on MPMAX tree were produced with MacClade software (Maddison and Maddison, 2005).

(A) Formula with graphical illustration and interpretation as per Farris (1989b).

(B) Example of synapomorphy of mandibular fossa position character.

(C) Example of autapomorphy in *Paranthropus* clade of lingual shape of maxillary canine character.

(D) Example of convergence homoplasy of suprameatal spine character.

(E) Example of reversal homoplasy of external auditory meatus size character.

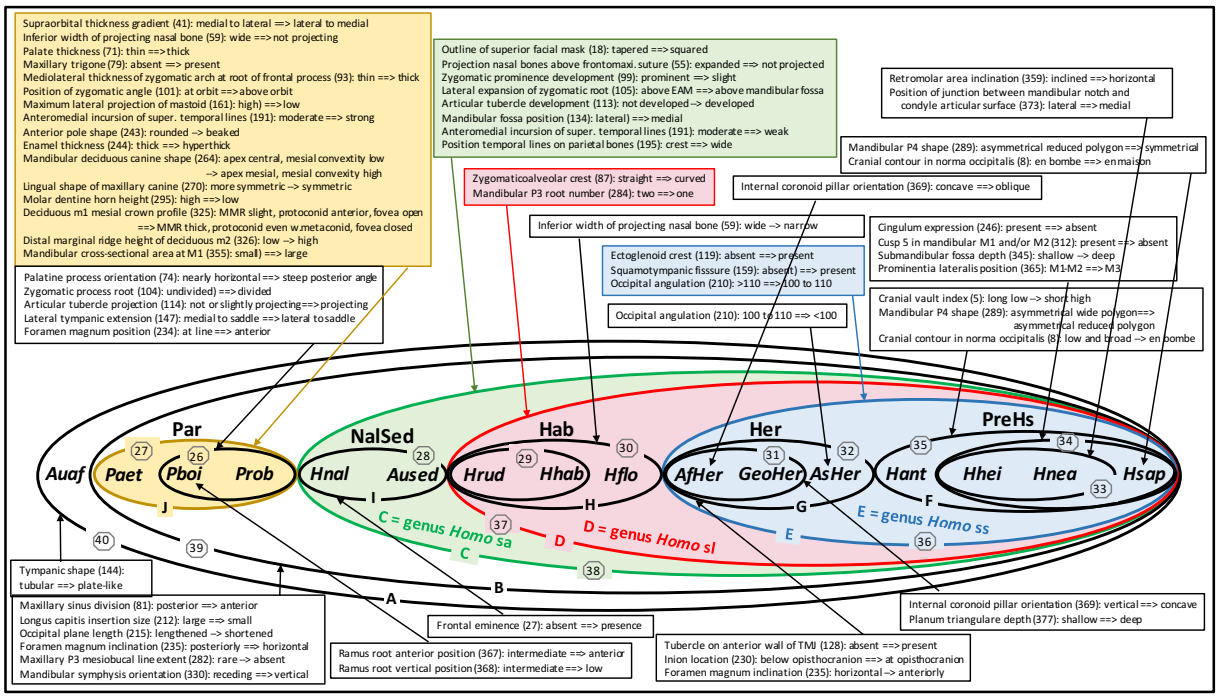

Figure S9. Character-state changes (apomorphies) in support of stem species elliptic boundaries 40 to 26 (tree nodes - LCAs) of MPMAX scenario. Related to Figures 1 and 2A, and Table S3

The species include *Au. africanus*, *Paranthropus* and *Homo* sister groups. Meaning of symbols: numbered stem boundaries correspond to nodes of Figure 1 tree, arrows from boxes to stem boundaries indicate supporting apomorphous character-state changes, ==> unambiguous characters and --> resolved ambiguous characters. ACCTRAN optimization is used for the treatment of ambiguities (Transparent Methods 7). The character changes highlighted for nested elliptic boundaries (stem taxa) A, B, C, D, E, F (PreHs), 34 and terminal *Hsap* (*H. sapiens*) are synapomorphies, i.e. morphological novelties passed on to succeeding nested monophyletic groups, whereas the novelties of the remaining lower sister groups J (Par), I (NalSed), H (Hab), G (Her) and stem boundaries 26, 31 and 33 are autapomorphies specific to these groups. Refer to the legend of Figure 1 for sister group definitions. The *Paranthropus* group Par with stem species J is the most supported clade thanks to 16 singular autapomorphies related to masticatory forces affecting mandibular, maxillar and postorbital morphology, along with a robust cranial architecture, which demonstrate that species of this group represent a parallel and distinct evolutionary lineage (Strait et al., 1997; Kimbel et al., 2004). For genus *Homo sensu amplo* (sa) C that includes all *Homo* species plus *Au. sediba*, eight subtle synapomorphous novelties come in support of this boundary, related essentially to facial changes and to a lesser extent cranial muscular insertion features: squared outline of superior facial mask (#18), not projected nasal bones above frontomaxillary suture (#55), slight zygomatic prominence development (#99), lateral expansion of zygomatic root above mandibular fossa (#105), developed articular tubercle (#113), medial mandibular fossa position (#134), weak anteromedial incursion of superior temporal lines (#191) and wide position temporal lines on parietal bones (#195). Boundary D, genus *Homo sensu lato* (sl) that includes all the *Homo* species minus *H. naledi*, is differentiated phylogenetically by two additional synapomorphies: curved zygomaticoalveolar crest (#87) and one mandibular P3 root (#284). Finally, genus *Homo sensu stricto* E, that excludes *H. rudolfensis*, *H. habilis* and *H. floresiensis*, is supported by three additional singular synapomorphies: presence of ectoglenoid crest (#119), presence of squamotympanic fisssure (#159) and occipital angulation between 100 and 110 degrees (#210).

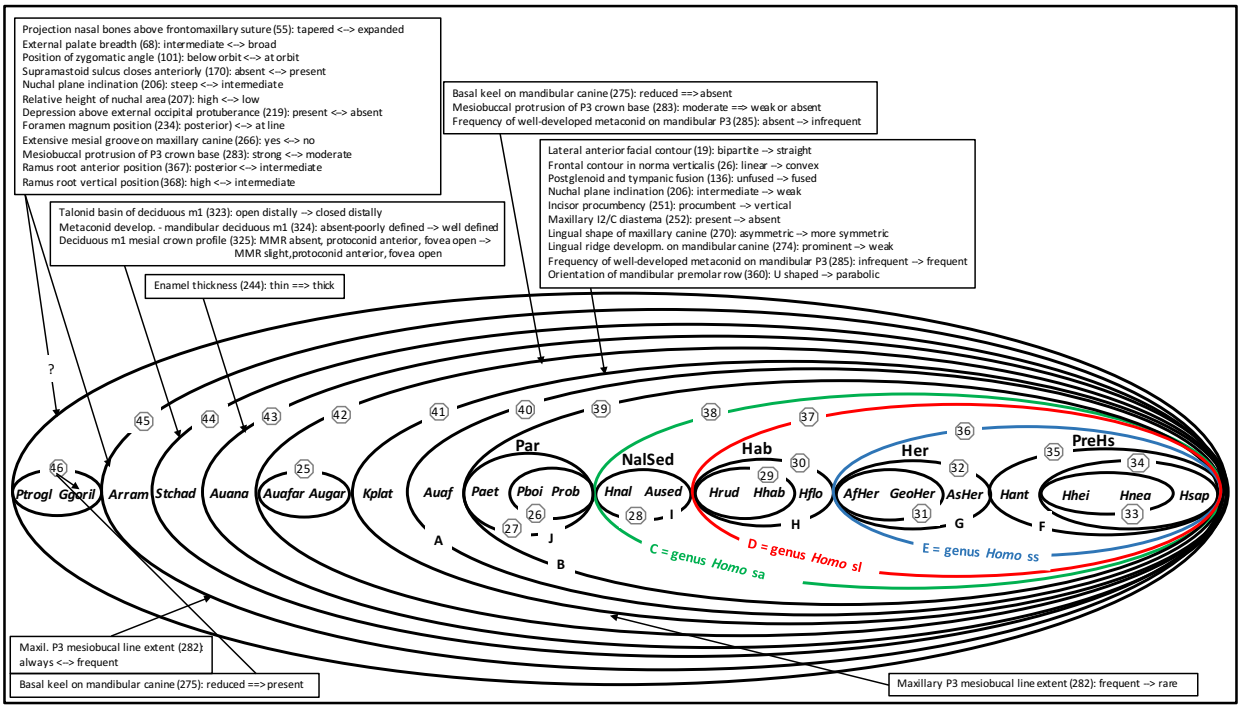

Figure S10. Character-state changes (apomorphies) in support of late Miocene - Pliocene stem species elliptic boundaries 46 to 41 (tree nodes - LCAs) of MPMAX scenario. Related to Figure 1

Symbols are as follows: numbered stem boundaries correspond to nodes of Figure 1 tree, arrows from boxes indicate assignment of apomorphous character-state changes to stem boundaries, unambiguous characters ==>, ambiguous characters --> and uncertain assignment of ambiguous characters at root <-->. ACCTRAN optimization method is used for the treatment of ambiguities (Transparent Methods 7). Most of the character apomorphies in support of the stem species elliptic boundaries/nodes 46 to 41 are ambiguous (Table S2), which renders their assignment to hypothetical ancestors (nodes/boundaries) uncertain and their anatomical interpretation arguable. Only three unambiguous apomorphies are identified. Enamel thickness (#244), changes from thin to thick at boundary 43 with *S. tchadensis* and *Ar. ramidus* sharing the archaic state thin with *G. gorilla* and *P. troglodytes*. This might explain the joint linkage of the former two in the polytomy of the consensus trees (Figure 3), and illustrate the probable shared phylogenetic position of these two hominins (White et al., 2009). At boundary 42, two synapomorphies appear: basal keel on mandibular canine (#275) changes from reduced to absent, while the mesiobuccal protrusion of P3 crown base (#283) evolves from moderate to weak or absent, bearing in mind that *Au. afarensis* manifested both states. These two dental novelties may support the phylogenetic inference of the evolutionary sequence *Ar. ramidus* → *Au. anamensis* → *Au. afarensis* based on dental and mandibular features (White et al., 2009). The large incidence of ambiguous characters is caused to a great extent by the high number of missing characters which makes the assignment at the boundaries (nodes of the tree) prone to equivocal interpretation, and therefore caution must be exercised. For example, character #55 (Projection nasal bones above frontomaxillary suture) is missing in *S. tchadensis*, *Ar. ramidus* and *Au. anamensis* but the change tapered to expanded is assigned by ACCTRAN at boundary 45, but could well be assigned at boundary 44 or 43, or even at the external boundary representing the first common ancestor which explains the symbol <--> given that eventuality.

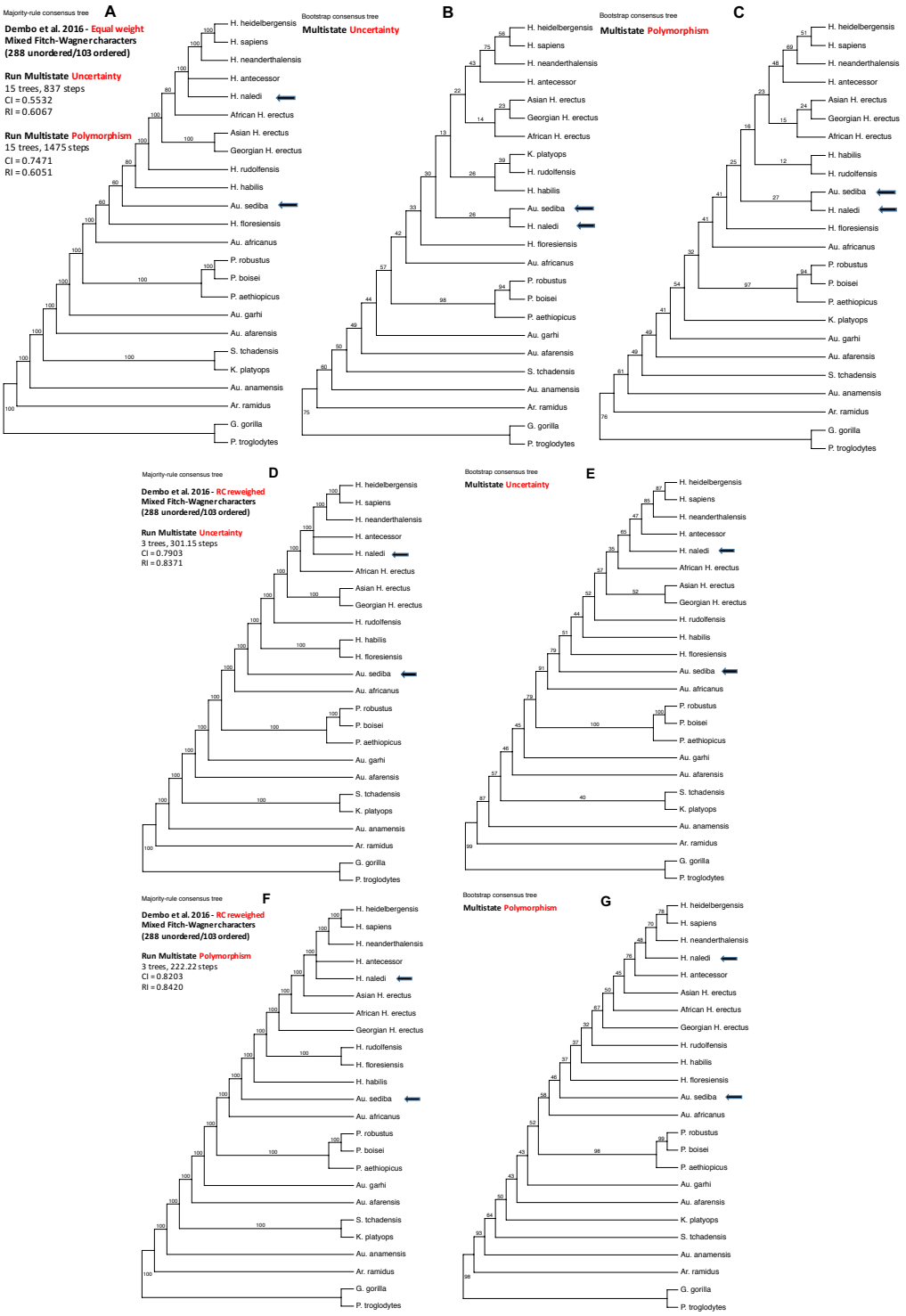

Figure S11. MP and bootstrap trees from PAUP (Swofford, 2020) heuristic searches with dataset split of 288 unordered characters and 103 ordered characters as per Dembo et al. 2016 MP analysis in their Supplementary Online Material. Related to results concerning *H. naledi* and *Au. sediba* in main text *2. Comparative validation of MPMAX optimal scenario*, and Table S5

Consensus MP and bootstrap trees include groups compatible with 50% majority-rule. Replicates P_{boot} are indicated for all the clades in the bootstrap trees.

(A) MP majority consensus tree with equally weighed characters under multistate taxa uncertainty or polymorphism settings. (B) Bootstrap consensus tree of run with equally weighed characters and uncertainty setting.

(C) Bootstrap consensus tree of run with equally weighed characters and polymorphism setting.

(D) MP majority consensus tree with RC reweighed characters and multistate taxa uncertainty setting.

(E) Bootstrap consensus tree of run with RC reweighed characters and uncertainty setting.

(F) MP majority consensus tree with RC reweighed characters and multistate taxa polymorphism setting.

(G) Bootstrap consensus tree of run with RC reweighed characters and polymorphism setting.

Table S1. Character diagnostics from output of MPMAX run 15. Related to Figures 1 and S6E

This run was executed with Dollo parsimony model, uncertainty setting for multistate taxa and characters reweighed with RCs with the full dataset. The list shows for each informative character its consistency index CI, retention index RI and rescaled consistency index RC = CI x RI. The RCs were used as weights in run 15 (Figure S6E) after executing initially run 13 with equal weigths (Figure S6A). The 74 apomorphies for the subsequent intermediate MP analysis (step 2 of Transparent Methods-Experimental Design) were selected on the basis of their character ri = 1 (Figure S8A, Transparent Methods 6) as recommended by Farris (1989b).

ri = (g – s) / (g – m) = RI character retention index
g = maximum number of steps
s = observed tree steps
m = minimum number of steps

Character diagnostics:

Character	Range	m Min steps	s Tree steps	g Max steps	CI	ri RI	RC	HI	G-fit
1	4	4	5	40	0.800	0.972	0.778	0.200	0.750
2	1	1	2	5	0.500	0.750	0.375	0.500	0.750
3	2	2	2	2	1.000	0/0	0/0	0.000	1.000
4	2	2	4	10	0.500	0.750	0.375	0.500	0.600
5	1	1	1	5	1.000	1.000	1.000	0.000	1.000
6	2	2	5	13	0.400	0.727	0.291	0.600	0.500
7	2	2	2	2	1.000	0/0	0/0	0.000	1.000
8	2	2	2	4	1.000	1.000	1.000	0.000	1.000
9	1	1	1	1	1.000	0/0	0/0	0.000	1.000
10	1	1	3	7	0.333	0.667	0.222	0.667	0.600
11	1	1	3	11	0.333	0.800	0.267	0.667	0.600
12	1	1	3	3	0.333	0.000	0.000	0.667	0.600
13	1	1	2	9	0.500	0.875	0.438	0.500	0.750
14	1	1	6	9	0.167	0.375	0.062	0.833	0.375
15	1	1	4	6	0.250	0.400	0.100	0.750	0.500
16	1	1	1	1	1.000	0/0	0/0	0.000	1.000
17	1	1	4	7	0.250	0.500	0.125	0.750	0.500
18	1	1	1	5	1.000	1.000	1.000	0.000	1.000
19	1	1	1	2	1.000	1.000	1.000	0.000	1.000
20	2	2	4	17	0.500	0.867	0.433	0.500	0.600
21	1	1	5	11	0.200	0.600	0.120	0.800	0.429
22	2	2	5	21	0.400	0.842	0.337	0.600	0.500
23	1	1	1	1	1.000	0/0	0/0	0.000	1.000
24	2	2	2	2	1.000	0/0	0/0	0.000	1.000
25	1	1	1	1	1.000	0/0	0/0	0.000	1.000
26	1	1	1	2	1.000	1.000	1.000	0.000	1.000
27	1	1	1	12	1.000	1.000	1.000	0.000	1.000
28	1	1	4	4	0.250	0.000	0.000	0.750	0.500
30	1	1	3	5	0.333	0.500	0.167	0.667	0.600
32	1	1	2	8	0.500	0.857	0.429	0.500	0.750
33	1	1	6	9	0.167	0.375	0.062	0.833	0.375
34	1	1	3	8	0.333	0.714	0.238	0.667	0.600
35	1	1	2	7	0.500	0.833	0.417	0.500	0.750
36	1	1	2	5	0.500	0.750	0.375	0.500	0.750
37	1	1	5	7	0.200	0.333	0.067	0.800	0.429
39	1	1	5	7	0.200	0.333	0.067	0.800	0.429
40	1	1	3	3	0.333	0.000	0.000	0.667	0.600
41	1	1	1	8	1.000	1.000	1.000	0.000	1.000
42	2	2	8	17	0.250	0.600	0.150	0.750	0.333
43	1	1	5	6	0.200	0.200	0.040	0.800	0.429
44	1	1	2	5	0.500	0.750	0.375	0.500	0.750
45	1	1	2	4	0.500	0.667	0.333	0.500	0.750
46	1	1	3	10	0.333	0.778	0.259	0.667	0.600
48	1	1	1	1	1.000	0/0	0/0	0.000	1.000
49	1	1	1	1	1.000	0/0	0/0	0.000	1.000
50	1	1	1	1	1.000	0/0	0/0	0.000	1.000
51	2	2	3	7	0.667	0.800	0.533	0.333	0.750
52	1	1	5	9	0.200	0.500	0.100	0.800	0.429
53	1	1	3	7	0.333	0.667	0.222	0.667	0.600
54	1	1	4	4	0.250	0.000	0.000	0.750	0.500
55	2	2	2	9	1.000	1.000	1.000	0.000	1.000
56	1	1	2	2	0.500	0.000	0.000	0.500	0.750
57	3	3	9	12	0.333	0.333	0.111	0.667	0.333
58	1	1	4	12	0.250	0.727	0.182	0.750	0.500
59	2	2	2	7	1.000	1.000	1.000	0.000	1.000
60	3	3	5	10	0.600	0.714	0.429	0.400	0.600
61	2	2	2	2	1.000	0/0	0/0	0.000	1.000
62	1	1	2	5	0.500	0.750	0.375	0.500	0.750
63	2	2	9	14	0.222	0.417	0.093	0.778	0.300
64	2	2	5	7	0.400	0.400	0.160	0.600	0.500
65	2	2	6	26	0.333	0.833	0.278	0.667	0.429
66	2	2	3	14	0.667	0.917	0.611	0.333	0.750
67	1	1	5	14	0.200	0.692	0.138	0.800	0.429
68	1	1	1	7	1.000	1.000	1.000	0.000	1.000
69	1	1	4	6	0.250	0.400	0.100	0.750	0.500
70	2	2	4	9	0.500	0.714	0.357	0.500	0.600
71	1	1	1	11	1.000	1.000	1.000	0.000	1.000
72	2	2	3	4	0.667	0.500	0.333	0.333	0.750
73	1	1	3	8	0.333	0.714	0.238	0.667	0.600
74	1	1	1	9	1.000	1.000	1.000	0.000	1.000
75	2	2	7	20	0.286	0.722	0.206	0.714	0.375
77	1	1	1	1	1.000	0/0	0/0	0.000	1.000
78	1	1	5	6	0.200	0.200	0.040	0.800	0.429
79	1	1	1	12	1.000	1.000	1.000	0.000	1.000
81	1	1	1	4	1.000	1.000	1.000	0.000	1.000
82	2	2	3	5	0.667	0.667	0.444	0.333	0.750
83	2	2	4	6	0.500	0.500	0.250	0.500	0.600
85	1	1	1	1	1.000	0/0	0/0	0.000	1.000
86	3	3	13	19	0.231	0.375	0.087	0.769	0.231
87	1	1	1	6	1.000	1.000	1.000	0.000	1.000
88	2	2	8	11	0.250	0.333	0.083	0.750	0.333
89	2	2	3	8	0.667	0.833	0.556	0.333	0.750
90	1	1	3	3	0.333	0.000	0.000	0.667	0.600
93	1	1	1	8	1.000	1.000	1.000	0.000	1.000
94	1	1	3	13	0.333	0.833	0.278	0.667	0.600
95	1	1	1	1	1.000	0/0	0/0	0.000	1.000
96	1	1	2	9	0.500	0.875	0.438	0.500	0.750
97	1	1	4	6	0.250	0.400	0.100	0.750	0.500
98	1	1	1	1	1.000	0/0	0/0	0.000	1.000
99	1	1	1	5	1.000	1.000	1.000	0.000	1.000
100	1	1	1	1	1.000	0/0	0/0	0.000	1.000
101	2	2	2	11	1.000	1.000	1.000	0.000	1.000
102	1	1	3	5	0.333	0.500	0.167	0.667	0.600
103	1	1	1	1	1.000	0/0	0/0	0.000	1.000
104	1	1	1	9	1.000	1.000	1.000	0.000	1.000
105	1	1	1	6	1.000	1.000	1.000	0.000	1.000
106	2	2	6	18	0.333	0.750	0.250	0.667	0.429
107	2	2	4	4	0.500	0.000	0.000	0.500	0.600
108	1	1	4	8	0.250	0.571	0.143	0.750	0.500
109	1	1	4	6	0.250	0.400	0.100	0.750	0.500
110	1	1	1	1	1.000	0/0	0/0	0.000	1.000
111	1	1	1	1	1.000	0/0	0/0	0.000	1.000
112	2	2	3	5	0.667	0.667	0.444	0.333	0.750
113	1	1	1	7	1.000	1.000	1.000	0.000	1.000
114	1	1	1	16	1.000	1.000	1.000	0.000	1.000
115	1	1	4	6	0.250	0.400	0.100	0.750	0.500
116	2	2	8	15	0.250	0.538	0.135	0.750	0.333
117	2	2	5	10	0.400	0.625	0.250	0.600	0.500
118	1	1	3	6	0.333	0.600	0.200	0.667	0.600
119	1	1	1	5	1.000	1.000	1.000	0.000	1.000
120	2	2	5	11	0.400	0.667	0.267	0.600	0.500
121	2	2	5	6	0.400	0.250	0.100	0.600	0.500
122	1	1	6	12	0.167	0.545	0.091	0.833	0.375
124	1	1	5	6	0.200	0.200	0.040	0.800	0.429
125	1	1	2	2	0.500	0.000	0.000	0.500	0.750
126	1	1	2	5	0.500	0.750	0.375	0.500	0.750
127	1	1	2	5	0.500	0.750	0.375	0.500	0.750
128	1	1	1	8	1.000	1.000	1.000	0.000	1.000
129	1	1	4	5	0.250	0.250	0.062	0.750	0.500
130	1	1	3	3	0.333	0.000	0.000	0.667	0.600
131	1	1	4	8	0.250	0.571	0.143	0.750	0.500
133	1	1	3	3	0.333	0.000	0.000	0.667	0.600
134	1	1	1	7	1.000	1.000	1.000	0.000	1.000
136	1	1	1	9	1.000	1.000	1.000	0.000	1.000
137	2	2	8	16	0.250	0.571	0.143	0.750	0.333
138	1	1	3	4	0.333	0.333	0.111	0.667	0.600
139	1	1	3	6	0.333	0.600	0.200	0.667	0.600
141	1	1	1	1	1.000	0/0	0/0	0.000	1.000
142	2	2	3	8	0.667	0.833	0.556	0.333	0.750
143	1	1	2	4	0.500	0.667	0.333	0.500	0.750
144	1	1	1	7	1.000	1.000	1.000	0.000	1.000
145	1	1	3	7	0.333	0.667	0.222	0.667	0.600
146	1	1	2	3	0.500	0.500	0.250	0.500	0.750
147	1	1	1	9	1.000	1.000	1.000	0.000	1.000
150	1	1	1	1	1.000	0/0	0/0	0.000	1.000
152	1	1	8	14	0.125	0.462	0.058	0.875	0.300
153	1	1	3	6	0.333	0.600	0.200	0.667	0.600
155	1	1	3	6	0.333	0.600	0.200	0.667	0.600
156	1	1	2	4	0.500	0.667	0.333	0.500	0.750
157	1	1	4	6	0.250	0.400	0.100	0.750	0.500
158	1	1	2	2	0.500	0.000	0.000	0.500	0.750
159	1	1	1	7	1.000	1.000	1.000	0.000	1.000
161	1	1	1	8	1.000	1.000	1.000	0.000	1.000
162	1	1	4	12	0.250	0.727	0.182	0.750	0.500
163	1	1	4	4	0.250	0.000	0.000	0.750	0.500
164	1	1	2	2	0.500	0.000	0.000	0.500	0.750
165	1	1	1	1	1.000	0/0	0/0	0.000	1.000
166	2	2	5	11	0.400	0.667	0.267	0.600	0.500
167	1	1	6	7	0.167	0.167	0.028	0.833	0.375
168	1	1	1	1	1.000	0/0	0/0	0.000	1.000
169	1	1	4	5	0.250	0.250	0.062	0.750	0.500
170	1	1	1	2	1.000	1.000	1.000	0.000	1.000
171	1	1	3	3	0.333	0.000	0.000	0.667	0.600
172	1	1	4	4	0.250	0.000	0.000	0.750	0.500
173	1	1	4	5	0.250	0.250	0.062	0.750	0.500
174	1	1	4	4	0.250	0.000	0.000	0.750	0.500
175	1	1	4	6	0.250	0.400	0.100	0.750	0.500
176	1	1	6	7	0.167	0.167	0.028	0.833	0.375
177	1	1	4	4	0.250	0.000	0.000	0.750	0.500
178	1	1	6	7	0.167	0.167	0.028	0.833	0.375
179	1	1	3	5	0.333	0.500	0.167	0.667	0.600
180	1	1	5	5	0.200	0.000	0.000	0.800	0.429
181	1	1	2	2	0.500	0.000	0.000	0.500	0.750
182	1	1	1	1	1.000	0/0	0/0	0.000	1.000
183	1	1	4	11	0.250	0.700	0.175	0.750	0.500
184	1	1	2	8	0.500	0.857	0.429	0.500	0.750
185	1	1	2	3	0.500	0.500	0.250	0.500	0.750
187	1	1	3	6	0.333	0.600	0.200	0.667	0.600
188	1	1	4	7	0.250	0.500	0.125	0.750	0.500
189	1	1	2	4	0.500	0.667	0.333	0.500	0.750
190	1	1	2	10	0.500	0.889	0.444	0.500	0.750
191	2	2	2	24	1.000	1.000	1.000	0.000	1.000
192	3	3	4	16	0.750	0.923	0.692	0.250	0.750
193	1	1	4	6	0.250	0.400	0.100	0.750	0.500
194	1	1	3	5	0.333	0.500	0.167	0.667	0.600
195	1	1	1	5	1.000	1.000	1.000	0.000	1.000
197	1	1	1	1	1.000	0/0	0/0	0.000	1.000
198	2	2	3	7	0.667	0.800	0.533	0.333	0.750
199	1	1	1	1	1.000	0/0	0/0	0.000	1.000
200	1	1	3	4	0.333	0.333	0.111	0.667	0.600
201	1	1	6	9	0.167	0.375	0.062	0.833	0.375
202	1	1	1	1	1.000	0/0	0/0	0.000	1.000
203	1	1	3	7	0.333	0.667	0.222	0.667	0.600
204	1	1	2	5	0.500	0.750	0.375	0.500	0.750
205	1	1	2	7	0.500	0.833	0.417	0.500	0.750
206	2	2	2	5	1.000	1.000	1.000	0.000	1.000
207	1	1	1	2	1.000	1.000	1.000	0.000	1.000
208	2	2	6	13	0.333	0.636	0.212	0.667	0.429
209	2	2	3	9	0.667	0.857	0.571	0.333	0.750
210	2	2	2	4	1.000	1.000	1.000	0.000	1.000
211	1	1	2	5	0.500	0.750	0.375	0.500	0.750
212	1	1	1	3	1.000	1.000	1.000	0.000	1.000
213	2	2	3	10	0.667	0.875	0.583	0.333	0.750
215	1	1	1	5	1.000	1.000	1.000	0.000	1.000
216	1	1	2	4	0.500	0.667	0.333	0.500	0.750
217	1	1	3	6	0.333	0.600	0.200	0.667	0.600
218	1	1	1	1	1.000	0/0	0/0	0.000	1.000
219	1	1	1	6	1.000	1.000	1.000	0.000	1.000
220	1	1	4	11	0.250	0.700	0.175	0.750	0.500
221	1	1	4	4	0.250	0.000	0.000	0.750	0.500
222	1	1	1	1	1.000	0/0	0/0	0.000	1.000
223	1	1	1	1	1.000	0/0	0/0	0.000	1.000
224	2	2	2	2	1.000	0/0	0/0	0.000	1.000
225	1	1	5	5	0.200	0.000	0.000	0.800	0.429
226	1	1	3	5	0.333	0.500	0.167	0.667	0.600
227	1	1	4	13	0.250	0.750	0.188	0.750	0.500
228	1	1	2	4	0.500	0.667	0.333	0.500	0.750
229	1	1	2	6	0.500	0.800	0.400	0.500	0.750
230	1	1	1	3	1.000	1.000	1.000	0.000	1.000
231	1	1	1	1	1.000	0/0	0/0	0.000	1.000
232	2	2	12	26	0.167	0.583	0.097	0.833	0.231
233	1	1	2	9	0.500	0.875	0.438	0.500	0.750
234	2	2	2	12	1.000	1.000	1.000	0.000	1.000
235	2	2	2	4	1.000	1.000	1.000	0.000	1.000
236	2	2	4	6	0.500	0.500	0.250	0.500	0.600
237	2	2	3	7	0.667	0.800	0.533	0.333	0.750
238	2	2	2	2	1.000	0/0	0/0	0.000	1.000
239	2	2	4	7	0.500	0.600	0.300	0.500	0.600
240	2	2	3	9	0.667	0.857	0.571	0.333	0.750
241	1	1	4	4	0.250	0.000	0.000	0.750	0.500
242	1	1	3	4	0.333	0.333	0.111	0.667	0.600
243	1	1	1	8	1.000	1.000	1.000	0.000	1.000
244	2	2	2	18	1.000	1.000	1.000	0.000	1.000
245	2	2	3	12	0.667	0.900	0.600	0.333	0.750
246	1	1	1	7	1.000	1.000	1.000	0.000	1.000
248	1	1	7	10	0.143	0.333	0.048	0.857	0.333
249	2	2	8	18	0.250	0.625	0.156	0.750	0.333
250	1	1	2	3	0.500	0.500	0.250	0.500	0.750
251	1	1	1	2	1.000	1.000	1.000	0.000	1.000
252	1	1	1	12	1.000	1.000	1.000	0.000	1.000
253	2	2	8	16	0.250	0.571	0.143	0.750	0.333
255	2	2	5	9	0.400	0.571	0.229	0.600	0.500
256	2	2	6	9	0.333	0.429	0.143	0.667	0.429
257	1	1	2	7	0.500	0.833	0.417	0.500	0.750
258	1	1	3	12	0.333	0.818	0.273	0.667	0.600
260	2	2	3	6	0.667	0.750	0.500	0.333	0.750
261	1	1	5	6	0.200	0.200	0.040	0.800	0.429
262	1	1	1	1	1.000	0/0	0/0	0.000	1.000
263	2	2	4	6	0.500	0.500	0.250	0.500	0.600
264	1	1	1	7	1.000	1.000	1.000	0.000	1.000
265	2	2	4	14	0.500	0.833	0.417	0.500	0.600
266	1	1	1	2	1.000	1.000	1.000	0.000	1.000
267	1	1	4	9	0.250	0.625	0.156	0.750	0.500
268	1	1	1	1	1.000	0/0	0/0	0.000	1.000
269	1	1	3	4	0.333	0.333	0.111	0.667	0.600
270	2	2	2	16	1.000	1.000	1.000	0.000	1.000
271	1	1	2	4	0.500	0.667	0.333	0.500	0.750
272	1	1	2	5	0.500	0.750	0.375	0.500	0.750
273	1	1	2	4	0.500	0.667	0.333	0.500	0.750
274	1	1	1	3	1.000	1.000	1.000	0.000	1.000
275	2	2	2	5	1.000	1.000	1.000	0.000	1.000
276	1	1	3	10	0.333	0.778	0.259	0.667	0.600
277	2	2	5	23	0.400	0.857	0.343	0.600	0.500
278	1	1	3	4	0.333	0.333	0.111	0.667	0.600
279	1	1	1	1	1.000	0/0	0/0	0.000	1.000
280	1	1	3	3	0.333	0.000	0.000	0.667	0.600
281	1	1	4	5	0.250	0.250	0.062	0.750	0.500
282	3	3	3	9	1.000	1.000	1.000	0.000	1.000
283	2	2	2	6	1.000	1.000	1.000	0.000	1.000
284	1	1	1	5	1.000	1.000	1.000	0.000	1.000
285	2	2	2	9	1.000	1.000	1.000	0.000	1.000
286	3	3	6	13	0.500	0.700	0.350	0.500	0.500
287	3	3	6	8	0.500	0.400	0.200	0.500	0.500
288	1	1	2	7	0.500	0.833	0.417	0.500	0.750
289	2	2	2	7	1.000	1.000	1.000	0.000	1.000
290	2	2	11	22	0.182	0.550	0.100	0.818	0.250
291	1	1	5	5	0.200	0.000	0.000	0.800	0.429
293	1	1	1	1	1.000	0/0	0/0	0.000	1.000
294	1	1	1	1	1.000	0/0	0/0	0.000	1.000
295	1	1	1	5	1.000	1.000	1.000	0.000	1.000
296	3	3	4	36	0.750	0.970	0.727	0.250	0.750
297	1	1	1	1	1.000	0/0	0/0	0.000	1.000
298	1	1	1	1	1.000	0/0	0/0	0.000	1.000
299	4	4	10	47	0.400	0.860	0.344	0.600	0.333
300	1	1	4	10	0.250	0.667	0.167	0.750	0.500
301	1	1	3	5	0.333	0.500	0.167	0.667	0.600
302	1	1	2	7	0.500	0.833	0.417	0.500	0.750
303	2	2	4	12	0.500	0.800	0.400	0.500	0.600
304	1	1	1	1	1.000	0/0	0/0	0.000	1.000
305	4	4	8	12	0.500	0.500	0.250	0.500	0.429
306	2	2	4	5	0.500	0.333	0.167	0.500	0.600
307	1	1	3	7	0.333	0.667	0.222	0.667	0.600
308	4	4	10	20	0.400	0.625	0.250	0.600	0.333
309	2	2	4	6	0.500	0.500	0.250	0.500	0.600
311	1	1	2	4	0.500	0.667	0.333	0.500	0.750
312	1	1	1	7	1.000	1.000	1.000	0.000	1.000
313	1	1	3	11	0.333	0.800	0.267	0.667	0.600
314	1	1	3	7	0.333	0.667	0.222	0.667	0.600
315	1	1	1	1	1.000	0/0	0/0	0.000	1.000
316	2	2	4	8	0.500	0.667	0.333	0.500	0.600
319	1	1	4	7	0.250	0.500	0.125	0.750	0.500
320	1	1	3	5	0.333	0.500	0.167	0.667	0.600
322	2	2	4	14	0.500	0.833	0.417	0.500	0.600
323	1	1	1	3	1.000	1.000	1.000	0.000	1.000
324	1	1	1	3	1.000	1.000	1.000	0.000	1.000
325	2	2	2	14	1.000	1.000	1.000	0.000	1.000
326	1	1	1	7	1.000	1.000	1.000	0.000	1.000
327	1	1	1	1	1.000	0/0	0/0	0.000	1.000
329	2	2	6	17	0.333	0.733	0.244	0.667	0.429
330	1	1	1	5	1.000	1.000	1.000	0.000	1.000
331	2	2	5	15	0.400	0.769	0.308	0.600	0.500
333	1	1	5	10	0.200	0.556	0.111	0.800	0.429
334	1	1	2	3	0.500	0.500	0.250	0.500	0.750
335	1	1	1	1	1.000	0/0	0/0	0.000	1.000
338	1	1	1	1	1.000	0/0	0/0	0.000	1.000
339	3	3	11	30	0.273	0.704	0.192	0.727	0.273
340	1	1	3	10	0.333	0.778	0.259	0.667	0.600
341	1	1	1	1	1.000	0/0	0/0	0.000	1.000
342	1	1	1	1	1.000	0/0	0/0	0.000	1.000
343	1	1	1	1	1.000	0/0	0/0	0.000	1.000
344	1	1	1	1	1.000	0/0	0/0	0.000	1.000
345	1	1	1	4	1.000	1.000	1.000	0.000	1.000
346	1	1	2	2	0.500	0.000	0.000	0.500	0.750
347	2	2	5	19	0.400	0.824	0.329	0.600	0.500
348	1	1	8	12	0.125	0.364	0.045	0.875	0.300
349	3	3	9	23	0.333	0.700	0.233	0.667	0.333
350	1	1	2	2	0.500	0.000	0.000	0.500	0.750
351	1	1	2	7	0.500	0.833	0.417	0.500	0.750
352	1	1	2	2	0.500	0.000	0.000	0.500	0.750
353	1	1	4	4	0.250	0.000	0.000	0.750	0.500
355	1	1	1	15	1.000	1.000	1.000	0.000	1.000
356	1	1	2	9	0.500	0.875	0.438	0.500	0.750
357	1	1	4	6	0.250	0.400	0.100	0.750	0.500
358	1	1	1	1	1.000	0/0	0/0	0.000	1.000
359	1	1	1	2	1.000	1.000	1.000	0.000	1.000
360	1	1	1	7	1.000	1.000	1.000	0.000	1.000
361	1	1	2	10	0.500	0.889	0.444	0.500	0.750
364	1	1	1	1	1.000	0/0	0/0	0.000	1.000
365	2	2	2	6	1.000	1.000	1.000	0.000	1.000
366	1	1	3	4	0.333	0.333	0.111	0.667	0.600
367	2	2	2	3	1.000	1.000	1.000	0.000	1.000
368	2	2	2	3	1.000	1.000	1.000	0.000	1.000
369	2	2	2	6	1.000	1.000	1.000	0.000	1.000
370	1	1	1	1	1.000	0/0	0/0	0.000	1.000
371	1	1	2	3	0.500	0.500	0.250	0.500	0.750
372	1	1	1	1	1.000	0/0	0/0	0.000	1.000
373	1	1	1	2	1.000	1.000	1.000	0.000	1.000
374	1	1	1	1	1.000	0/0	0/0	0.000	1.000
375	2	2	2	2	1.000	0/0	0/0	0.000	1.000
376	2	2	5	5	0.400	0.000	0.000	0.600	0.500
377	1	1	1	3	1.000	1.000	1.000	0.000	1.000
378	1	1	1	1	1.000	0/0	0/0	0.000	1.000
379	1	1	2	2	0.500	0.000	0.000	0.500	0.750
381	1	1	1	1	1.000	0/0	0/0	0.000	1.000
384	2	2	3	3	0.667	0.000	0.000	0.333	0.750
385	1	1	1	1	1.000	0/0	0/0	0.000	1.000
386	1	1	2	3	0.500	0.500	0.250	0.500	0.750
387	1	1	1	1	1.000	0/0	0/0	0.000	1.000
388	2	2	3	3	0.667	0.000	0.000	0.333	0.750
391	1	1	1	1	1.000	0/0	0/0	0.000	1.000

(41 constant characters not shown)

Table S2. List of 74 apomorphies in ascending identifying numbers in support of tree nodes / elliptic boundaries (LCAs) of MPMAX scenario. Related to Figures 3, S9 and S10

Apomorphies are selected from run output with ri = 1 (Table S1) and meaning of symbols is as follows: ==> unambiguous characters, --> ACCTRAN resolved ambiguous characters (Transparent Methods 7), <--> ACCTRAN uncertain assignment of ambiguous characters at root, # character number, *S = synapomorphy, *A = autapomorphy.

Morphological apomorphies with R = 1	#	*	State changes in the cladogram
Cranial vault index	5	S	node 36 (long low) --> node 35 (short high)
Cranial contour in norma occipitalis	8	S	node 36 (low and broad) ==> node 35 (en bombe)
		S	node 34 (en bombe) --> *H. sapiens* (en maison)
Outline of superior facial mask	18	S	node 39 (tapered) ==> node 38 (squared)
Lateral anterior facial contour	19	S	node 42 (bipartite) --> node 41(straight)
Frontal contour in norma verticalis	26	S	node 42 (linear) --> node 41 (convex)
Frontal eminence	27	A	node 38 (absent) ==> node 28 (presence)
Supraorbital thickness gradient	41	A	node 39 (med. to lateral) ==> node 27 (later. to medial)
Projection nasal bones above frontomaxillary suture	55	S	node 46 (tapered) <--> node 45 (expanded)
		S	node 39 (expanded) ==> node 38 (not projected)
Inferior width of projecting nasal bone	59	A	node 39 (wide) ==> node 27 (not projecting)
		A	node 37 (wide) --> node 30 (narrow)
External palate breadth	68	S	node 46 (intermediate) <--> node 45 (broad)
Palate thickness	71	A	node 39 (thin) ==> node 27 (thick)
Palatine process orientation	74	A	node 27 (nearly horiz.) ==> node 26 (steep post. angle)
Maxillary trigone	79	A	node 39 (absent) ==> node 27 (present)
Maxillary sinus division	81	S	node 40 (posterior) ==> node 39 (anterior)
Zygomaticoalveolar crest	87	S	node 38 (straight) ==> node 37 (curved)
Mediolateral thickness of zygomatic arch at root of frontal process	93	A	node 39 (thin) ==> node 27 (thick)
Zygomatic prominence development	99	S	node 39 (prominent) ==> node 38 (slight)
Position of zygomatic angle	101	S	node 46 (below orbit) <--> node 45 (at orbit)
		A	node 39 (at orbit) ==> node 27 (above orbit)
Zygomatic process root	104	A	node 27 (undivided) ==> node 26 (divided)
Lateral expansion of zygomatic root	105	S	node 39 (above EAM) ==> node 38 (above mand.fossa)
Articular tubercle development	113	S	node 39 (not developed) --> (developed) node 38
Articular tubercle projection	114	A	node 27 (not-slightly projecting)==> node 26 (projecting)
Ectoglenoid crest	119	S	node 37 (absent) ==> node 36 (present)
Tubercle on anterior wall of TMJ	128	A	node 36 (absent) ==> node 32 (present)
Mandibular fossa position	134	S	node 39 (lateral) ==> node 38 (medial)
Postglenoid and tympanic fusion	136	S	node 42 (unfused) --> node 41 (fused)
Tympanic shape	144	S	node 41 (tubular) ==> node 40 (plate-like)
Lateral tympanic extension	147	A	node 27 (medial to saddle) ==> node 26 (lat. to saddle)
Squamotympanic fisssure	159	S	node 37 (absent) ==> node 36 (present)
Maximum lateral projection of mastoid	161	A	node 39 (high) ==> node 27 (low)
Supramastoid sulcus closes anteriorly	170	S	node 46 (absent) <--> node 45 (present)
Anteromedial incursion of superior temporal lines	191	A	node 39 (moderate) ==> node 27 (strong)
		S	node 39 (moderate) ==> node 38 (weak)
Position temporal lines on parietal bones	195	S	node 39 (crest) ==> node 38 (wide)
Nuchal plane inclination	206	S	node 46 (steep) <--> node 45 (intermediate)
		S	node 42 (intermediate) --> node 41 (weak)
Relative height of nuchal area	207	S	node 46 (high) <--> node 45 (low)
Occipital angulation	210	S	node 37 (>110) ==> node 36 (100 to 110)
		A	node 32 (100 to 110) ==> Asian *H. erectus* (<100)
Longus capitis insertion size	212	S	node 40 (large) ==> node 39 (small)
Occipital plane length	215	S	node 40 (lenghtened) --> node 39 (shortened)
Depression above external occipital protuberance	219	S	node 46 (present) <--> node 45 (absent)
Inion location	230	A	node 36 (below opisthocranion) ==> node 32 (at opisth.)
Foramen magnum position	234	S	node 46 (posterior) <==> node 45 (at line)
		A	node 27 (at line) ==> node 26 (anterior)
Foramen magnum inclination	235	S	node 40 (posteriorly) ==> node 39 (horizontal)
		A	node 36 (horizontal) --> node 32 (anteriorly)
Anterior pole shape	243	A	node 39 (rounded) --> node 27 (beaked)
Enamel thickness	244	S	node 44 (thin) ==> node 43 (thick)
		A	node 39 (thick) ==> node 27 (hyperthick)
Cingulum expression	246	S	node 35 (present) ==> node 34 (absent)
Incisor procumbency	251	S	node 42 (procumbent) --> node 41 (vertical)
Maxillary I2/C diastema	252	S	node 42 (present) --> node 41 (absent)
Mandibular deciduous canine shape	264	A	node 39 (apex cent., mesial convext.low) --> node 27 (apex mesial, mesial convexity high)
Extensive mesial groove on maxillary canine	266	S	node 46 (yes) <==> node 45 (no)
Lingual shape of maxillary canine	270	S	node 42 (asymmetric) --> node 41 (more symmetric)
		A	node 39 (more symmetric) --> node 27 (symmetric)
Lingual ridge developm. on mandibular canine	274	S	node 42 (prominent) --> node 41 (weak)
Basal keel on mandibular canine	275	A	node 46 (reduced) ==> *Gorilla* (present)
		S	node 43 (reduced) ==> node 42 (absent)
Maxillary P3 mesiobucal line extent	282	S	node 46 (always) <--> node 45 (frequent)
		S	node 42 (frequent) --> node 41 (rare)
		S	node 40 (rare) --> node 39 (absent)
Mesiobuccal protrusion of P3 crown base	283	S	node 46 (strong) <==> node 45 (moderate)
		S	node 43 (moderate) ==> node 42 (weak or absent)
Mandibular P3 root number	284	S	node 38 (two) ==> node 37 (one)
Frequency of well-developed metaconid on mandibular P3	285	S	node 43 (absent) --> node 42 (infrequent)
		S	node 42 (infrequent) --> node 41 (frequent)
Mandibular P4 shape	289	S	node 36 (asym. wide pol.) ==> node 35 (asym. reduc. pol)
		A	node 34 (asym. reduc. pol) ==> *H. sapiens* (symmetrical)
Molar dentine horn height	295	A	node 39 (high) ==> node 27 (low)
Cusp 5 in mandibular M1 and/or M2	312	S	node 35 (present) ==> node 34 (absent)
Talonid basin of deciduous m1	323	S	node 45 (open distally) --> node 44 (closed distally)
Metaconid development on mandibular deciduous m1	324	S	node 45 (absent-poorly defined) --> node 44 (well defin.)
Deciduous m1 mesial crown profile	325	S	node 45 (MMR absent, protoconid anterior, fovea open) --> node 44 (MMR slight, protocon. anterior, fovea open)
		A	node 39 (MMR slight, protoconid anterior, fovea open) ==> node 27 (MMR thick,protoconid even w.metaconid, fovea closed)
Distal marginal ridge height of deciduous m2	326	A	node 39 (low) --> node 27 (high)
Mandibular symphisis orientation	330	S	node 40 (receding) ==> node 39 (vertical)
Submandibular fossa depth	345	S	node 35 (shallow) --> node 34 (deep)
Mandibular cross-sectional area at M1	355	A	node 39 (small) ==> node 27 (large)
Retromolar area inclination	359	A	node 34 (inclined) ==> node 33 (horizontal)
Orientation of mandibular premolar row	360	S	node 42 (U shaped) --> node 41 (parabolic)
Prominentia lateralis position	365	S	node 35 (M1-M2) ==> node 34 (M3)
Ramus root anterior position	367	S	node 46 (posterior) <--> node 45 (intermediate)
		A	node 26 (intermediate) ==> *P. boisei* (anterior)
Ramus root vertical position	368	S	node 46 (high) <--> node 45 (intermediate)
		A	node 26 (intermediate) ==> *P. boisei* (low)
Internal coronoid pillar orientation	369	A	node 32 (vertical) ==> node 31 (concave)
		A	node 31 (concave) ==> African *H. erectus* (oblique)
Pos. junction between mand. notch and condylar articular surface	373	A	node 34 (lateral) ==> node 33 (medial)
Planum triangulare depth	377	A	node 32 (shallow) ==> node 31 (deep)

Table S3. Apomorphies in support of stem elliptic boundaries/tree nodes 40 to 26. Related to Figures 1, 2A and S9

Meaning of symbols is the same as for Table S2 with character numbers # in bracket (). Character changes highlighted for the higher order elliptic boundaries A, B, C, D, E and F are synapomorphies, i.e. morphological novelties passed on to succeeding concentric monophyletic groups, whereas the novelties of the lower order groups Par, NalSed, Hab and Her are autapomorphies specific to these groups. The inheritance of morphological novelties is a cumulative process with 2 distinctions : nested elliptic stem ancestors cumulate novelties, e.g. boundary E (genus *Homo sensu stricto*) posseses the synapomorphous character-state changes from A + B + C + D in addition to its three synapomorphies (present ectoglenoid crest #119, present squamotympanic fisssure #159, 100 to 110 occipital angulation #210), whereas non-nested elliptic stem ancestors such as Par, NalSed, Hab and Her cumulate novelties of preceding nested boundaries plus its autapomorphies, but its autapomorphies are not passed on, e.g. the *Paranthropus* group Par accumulate novelties from A + B + 16 autapomorphies, but its 16 autapomorphies are not passed on to C, D and E.

Elliptic boundary A = stem ancestor of *Au. africanus*, *Paranthropus* and *Homo* sister groups (1 synapomorphy)
Tympanic shape (144) : tubular ==> plate-like

Elliptic boundary B = stem ancestor of *Paranthropus* and *Homo* sister groups (6 synapomorphies)
Maxillary sinus division (81): posterior ==> anterior
Longus capitis insertion size (212): large ==> small
Occipital plane length (215): lengthened --> shortened
Foramen magnum inclination (235): posteriorly ==> horizontal
Maxillary P3 mesiobucal line extent (282): rare --> absent
Mandibular symphysis orientation (330): receding) ==> vertical

Elliptic boundary C = stem ancestor of genus *Homo sensu amplo* (8 synapomorphies)
Outline of superior facial mask (18): tapered ==> squared
Projection nasal bones above frontomaxi. suture (55): expanded ==> not projected
Zygomatic prominence development (99): prominent ==> slight
Lateral expansion of zygomatic root (105): above EAM ==> above mandibular fossa
Articular tubercle development (113): not developed --> developed
Mandibular fossa position (134): lateral) ==> medial
Anteromedial incursion of super. temporal lines (191): moderate ==> weak
Position temporal lines on parietal bones (195): crest ==> wide

Elliptic boundary D = stem ancestor of genus *Homo sensu lato* (2 synapomorphies)
Zygomaticoalveolar crest (87): straight ==> curved
Mandibular P3 root number (284): two ==> one

Elliptic boundary E = stem ancestor of genus *Homo sensu stricto* (3 synapomorphies)
Ectoglenoid crest (119): absent ==> present
Squamotympanic fissure (159): absent) ==> present
Occipital angulation (210): >110 ==> 100 to 110

Elliptic boundary F = PreHS = stem ancestor of
(((*H. heidelbergensis, H. neanderthalensis*), *H. sapiens*), *H. antecessor*) (3 synapomorphies)
Cranial vault index (5): long low --> short high
Mandibular P4 shape (289): asymmetrical wide polygon==> asymmetrical reduced polygon
Cranial contour in norma occipitalis (8): low and broad -->en bombe

Elliptic boundary G = Her = stem ancestor of ((Af.*H. erectus*, Geo. *H. erectus*), As.*H. erectus*) (3 autapomorphies)
Tubercle on anterior wall of TMJ (128): absent ==> present
Inion location (230): below opisthocranion ==> at opisthocranion
Foramen magnum inclination (235): horizontal --> anteriorly

Elliptic boundary H = Hab = stem ancestor of ((*H. rudolfensis, H. habilis*), *H. floresiensis*) (1 autapomorphy)
Inferior width of projecting nasal bone (59): wide --> narrow

Elliptic boundary I = NalSed = stem ancestor of (*H. naledi*, *Au. sediba*) (1 autapomorphy)
Frontal eminence (27): absent ==> presence

Elliptic boundary J = Par = stem ancestor of genus *Paranthropus* (16 autapomorphies)
Supraorbital thickness gradient (41): medial to lateral ==> lateral to medial
Inferior width of projecting nasal bone (59): wide ==> not projecting
Palate thickness (71): thin ==> thick
Maxillary trigone (79): absent ==> present
Mediolateral thickness of zygomatic arch at root of frontal process (93): thin ==> thick
Position of zygomatic angle (101): at orbit ==> above orbit
Maximum lateral projection of mastoid (161): high) ==> low
Anteromedial incursion of super. temporal lines (191): moderate ==> strong
Anterior pole shape (243): rounded --> beaked
Enamel thickness (244): thick ==> hyperthick
Mandibular deciduous canine shape (264): apex central, mesial convexity low --> apex mesial, mesial convexity high
Lingual shape of maxillary canine (270): more symmetric --> symmetric
Molar dentine horn height (295): high ==> low
Deciduous m1 mesial crown profile (325): MMR slight, protoconid ant., fovea open ==> MMR thick, protoc. even w. metaconid, fovea closed
Distal marginal ridge height of deciduous m2 (326): low --> high
Mandibular cross-sectional area at M1 (355): small) ==> large

Elliptic boundary 26 = stem ancestor of (*P. boisei, P. robustus*) (5 autapomorphies)
Palatine process orientation (74): nearly horizontal ==> steep posterior angle
Zygomatic process root (104): undivided ==> divided
Articular tubercle projection (114): not or slightly projecting==> projecting
Lateral tympanic extension (147): medial to saddle ==> lateral to saddle
Foramen magnum position (234): at line ==> anterior

Elliptic boundary 31 = stem ancestor of (African *H. erectus*, Georgian *H. erectus*) (2 autapomorphies)
Internal coronoid pillar orientation (369): vertical ==> concave
Planum triangulare depth (377): shallow ==> deep

Elliptic boundary 33 = stem ancestor of (*H. heidelbergensis, H. neanderthalensis*) (2 autapomorphies)
Retromolar area inclination (359): inclined ==> horizontal
Position of junction between mandibular notch and condyle articular surface (373): lateral ==> medial

Elliptic boundary 34 = stem ancestor of
((*H. heidelbergensis, H. neanderthalensis*), *H. sapiens*) (4 synapomorphies)
Cingulum expression (246): present ==> absent
Cusp 5 in mandibular M1 and/or M2 (312): present ==> absent
Submandibular fossa depth (345): shallow --> deep
Prominentia lateralis position (365): M1-M2 ==> M3

Table S4. Summary of *H. naledi* and *Au. sediba* MP phylogenetic positions. Related to results concerning *H. naledi* and *Au. sediba* in main text *2. Comparative validation of MPMAX optimal scenario*, and Figures S3-S6

Relative phylogenetic position of *H. naledi* and *Au. sediba*	Equal weight characters	RC reweighed characters
Fitch parsimony (Figure. S3) (unordered characters)	*Au. sediba*, in a polytomy with *H. floresiensis*, is close upstream to *H. naledi* and together are between *Au. africanus* and *Homo* clades.	*H. floresiensis* is between *Au. sediba* and *H. naledi*, and this group is in turn between *Au. africanus* and *Homo* clades.
Wagner parsimony (Figure. S4) (ordered characters)	*Au. sediba* and *H. naledi* are together upstream from *Homo* clades and downstream from *H. floresiensis* and *Au. africanus*.	Same as for equal weight.
Camin-Sokal parsimony (Figure. S5) (only convergence accounted for)	*Au. sediba* and *H. naledi*, with *H. floresiensis* in uncertainty setting and without in polymorphism setting, are a sister group of the *habiline* group that includes *Kenyanthropus*	*Au. sediba* and *H. naledi* are a sister group of the *habiline* group that includes *Kenyanthropus*
Dollo parsimony (Figure. S6) (only reversal accounted for)	For uncertainty setting *Au. sediba* and *H. naledi* are together as a sister group between *Paranthropus* and *Homo* clades. In polymorphism setting their group with *H. antecessor* is among *Homo* sister groups	For uncertainty setting *Au. sediba* and *H. naledi* are together as a sister group between *Paranthropus* and *Homo* clades. Under polymorphism setting both are a sister group of the *habiline* group that includes *Kenyanthropus*.

Table S5. Inconsistencies for the Popperian elimination of evolutionary scenarios applied to dataset split of 288 unordered characters and 103 ordered characters as per Dembo et al. 2016. Related to results concerning *H. naledi* and *Au. sediba* in main text *2. Comparative validation of MPMAX optimal scenario*, and Figure S11

The list of inconsistencies based on 4 MP bootstrap trees is determined according to the following criteria: 1) chronological placement of *S. tchadensis*, *K. platyops* and *Au. africanus* (1 = out of order chronologically, 0 = consistent chronologically); 2) presence of clade ((*H. heidelbergensis, H. neanderthalensis*), *H. sapiens*) (1 = no presence of clade, 0 = presence of clade); and 3) number of branches with bootstrap support values of less than 20 %.

	Inconsistency 1 Chronological order satisfied in bootstrap tree			Inconsistency 2 Presence of clade ((*H. heid, H. neand*), *H. sap*)	Inconsistency 3 Bootstrap support # clades < 20%	Sum of inconsistencies	CI	RI
Parsimony scenario	*S. tchadensis*	*K. platyops*	*Au. africanus*					
Dembo mixed characters equal weight - uncertainty	1	1	1	1	2	6	0.55	0.61
Dembo mixed characters equal weight - polymorphism	1	1	1	1	3	7	0.75	0.61
Dembo mixed characters RC weighed - uncertainty	1	1	1	1	0	4	0.79	0.84
Dembo mixed characters RC weighed - polymorphism	1	1	1	1	0	4	0.82	0.84

Other Supplemental Information for this manuscript includes the following:

Figure360. An Author Presentation of Figure 4